UNIVERSITÀ DEGLI STUDI DELL'AQUILA
Dipartimento Di Scienze Fisiche e Chimiche

Dottorato di Ricerca in Scienze Fisiche e Chimiche
XXXII Ciclo
SSD FIS/02

Three aspects on Compact Stars stability

Dottorando
Francesco TONELLI

Coordinatore del Corso
Prof. Antonio Mecozzi

Tutor
Prof. Luigi PILO

Relatore
Dott. Massimo MANNARELLI

Anno Accademico 2018-2019

Contents

1 Overview **1**
- 1.1 History . . . 2
- 1.2 The Birth of Neutron Star . . . 5
- 1.3 Observed properties of Compact Stars . . . 7

2 Spherical Compact Stars **13**
- 2.1 Neutron Stars . . . 13
- 2.2 Hydrostatic Equilibrium . . . 16
- 2.3 The EoS of Nuclear Matter . . . 17
- 2.4 Quark Stars . . . 20
  - 2.4.1 Overview on Quantum Chromodynamics . . . 21
  - 2.4.2 Quark Matter EoS . . . 23
- 2.5 Hybrid Stars . . . 24
- 2.6 Strange Stars . . . 26

3 Gravitational Wave Echoes from Compact Stars **29**
- 3.1 Theoretical aspects on GW Echoes . . . 30
- 3.2 GW Echo observation . . . 34
- 3.3 GW echo from Strange Stars . . . 35
  - 3.3.1 The Model . . . 38

4 The Neutron-Mirror Neutron mixing in Neutron Stars **42**
- 4.1 Mirror World . . . 42
- 4.2 Mirror neutron-neutron mixing . . . 45
- 4.3 Mirror neutron-neutron mixing in Neutron Stars . . . 46
  - 4.3.1 Two fluid description . . . 47
  - 4.3.2 Total Baryon Density Curves . . . 51
  - 4.3.3 Transformation rate time . . . 55
  - 4.3.4 TOY model for Mass distribution of Mixed Stars . . . 59

5 Radial Oscillations of Compact Stars **64**
5.1 Radial oscillation in Newtonian Limit 65
5.2 Radial oscillation in General Relativity 68
5.3 Numerical Method 73
5.4 Radial Oscillation with a Phase transition 79

6 Conclusions **84**

A Numerical results **110**

Abstract

This thesis is aim to explore three different aspects of Compact Stars, the densest and the smallest stars known. Compact Stars are a very interesting subject of study because of their extreme conditions, making them a laboratory to test our knowledge on the properties of dense matter.

The first aspect is the possible Gravitational wave echoes emission from the merging of Compact Stars. In this thesis we examine the possibility that the ultracompact object produced in the GW170817 event is a Strange Star, and we evaluate the frequency of the corresponding Gravitational wave echoes. GW170817 event is the first merging observation compatible with the coalescence of a binary Compact Stars system and the nature of its final product is still unclear. It has recently been claimed that in the GW170817 event a gravitational wave echoes at a frequency of about 72 Hz have been produced with a $4.2\,\sigma$ significance level. The merging of Compact Stars can lead to the emission of gravitational wave echoes if the postmerger object features a photon sphere capable of partially trapping the gravitational waves. Our study can in principle give us some fundamental information on Compact stars' equation of state. Indeed, if the postmerger object was a strange stars it would be proved the hypothesis of Bodmer and Witten that collapsed nuclei are the true fundamental state of matter. However, the frequency obtained even considering a final object described by an ultrastiff strange star is about two order of magnitude bigger than the experimental measurement. This could be a signature that the remnant of GW170817 is a Black Hole.

The second aspect is the possible presence of Mirror matter into a Neutron Star. Mirror matter is a non conventional dark matter candidate, firstly suggested by Lee and Yang in 1956 which proposed the existence of a hidden sector of particles and interactions to restore the parity symmetry. Mirror matter communicates with our world only through gravity. In this thesis we assume that neutrons could oscillate into Mirror neutrons inside a Neutron Star. This phenomenon has interesting implications. Whether the measurements of radii will improve in the following years, this kind of phenomenon could lead to the detection of stars with equal masses but different radii corresponding to stars composed of different fraction of Mirror matter. Furthermore, whether the oscillation of neutron is possible, a large number of stars could produce Mirror matter and eventually collapse in a Black Hole without any violent explosion.

The last aspect is the radial oscillation of Compact Stars. In this thesis we develop a numerical algorithm for the solution of the Sturm-Liouville differential equation governing the stationary radial oscillations of Compact Stars. Our method is based on the *Numerov Method* that turns the Sturm-Liouville differential equation in an eigenvalue problem. In our model we provide a strategy to deal with the star boundaries. Assuming that the fluctuations obey the same equation of state of the background, we analyze different stellar models using several equation of state. With our model it is possible to test the paradigm that the last stable configuration corresponds to the null eigenfrequency. We obtain this result using continuous equation of state providing a stability test of our method. In addition, in order to correctly treat equations of state with discontinuous speed of sound, we develop an innovative numerical method that can be used to analyze the stability of Compact Stars.

Chapter 1

Overview

Compact Stars (CSs) are one of the possible final stages of stellar evolution. Unlike luminous stars, CSs do not *burn* nuclear fuel but they are supported against gravitational collapse mainly by the degeneracy pressure of neutrons. These features, together with the extreme internal condition, make CSs a very intriguing subject of study.

We know from observation that CSs rotate as fast as a few hundred rounds per second. Due to the very fast rotation, the huge centrifugal force must be balanced by gravity, otherwise the matter will be ripped apart [1]. The balance between gravity and centrifugal force gives us the lower limit on the stellar density: with CSs 10^{14} times denser than Earth [1]. Thus the typical central density of CSs can be up to $5-10$ times the nuclear saturation density ρ_s, i.e. the typical density of heavy nuclei. Furthermore, sometimes it is possible to measure with good accuracy the CSs mass. The typical mass of CSs is about $1.4M_\odot$, where $M_\odot = 1.989 \times 10^{33}$ g indicates the solar mass. Thus, considering that the mean density is of the order of $\bar{\rho} \sim 10^{15}\mathrm{g/cm}^3$, we can infer that the typical radius ($R \propto \sqrt[3]{M/\rho}$) is of the order of 10 kilometers. By all means CSs are the smallest and the densest stars known. These extreme conditions are irreproducible in terrestrial laboratory, so CSs can be viewed as a laboratory for studying the properties of nuclear and exotic matter at supranuclear densities [1–4].

To build an accurate model of CSs we need to find a relation between a macroscopic object and the fundamental interactions of matter. Remembering that the Gravitational Potential at the surface of a star is $\Phi = GM/R$, a CS has a Gravitational Potential five order bigger than a luminous star. Thus, for an accurate description of CSs we should use the theory of General Relativity. For a detailed treatment of General Relativity see for instance [5–10].The link between microscopic physics and General Relativity is

given by the Einstein equation:

$$G^{\mu\nu} = 8\pi T^{\mu\nu}, \tag{1.1}$$

where $G^{\mu\nu}$ is the Einstein's tensor and $T^{\mu\nu}$ is the stress energy tensor. The Einstein tensor is defined as:

$$G_{\mu\nu} = R_{\mu\nu} - \frac{1}{2} R g_{\mu\nu}, \tag{1.2}$$

where $R_{\mu\nu}$ is the Ricci's tensor, R is the Ricci's scalar and $g_{\mu\nu}$ is the metric tensor of the spacetime. In our studies we focus on static and spherical CSs, thus the appropriate metric tensor is the well known Schwarzschild metric. The Ricci's tensor and the Ricci's scalar are combination of derivatives of the metric tensor, for a complete discussion see for instance [5–7]. Instead the form of the stress energy tensor strongly depends on the Equation of State (EoS) of matter, that is a relation between the thermodynamic quantities.

The EoS for densities smaller than the nuclear saturation density are well known. They are based on experimental data of neutron scattering and on theories of Coulomb system [2]. Furthermore, using many-body theories, it is possible to narrowly calculate the EoS up to $2\,\rho_s$. Anyway, the determination of EoS at density up to $10 - 15\,\rho_s$ remains an open problem. Our main goal is to find a link between the internal structure of CSs and some astrophysical observables. In this way, some important information on microphysics and on the strong interaction could be extracted. The electromagnetic signals give us some important information, but these signals are supposed to be related to the atmospheric properties of CSs.

Rapidly rotating CSs lose axial symmetry (e.g., due to r-mode instability) and emit gravitational waves. Compact binaries containing CSs are even much more efficient sources of gravitational radiation (especially at the final inspiral stage). Gravitational radiation of double neutron star binaries and neutron star-white dwarf binaries has already been observed indirectly, by detecting relativistic decay of pulsar orbits [2]. Furthermore the 17th of August 2017 a first direct detection of Gravitational radiation from binary neutron stars was made. From this observation, for instance, parameters like tidal deformability can be calculated and this can give us important constraints on the EoS of the matter.

1.1 History

The history of Neutron Star (NS), the widely studied CS class, began in 1930s. Despite Sir James Chadwick announced the experimental discovery

of the neutron in 1932 [11], few months earlier, Landau had already speculated on the possible existence of stars more compact than White Dwarfs, containing matter at nuclear density [12]. However, the NS first prediction was made by Baade and Zwicky in 1934. We report few passages of their inspired papers. In their first work they suggested that: *supernovae represent the transition from ordinary stars to neutron stars, which in their final stages consist of extremely closely packed neutrons* [13]. In their following publication they also stated that NSs: *may possess a very small radius and an extremely high density. As neutrons can be packed much more closely than ordinary nuclei and electrons, the gravitational packing energy in a cold neutron star may become very large, and, under certain circumstances, may far exceed the ordinary nuclear packing fractions* [14].

A milestone in the development of NS models was achieved in 1939 by Tolman, Oppenheimer and Volkoff. Tolman and Oppenheimer, together with Oppenheimer's student Volkoff, independently derived the equation of the hydrostatic equilibrium in the framework of General Relativity [15, 16]. Furthermore, Oppheneimer and Volkoff numerically solved this equation considering the simplest composition possible: an ideal Fermi gas of neutrons at very high density [15]. For this particular model they obtained a maximum gravitational mass of $0.7\,M_{\odot}$. This result was in disagreement with Chandrasekhar limit on the mass of a white dwarf, i.e. $1.4\,M_{\odot}$. Thus, Opphenheimer and Volkoff interpreted their result as the impossibility to generate NSs from supernovae explosion.

Another important issue at that time was the understanding of the stellar pressure source. In 1937, Gamow [17] and Landau [18] independently suggested that any (normal) star could contain a NS in its own core. This would have initiated a slow "accretion" of stellar matter within the normal star onto its neutron star core, so that the stellar energy could have been supplied by the gravitational energy release in the course of that accretion [2]. However, soon after, Bethe and Critchfield clarified the connection between stellar pressure and thermonuclear reactions [19]. When the idea of Gamow and Landau faded, NSs were ignored by the scientific community for about thirty years [3]. Nonetheless, before the discovery of the first NS some important theoretical aspects were explored.

The widest studied theoretical problem in the fifties was the construction of the EoS of dense stellar matter. The first realistic attempt was due to Wheeler and his collaborators [20]. They used the semiempirical mass formula together with the EoS of degenerate electrons for the external layers and they assumed a core composed by a mixture of neutrons, protons and electrons in beta equilibrium. In 1959, Cameron constructed a NS model using the Skyrme EoS for high-density matter obtaining that nuclear forces

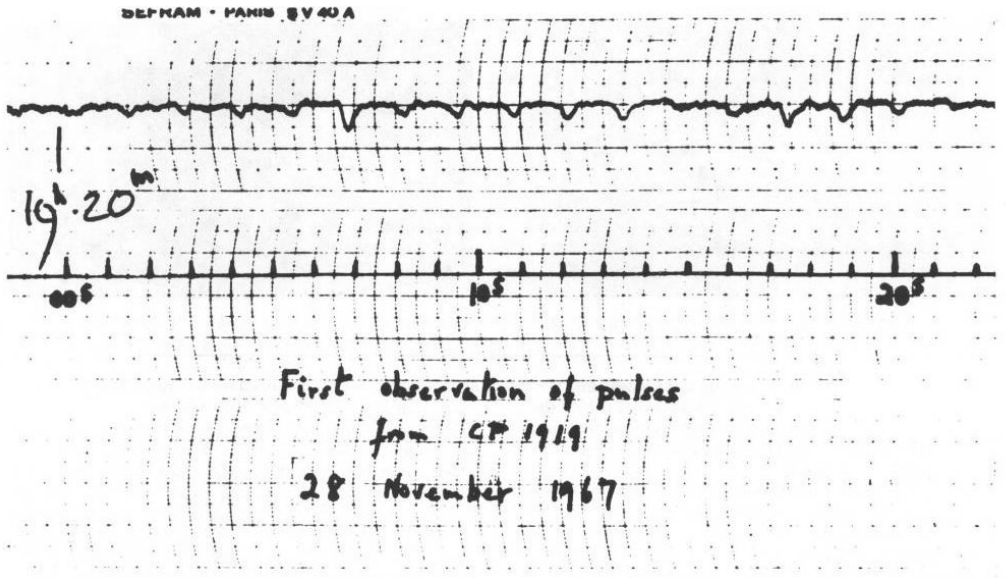

Figure 1.1: Periodic radio pulses observed by J. Bell. In the figure it is possible to see the pulses spaced 1.3s from each other (the horizontal axis represent the time). Figure taken by http://www.cv.nrao.edu

considerably stiffen the EoS [21]. Using his model he calculated a NS's maximum mass of $M \simeq 2\,M_{\odot}$. This result showed that NSs could be formed as proposed by Baade and Zwicky. Moreover, few years later the experimental discovery of the first NS, the hypothesis of the presence of exotic particles as hyperons [21–23] or free quarks [24, 25] in the core of a CS was proposed.

Before keep going on the history of NSs, let us answer to a question: Why are NSs the only stars which existence and origin have been successfully predicted much before their discovery? The answer is their typical thermal emission. The first cooling calculation, performed by Chiu and Salpeter [26], had already shown that the surface temperature of a NS should be of the order of $T \sim 10^6$ K. Thus, assuming a blackbody radiation emission, for the Wien law the emission of NSs has a maximum wavelength of $\lambda = 29$ Å: NSs emit mainly in X-ray. However X-ray cannot penetrate the Earth's atmosphere so we do not expect to reveal the NSs presence on the Earth.

Several important results were obtained during the era of X-ray astronomy, the 1960s [2]. In the beginning of this decade the first X-ray detectors were launched on rockets and balloons. In 1962, Giacconi et al [27], discovered the first cosmic, nonsolar X-ray Source. This detection generated a great interest in NSs and dozens of theorists speculated that the X-ray telescope was observing a young, warm NS. However, another important milestone for the detection of NSs was the discovery of a weak variable radio source, made

by Hewish and his student Bell in 1967. The source had been observed for months and it was found to be extremely regular, see Figure 1.1. They measured with good accuracy the period: 1.3373012 s. This is the discovery of the first *Pulsar* (now known as PSR B1919+21) and it was announced by Hewish *et al.* in 1968 [28]. Soon after the announcement, Gold speculated on the possibility that pulsars could be rotating NSs [29], and his idea is generally accepted today.

Between 1968 and 1969, two famous pulsars were detected: the Vela and the Crab Pulsars. Vela and Crab Pulsars are located in supernova remnants, providing evidence for the hypothesis of Baade and Zwicky: NSs are the remnant of supernova explosions. Furthermore, optical and X-rays observation of binary X-ray sources allow us to estimate the mass and the radius of NSs and this, as we shall see later, is a test for the various proposed EoS of matter. So far about 2000 NSs have been identified. In the following sections, after a brief discussion on NS birth, we shall talk about some properties we can infer and calculate from X-ray and radio emission of NSs.

1.2 The Birth of Neutron Star

Luminous Stars remain stable from ten to thousand million of years. During this period stars balance the gravitational pull melting light element in heavier nuclei, producing in this way a radiation pressure. The different fate of the stars depends on the mass of the progenitor, and massive stars can evolve in compact object. Stars with mass between 8 and 20 $M_\odot$ seem to be able to fuse elements up to iron, the endpoint of exothermic reaction [41], see Figure 1.2.

When iron is produced, the core of the star reaches the thermal equilibrium. In this phase the star is sustained by the degeneracy pressure of electrons. Elements cannot be fused in the core, so massive stars start to burn elements in the outer shells yielding a growing of the core. When the core mass reaches the Chandrasekhar limit, electrons become relativistic reducing their pressure contribution. The nuclear fusion processes and the electron degeneracy pressure are not sufficient to balance the gravitational pull and the core begins to contract. This contraction of matter inside the core squeezes neutrons and protons outside the nuclei releasing a huge amount of energy. Protons are now capable to capture electrons by inverse β-decay process:

$$p^+ + e^- \rightarrow n + \nu_e, \tag{1.3}$$

producing a large number of neutrons and electron neutrinos. This large number of neutrons generates a short-range nuclear repulsion that balances

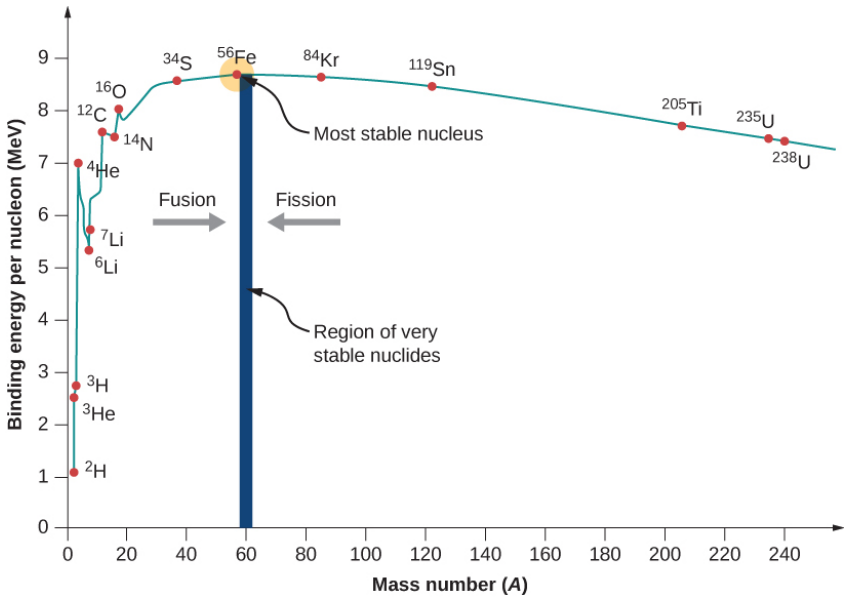

Figure 1.2: Binding energy per nucleon in MeV for different types of Nuclei. ^{56}Fe is the endpoint of exothermic reaction and it has the biggest binding energy per nucleon, i.e. about 8 MeV per nucleon. [40]

the gravitational pull. For this reason, the core bounces back the in-falling outer layer of the star resulting in a shock wave that propagates in the stellar medium. This mechanism is roughly the explosion mechanism of a Type-II Supernova. In the following we focus on the evolution of the core, for more details on the fate of the external layers see for instance [1–3].

In the center of a Type-II Supernova it is believed that a hot, lepton rich, compact object, called *proto-neutron star*, remains. The temperature of a proto-neutron star is of the order of tens of MeV and the lepton fraction, i.e. the number of leptons per baryons, can be as large as $Y_e \sim 0.4$. The formation of this kind of object takes a very short time, about few tens of milliseconds. These features qualitatively change the matter inside a proto-neutron star, making the EoS stiffer. In the subsequent evolution, the proto-neutron star deleptonizes and cools down mainly through the inverse beta decay. During its formation, because of the high temperature, proto-neutron star is opaque to neutrinos. So, neutrinos are trapped in a very high density region ($n \sim 6 \times 10^{-3}\,\mathrm{fm}^{-3}$) [42], called the *neutrino sphere*, and it takes about 10 s to diffuse. $10 - 30$ seconds after the core bounce, the star deleptonizes and very rapidly cools down through neutrinos emission. After few minutes, when the temperature of the core is less than $1\,MeV$, a cold NS is formed.

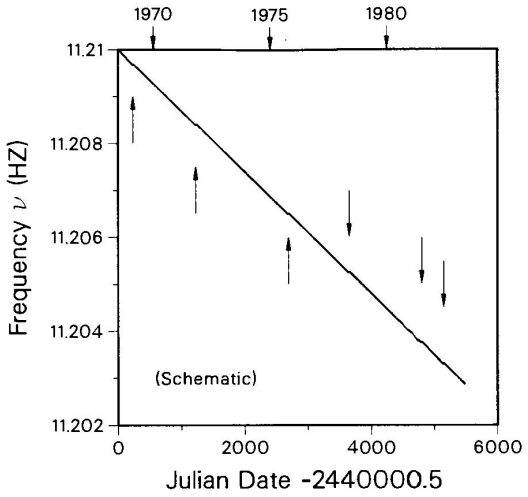

Figure 1.3: Slow variation of Vela Pulsar's rotational frequency with time: $\dot{P} = 1.2503 \times 10^{-13} s/s$. The arrows indicates the observed glitches [1].

1.3 Observed properties of Compact Stars

The widely observed astrophysical object associated to CSs are *Pulsars*. Pulsars are highly magnetized rotating CSs that emit magneto dipole radiation [29, 30]. This radiation is typically in the radio frequency band (Radio Pulsars) and rarely in the X-ray (X-ray Pulsars) or γ-ray band (γ-ray Pulsars). The radiation is emitted along the magnetic axis with a spread of about 10 degrees [1]. In general the magnetic field dipole axis is not aligned with the rotation axis. The rotation of the magnetic axis around the rotation axis implies that we can observe the emitted radiation only if we lie on the cone of the radiation swept out by the star, and if the source is not too far from the Earth [2]. Using the Radio telescopes, several hundred pulsars from our galaxy and from the nearby Magellanic Cloud have been detected, for instance [31–38]. Many of them show a very stable period. As a consequence we can measure with good precision the rotational period of a Pulsar P, i.e. the time interval between two subsequent pulses. Furthermore, we can also measure with good accuracy the time derivative $\dot{P}$, and sometimes the second time derivative $\ddot{P}$ [2]. The emission of electromagnetic radiation is made at the expenses of the rotational energy, thus isolated Pulsars show a regular spin down. For instance, rotational frequency of Vela Pulsar in function of time is shown in Figure 1.3.

It is very interesting to note that the period of several Pulsars shows some sudden jumps. These events are called *Glitches*. After one glitch the

frequency of a NS can vary from [1]:

$$\frac{\Delta\nu}{\nu} = 10^{-8} - 10^{-6}. \tag{1.4}$$

The mechanism responsible for glitches is not yet completely known. However, the mainly accepted idea is that glitches are associated with a sudden unpinning of vortices of nuclear superfluid in the NS crust [43–46]. When a superfluid rotates, it generates vortices. Vortices are regions of space in which the fluid is in normal phase and around them superfluid rotates with non vanishing speed. It is possible to demonstrate that the angular momentum of a rotating superfluid is in direct proportion with the number of vortices [4]. If a vortex line annihilate on the NS crust, it yields angular momentum to it and we could observe a sudden spin up of the star.

From observation of Pulsar's period and remembering the typical radii of CSs, we can estimate some important properties. For instance we can estimate the pulsar rotational energy, which is defined by:

$$E_{rot} = \frac{I\Omega^2}{2}, \tag{1.5}$$

where I is the moment of Inertia and $\Omega = 2\pi/P$ is the Pulsar frequency. Using the Crab Pulsar observed values of $P = 33.08\,ms$ and assuming the typical value for $I = 10^{45}\,\mathrm{g\,cm^2}$ ($I \propto M_\odot R^2$, with $M_\odot \sim 10^{33}$ g and $R \sim 10^6$ cm), we obtain that typical rotation energy is about $E_{rot} \sim 2 \times 10^{49}$ erg [2]. From the measure of $\dot{P}$ we can infer the rotational energy release as $\dot{E}_{rot} = I\Omega\dot{\Omega}$.

From the measured values of P and $\dot{P}$ we can estimate the Pulsar magnetic field and the Pulsar characteristic age. Assuming that the star's magnetic field is dipolar, and that the magnetic dipole energy loss rate is equal to the rotational energy release $\dot{E}_{rot}$, we obtain:

$$I\dot{\Omega} = \mathcal{N}, \quad \text{where} \quad \mathcal{N} = -\frac{2\Omega^3 B_{eff}^2 R^6}{3c^3}, \tag{1.6}$$

is the torque acting on the pulsar due to the magnetic dipole radiation, $B_{eff} = B_{eq}\sin\alpha$, B_{eq} is the magnetic field at the equator and α is the angle between the magnetic and rotational axes. From Eq.(1.6), we obtain:

$$B_{eff} = \left(\frac{3Ic^3}{8\pi^2 R^6} P\dot{P}\right)^{1/2} \sim 3.2 \times \frac{I_{45}^{1/2}}{R_6^3}\sqrt{P\dot{P}}G, \tag{1.7}$$

where I_{45} is the momentum of inertia in units of $10^{45}\,\mathrm{g\,cm^2}$ and $R_6 = R/10^6$ cm. Assuming $I_{45} = 1$ and $R_6 = 1$ and using the measured values of P and

$\dot{P}$ we can obtain the value of B_{eff}, that could be treated as the characteristic pulsar magnetic field (of the order of 10^{12} G [47]).

From Eq.(1.6) we can also estimate the pulsar age. In general, we can define the spin down torque as $N = -A\Omega^n$, where n is the *braking index*. Assuming a constant n, from Eq.(1.6) we obtain: $P^{n-1}\dot{P} = \text{const}$ [2]. Integrating from a time $t = 0$ (associated to stellar birth), to the current age t, one obtains:

$$t = \frac{P(t)}{(n-1)\dot{P}(t)}\Big(1 - \Big(\frac{P(0)}{P(t)}\Big)^{n-1}\Big). \tag{1.8}$$

Considering that newly born Pulsar rotated much faster than now ($P(t) << P(0)$), we can consider for old Pulsars, $t = P/((n-1)\dot{P}$ [2]. For magnetic dipole model, braking index is $n = 3$ and so the last expression reduces to:

$$t_c = \frac{P}{2\dot{P}}, \tag{1.9}$$

where t_c is called *characteristic pulsar age*. For instance, the characteristic age of Crab pulsar is $t_c = 1240$ years in qualitative agreement with its true age (~ 970 years).

Using the observed data and the inferred magnetic field we can study the time evolution of Pulsars. In Figure 1.4 some observed pulsars are shown. It is possible to note that stronger magnetic field, (on the order of $10^{12} - 10^{13}$G) induces a faster spin down. During the evolution in time, Pulsars located on the top of the figure are moving toward right (because they are loosing rotational energy), and toward down (because of magnetic field decay). Owing to loosing of rotational energy, stars induce weaker electric field and could not have enough energy to produce a sensible outflow of charged particle from their surface. In this case they cease to be observable as Pulsars and they enter in the right bottom corner of the Figure 1.4. In Figure 1.4 the silent region is divided from *radiative* part by the *Pulsar death line* (dashed blue line). However, some Pulsars with P of the order of milliseconds have been observed. These stars are called Millisecond Pulsars and they are believed to be spun-up by accretion of matter. Falling matter onto a CS could produce a X-ray burst and, from conservation of angular momentum, the star should spin-up. These stars are observed with a low magnetic field, $B \sim 10^8\, G$ and with low time derivative of the period. That presumably means that these are old stars and probably they have crossed back the pulsar death line. After accretion of matter, the spin is big enough to sustain magnetosphere activity, and stars can be seen as pulsars [49].

An accurate measurements concerning CSs are mass determination [50]. About the 90 % of pulsars are isolated and we cannot measure their masses;

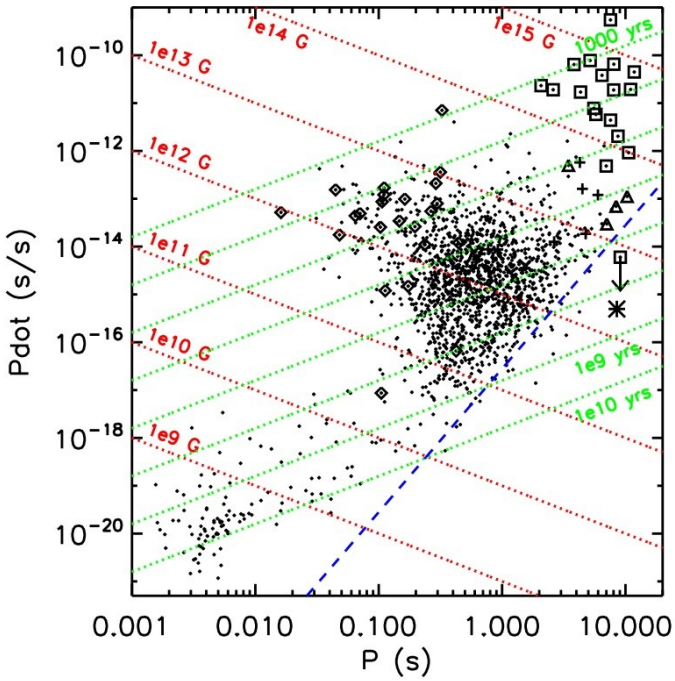

Figure 1.4: Period and its time derivative for Pulsars. Line of constant Magnetic field strength and characteristic time are indicated in the plot (dashed red and dashed green lines respectively). Pulsars located in the highest part of the Figure are younger and they are spinning down. Due to the spin-down they could cross the *death line* (dashed blue line). Death line divide the *radiative* behavior, i.e. active Pulsar, from the *silent* region where stars have not enough rotational energy to emit radiation. However, due to accretion, stars located in the silent region, should cross back the death line and start to emit again. [48]

precise calculation can be performed for those CSs in binary system. Up to now, around 33 relatively precise mass measurement have been performed. The mass is defined measuring some parameters of the system such as the binary period P, the projection of pulsar's semimajor axis on the line of sight $a_p \sin i$ (with i the orbit's inclination angle), the eccentricity e, etc. The observed parameters yield the so called mass function:

$$f_p = \left(\frac{2\pi}{P}\right)^2 \frac{(a_p \sin i)^3}{G} = \frac{(M_c \sin i)^3}{M^2}, \tag{1.10}$$

where $M = M_c + M_p$ is the total mass; M_p and M_c are the mass of the pulsar and of the companion respectively. Binary systems are compact system and

General Relativity effect can often be observed [50]. Using Post-keplerian approximation we can infer some parameters like the advance of periastron, the gravitational redshift, the Shapiro delay time, etc. Utilizing one of these parameters together with the mass function it is possible to uniquely determine the masses of both stars in a binary system, see Figure 1.5.

In Figure 1.5 masses are divided in four different groups. The groups differs from the companion type: X-ray/optical binaries, double neutron stars binaries, white dwarf-neutron star binary, and main sequence-neutron star binary. It is interesting to note that the mean mass of all these groups is about $1.4\,M_\odot$ but their distribution are quite different. For instance, the distribution of double neutron stars is peaked over $1.4\,M_\odot$ and do not show a broad dispersion. This could be a signature of a common evolution of the binary system [50]. This condition is relaxed in the other class of binaries. For instance, in the compact star-white dwarf binary (in Figure 1.5 the grey region) some stars with mass higher than $1.4\,M_\odot$ have been observed.

The existence of CSs with masses of the order of $2\,M_\odot$ could be a key to test the EoS of matter. The largest CS mass can rule out the EoS that fall below this value [51]. The most massive and well-measured CS mass is $2.01 \pm 0.04 M_\odot$ for PSR J0751+1807 [52]. Furthermore there is a particular class of millisecond pulsar, the black widows, that seems to have a very large mass [53]. However, the large errors in black widows mass measurements need caution.

Presently no high-accuracy measurement of NS radii has been done. There are several astrophysical observation that could be used for the extraction of radius, for instance: the thermal X-ray and optical fluxes from isolated and quiescent neutron stars [54], gravitational radiation from tidal disruption of merging neutron stars [55, 56] , etc.. For example, the study of thermal X-ray in low mass X-ray binaries gives us the so-called radiation radius:

$$R_\infty = \frac{R}{\sqrt{1 - 2GM/(Rc^2)}}, \tag{1.11}$$

by measurement of the star luminosity and the use of the Stefan-Boltzmann law. This kind of estimate gives radii of the order of $10\,km$. Unfortunately this measure is complicated because the X-ray emission depends on the composition of the atmosphere of the star and on the strength and distribution of the magnetic field. Any measurement of this sort effectively gives R/d, where d is the distance of NS, and the determination of distance of the star is very difficult. We do not focus on this work on the techniques of radii estimation, for a detailed description of this method and of the other methods see for instance [1–3, 50, 51, 57–61].

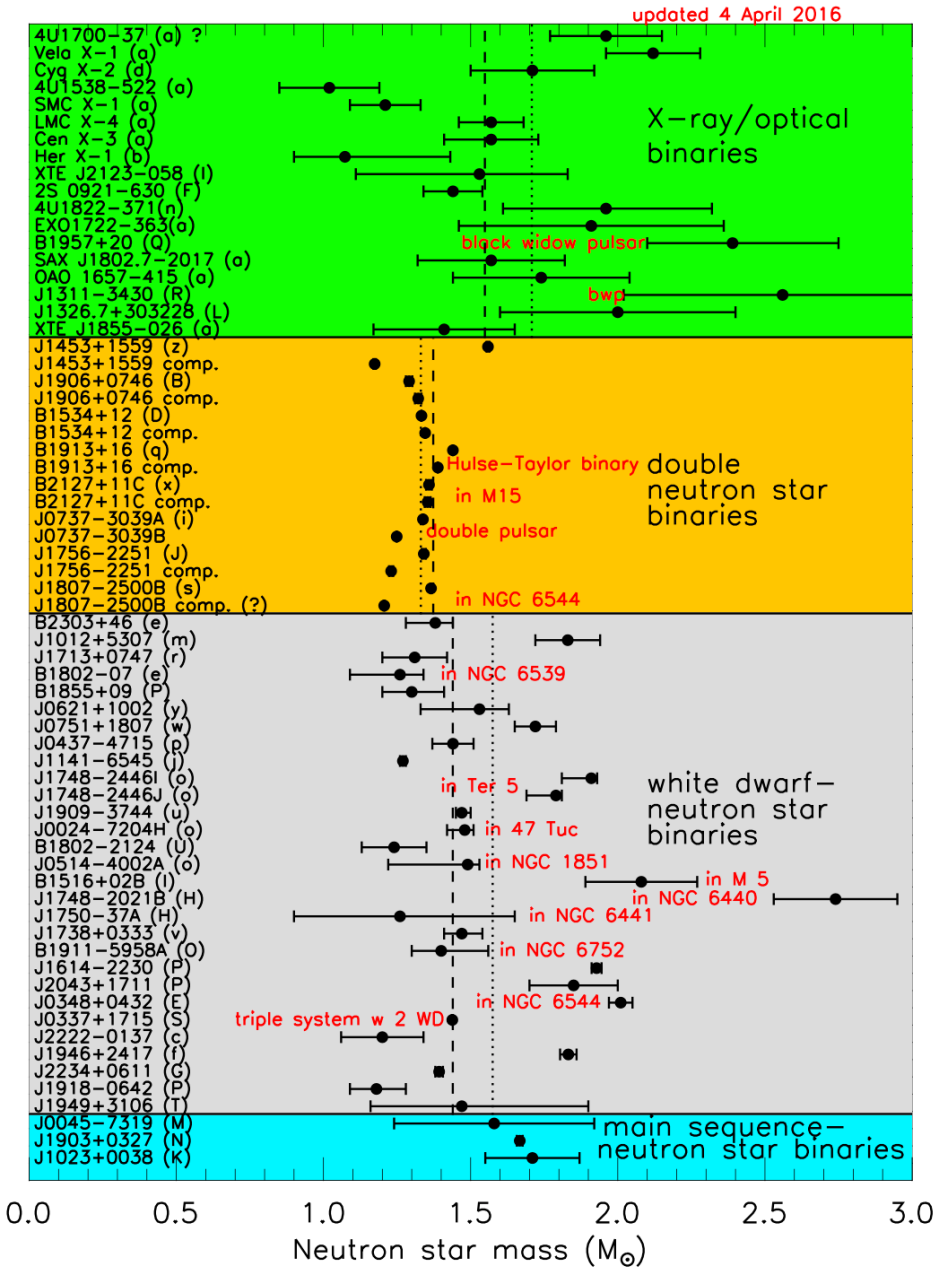

Figure 1.5: Observed neutron star masses, figure taken from [50]. In the region with green background are shown the measured mass for X-ray/optical binaries: the errorbars show large uncertainties on these measurement. In orange the most precise measurement of NS mass: the double neutron star binaries. In grey and blue are shown respectively the white dwarf-neutron star binaries and the main sequence-neutron star binaries.

Chapter 2

Spherical Compact Stars

In this Chapter we focus on the stable solution of a non-rotating, non-magnetic CS. We derive the equation of hydrostatic equilibrium in general relativity and we focus on some EoSs useful for the following chapters. This chapter is organized as follows: in the first section we analyze the structure of the most widely studied CS class: Neutron Stars. Then we derive the TOV equation and some basic EoSs for the nuclear matter. In the last two sections we analyze the possible presence of quark matter in CS, deriving the possible EoSs and discussing the models of hybrid and strange star.

2.1 Neutron Stars

According to current theories, it is possible to subdivide a NS in different regions characterized by typical values of the energy density. As shown in Figure 2.1, NS can be divided in an *Atmosphere* and four internal regions: the *outer crust*, the *inner crust*, the *outer core*, and the *inner core*.

The *Atmosphere*, is the most external part. It is mainly composed of Hydrogen, Helium and non degenerate electrons. It extents from $10\,cm$ for hot NSs (NSs with external temperature of $10^6 K$) to few mm for cold stars. The density in this region is smaller than $\rho \sim 7. \times 10^6\, g/cm^3$. Despite the limited thickness, the Atmosphere properties are fundamental for the determination of some NS observables like the mass and the radius. The NS atmosphere properties have been studied by many authors [62–66] but the developed models seem far from being complete.

The *outer crust* extends from the atmosphere bottom to the layer whose density is the neutron drip density $\rho = \rho_{ND} \sim 4.3 \times 10^{11}\mathrm{g/cm}^3$. The outer crust typical temperature is of the order of tens of KeV and it is believed to be mainly composed of ions and electrons. This region, considering the very high

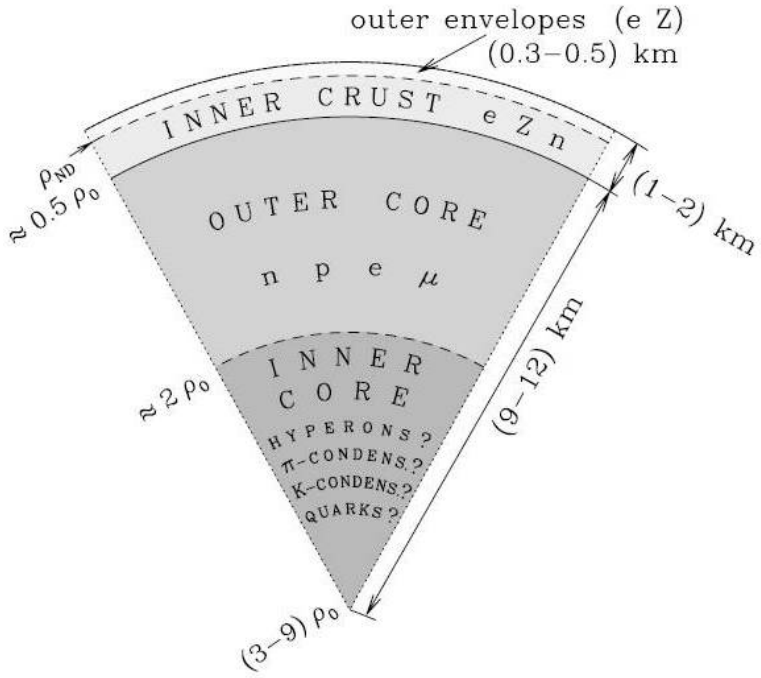

Figure 2.1: Schematic structure of a neutron star [2]. The outer envelopes are formed by the Atmosphere and the outer crust, regions rich of electrons and ions. The inner crust is a thin layer of few kilometers thick, formed by neutron rich nuclei, neutrons and electrons. The outer core and the inner core form the biggest part of the star. The outer core is composed of neutrons, protons, electron and muons, while the composition of the inner core is uncertain. In this figure ρ_0 indicates the nuclear saturation density.

temperature and the low density, should be liquid. However, in deeper layers density grows. Ions should form a strongly coupled Coulomb solid immersed in a strongly degenerate and ultrarelativistic electrons gas [67–69]. As the matter compression increases, it becomes more favorable to have proton poor ions. Indeed the electron Fermi energy grows with increasing density favoring the electron capture process [70,71]. When the density reaches ρ_{ND}, neutrons start to drip out from nuclei producing a free neutron gas [2].

The *inner crust* occupies the density range $\rho_{ND} < \rho < 0.5\rho_s$,where $\rho_s \simeq 2.5 \times 10^{14} g/cm^3$ is saturation nuclear matter density. It may be about one kilometer thick and it is formed mainly of electrons, free neutrons, and neutron-rich atomic nuclei. As the density grows the number of protons drop down and very exotic nuclei, like zirconium with 1500 nucleons, can be present [67]. Moreover, in this region various *Pasta phases* could be realized [72–74]. In this phases nuclei form sheets immersed in liquid nuclear matter. With increasing densities different type of *pasta*, characterized by different space modulation, are energetically favored. The most important

feature of these *pasta phases* is that nucleons form a crystal while free neutrons might be in a superfluid state [75, 76].

Going inward in the star, with density in the range $0.5\,\rho_s < \rho < 2\,\rho_s$, we suppose the existence of a region called *outer core*. This layer is several kilometer thick and its matter consists mainly of neutrons with a few percent of protons p, electrons, and possibly muons μ (the so called npeμ composition) [2]. Neutrons, Protons, Electrons and Muons inside the core are in statistical equilibrium, meaning that the beta decay and its inverse process are in equilibrium. In this region the npeμ plasma is strongly degenerate and electrons and muons form an almost ideal Fermi gas [2]. Neutrons and protons could be in superfluid and superconductive, state respectively. They form a Fermi liquid and their interactions are due to nuclear forces.

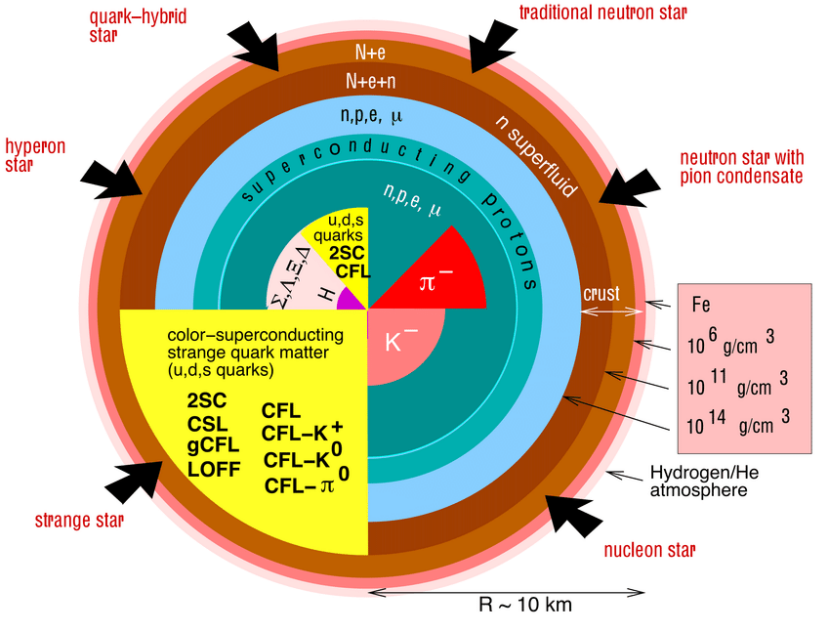

Figure 2.2: Compact Stars model zoo [77]. The models differ from each other by the internal composition: star with core made of pion (kaon) condesate, hyperons or quark matter are shown. In the bottom left the hypotetical strange star model is depicted.

The central part of the star is called the *inner core*. It can have a radius of several kilometers and its density is $\rho > 2\,\rho_s$. This is the most interesting part of a NS. Since the energy density is higher than the central density of heavy nuclei, several models have been put forward, see Figure 2.2. The models developed concerned the possible presence of Hyperons [21–23], condensates of pions [78, 79] or kaons [80, 81]. Moreover some models take into account the possible presence of deconfined quarks in Compact stars [82–84].

2.2 Hydrostatic Equilibrium

The equilibrium configuration of stars is determinated by the equilibrium between gravitational pull and hydrostatic counteraction. An important mathematical result in the theory of stellar compact object is the derivation of the Tolman Oppenheimer Volkoff (TOV) equation, a differential equation that generalizes the hydrostatic equilibrium in General Relativity. The TOV equation allows us, for a given EoS to determine the equilibrium stellar configuration.

To derive the TOV equation we have to start from Eq. (1.1), adding two main ingredients. First of all let us derive the stress energy tensor $T^{\mu\nu}$, considering the source as a perfect fluid [15,16]. That means that the pressure is a function only of the energy density, so the stress energy tensor can be defined as:

$$T^{\mu\nu} = -p(r)g^{\mu\nu} + (p(r) + \rho(r))u^{\mu}u^{\nu}, \tag{2.1}$$

where we are indicating with $p(r)$ the pressure, with $\rho(r)$ the energy density, with $g^{\mu\nu}$ the metric tensor and with u^{μ} the velocity four-vector. To define the Einstein tensor (Eq. (1.1)) we consider the most general static spherical symmetric metric:

$$ds^2 = e^{2\Phi}dt^2 - e^{2\lambda}dr^2 - r^2 d\Omega^2, \tag{2.2}$$

with $d\Omega^2 = d\theta^2 + r^2 d\phi^2$, $\phi = \phi(r)$ and $\lambda = \lambda(r)$. The functions ϕ and λ depend on the radial distribution of matter. Following these hypotheses we can define the metric tensor as:

$$g_{\mu\nu} = \mathrm{diag}(-e^{2\phi}, e^{2\lambda}, r^2, r^2 \sin^2\vartheta), \tag{2.3}$$

thus the stress energy tensor becomes:

$$T_{\mu\nu} = \mathrm{diag}(-\rho e^{2\phi}, p e^{2\lambda}, p r^2, p r^2 \sin^2\vartheta). \tag{2.4}$$

From the energy momentum conservation, using Bianchi identity, we obtain the equation of hydrostatic equilibrium in General relativity:

$$\frac{1}{p+\rho}\frac{dp}{dr} = -\frac{d\phi}{dr}. \tag{2.5}$$

Furthermore, let us derive the time and radial components of the Einstein Equation (1.1):

$$G_{00} = \frac{e^{2\phi}}{r^2}\big(1 - e^{-2\phi}(1 - 2r\lambda')\big), \tag{2.6}$$

$$G_{11} = \frac{e^{2\lambda}}{r^2}\big(-1 + e^{-2\lambda}(1 + 2r\phi')\big), \tag{2.7}$$

for details on the derivation, see for instance [5–8]. Defining $m(r)$ as the stellar gravitational mass inside a radius r, from Eq.(2.7) we obtain:

$$e^{-2\lambda} = 1 - 2\frac{m(r)}{r}, \tag{2.8}$$

$$\frac{dm}{dr} = 4\pi\rho r^2. \tag{2.9}$$

Using the equation of hydrostatic equilibrium in the radial component of the Einstein equation, we obtain the TOV equation:

$$\frac{dp}{dr} = -\frac{\rho m}{r^2}\left(1+\frac{p}{\rho}\right)\left(1+\frac{4\pi P r^3}{m}\right)\left(1-\frac{2Gm}{r}\right), \tag{2.10}$$

which is a relation between energy density and pressure in the stellar interior.

For a given EoS, $p(\rho)$ it is possible to solve the closed system formed by Eq. (2.9) and Eq. (2.10). From Eq. (2.9) it is possible to obtain the total mass of the star integrating it up to the stellar radius, i.e. the radius at which pressure vanishes. It is important to note that TOV equation have been derived for a static, spherical symmetric metric. Assuming the total mass of the star M, Eq.(2.9) must match at the surface of the star the Schwarzschild solution, i.e. the spherical symmetric solution of Einstein equation.

To solve the system formed by Eq. (2.9) and Eq. (2.10) we must impose two boundary conditions. Both boundary conditions are given at the center of the star. We define the central density of the star, generally of the order of $\rho_c \sim 10^{15} g/cm^3$ and we impose a zero gravitational mass, $M(r)_{r=0} = 0$. Solving this system we find a family of solutions depending on the central density. This family gives us a unique relation between radius and mass of the star and this relation could be used for comparison with astrophysical observations and to obtain some constraint on the properties of hadronic matter. See for more details [1–3, 50, 51].

2.3 The EoS of Nuclear Matter

NSs are supposed to be "cold", that is the temperature of the system is much less than the chemical potential. Infact, in NSs the chemical potential of nucleons is much bigger than the nucleon mass $\mu_n, \mu_p >> m_N$ (where $m_N \sim 1GeV$), while NS typical temperature is some orders of magnitude smaller ($T \sim 1 - 100\, keV$). In general, the equilibrium configuration will depend on the matter content and is mainly produced by highly degenerate fermions. This implies that we have to provide a functional relation of the

type $p = f(\rho, T)$ where $f(\rho, T)$ is the EoS. However, due to the negligible temperature, we can assume that $T = 0$ obtaining a barotropic EoS:

$$p = f(\rho). \tag{2.11}$$

This relation implies that irrespective of any effect of gravity, the pressure and the matter density are functionally related.

The EoS of the NS crust is based on reliable experimental data on atomic nuclei, on nucleon scattering and on the well elaborated theory of strongly coupled Coulomb systems [2, 70]. By contrast, for $\rho > \rho_S$ the EoS should be extrapolated from available empirical information because matter at such high density is neutron rich and cannot be reproduced in laboratory. To describe the high density range various approaches have been developed: for instance the Brueckner-Bethe-Goldstone perturbative expansion of strong interaction [85–91] and the Green's functional theories [90,92–94]. For detailed review on nuclear EoS calculation see [95]. However, no exact calculation have been performed yet and the reliability of these theoretical models decreases with growing ρ.

In general, the EoSs can be subdivided into soft, moderate and stiff. The rigidity of an EoS depends on the adiabatic compressibility of matter:

$$k = \rho\left(\frac{\partial p}{\partial \rho}\right)_s, \tag{2.12}$$

where the suffix s indicates that the partial derivative is made at constant entropy. The range of maximum masses varies from $M_{max} \sim 1.4\,M_\odot$ for softest EOSs to $M_{max} \sim 2.5 M_\odot$ for the stiffest EoS. The stiffness of an EoS is related to the increase of pressure for a given density. The stiffest is the EoS the biggest is the pressure and thus, the more is the support against gravity, meaning that the stiffest is the EoS the bigger is the maximum mass.

Very stiff EoS can possibly be attributed only to nucleon matter [2]. At very high density, fermions in nuclear matter fill their Fermi spheres and the degeneracy pressure could produce a stiff EoS. However, whether different particles could start to being produced the degeneracy pressure drop down. The presence of Hyperons or bosons considerably softens the EoS. Indeed populating NS core with Hyperons, leads to the hyperon puzzle: pressure contribution falls down and typically the maximum mass is less than $2\,M_\odot$. Despite populate the NS cores with hyperons seems natural, the resulting EoS contradicts the observation of very massive NSs.

A review of the most important EoS can be found in [96, 97]. In Figure 2.3 we show the results obtained comparing different EoSs. One EoS widely used in this thesis is the SLy EoS [98] a moderately stiff EoS constructed by Douchin and Haensel. This EoS is based on the Skyrme effective

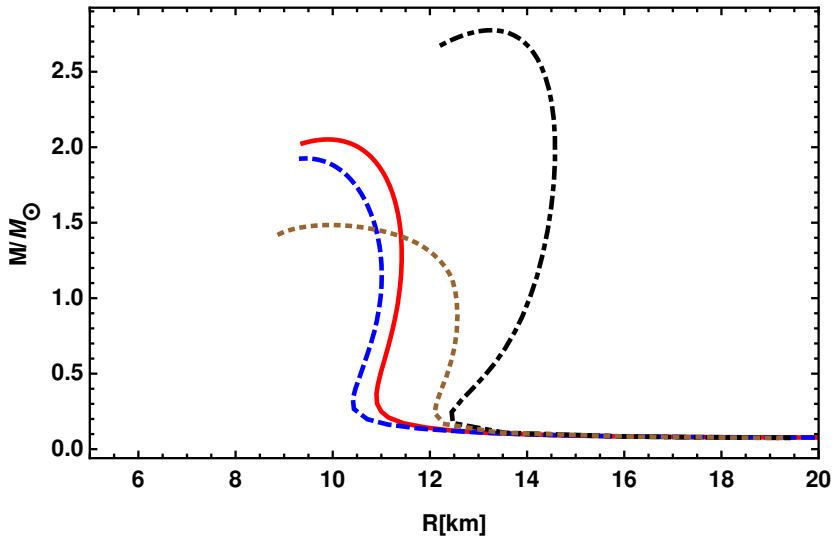

Figure 2.3: MR diagram for different EoSs. In Figure we show the solution of SLy EoS [98] (solid red line), the BBB EoS [99] (dashed blue line), the MS1 EoS [100] (dot dashed black line) and the pcl1 EoS [101] (dotted brown line). The pcl1 EoS is constructed assuming the presence of quarks and Hyperons in the core

nucleon-nucleon interaction and it has two important properties: it is a reliable EoS from $\rho \sim 10^8 g/cm^3$ down to the center, i.e. it is a unified crust-core EoS and it has a maximum mass of $2.05\, M_\odot$ in accordance with the recent observations.

Another possible approach to define an EoS of Nuclear Matter is to use polytropes. A polytrope is a simple law that relates the pressure and the energy density via the adiabatic index:

$$p = K\rho^\Gamma, \tag{2.13}$$

where K is a constant and Γ is the adiabatic index. The adiabatic index strongly depends on the system, see Table 2.1.

Γ	Described System
5/3	Non relativistic Fermi gas
4/3	Relativistic Fermi gas
1	Ultra Relativistic Fermi gas
2	Neutron Star central region
$\to \infty$	Homogeneous star

Table 2.1: Typical values of adiabatic index for different system.

In principle it is possible to describe any complicated EoS joining several polytropes. For instance we show in Figure 2.4 the results obtained joining two polytropes, the first describing the central part of the star and the second the external crust. Choosing $\Gamma_1 = 3$ for the central part (i.e. a stiff EoS) and $\Gamma_2 = 4/3$ for the external part, we join the polytropes at:

$$\rho_t = \rho_s/t, \tag{2.14}$$

where ρ_t is the transition density and t is a parameter. To determine the constants we use that pressure and saturation density are known. We set the constant K_1 as:

$$K_1 = \frac{p_s}{\rho_s^3}, \tag{2.15}$$

while imposing the continuity of pressure and density we obtain:

$$K_2 = K_1 \rho_t^{\Gamma_1 - \Gamma_2}. \tag{2.16}$$

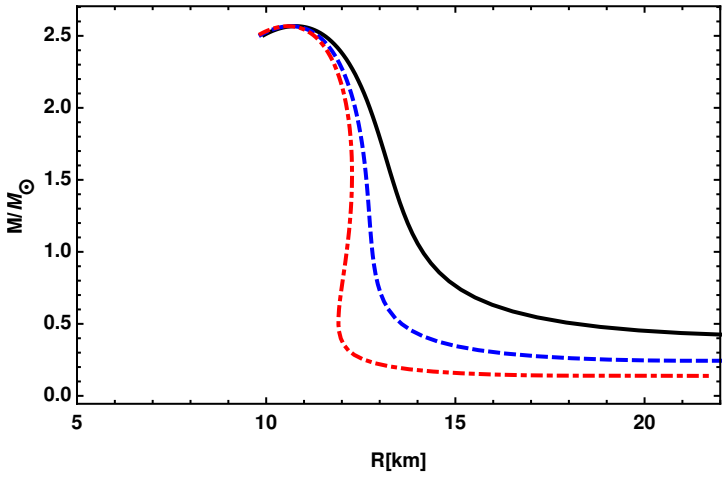

Figure 2.4: Mass-radius diagram for star described by two polytropes with $\Gamma = 3$ for the inner part and $\Gamma = 4/3$ for the crust. The curves are obtained joining the polytropes at different transition pressure. Polytropes are joined at $p_t = p_s$ (solid black line), $p_t = p_s/2$ (dashed blue line), $p_t = p_s/4$, (dotdashed red line).

2.4 Quark Stars

Two main aspects of neutron matter represent a challenge to our understanding of the strong interaction. The first aspect is that nuclei in terrestrial elements are almost isospin symmetric meaning that the majority of nuclei have

(almost) the same number of protons and neutrons. Conversely, neutrons are the dominant component of nuclear matter inside a NS. The second is that densities in the core are of the order of tens ρ_S. These two aspects imply that the extrapolated models for nuclear interaction, as already said, are far to be reliable. Furthermore, remembering that the baryon density n_b at ρ_s is $n_b \simeq 0.16$ baryons/fm^3, at tens of ρ_s the volume per particles is less than 1 fm^3 and the nucleons could overlap. However overlapping of nuclei is not energetically favored because of the Pauli exclusion principle and the short range strongly repulsive nuclear potential. One of the possible solutions of this puzzle is the presence in a Compact Object of deconfined quarks.

We do not know whether at the densities reachable in a CS the quark content of nucleons can be liberated [102]. We have some information from accelerators experiment in which the quarks form the so called Quark Gluon Plasma [103–105]. Quark Gluon Plasma is a state of hot matter in which the quarks are deconfined. However, this state of matter is produced in relativistic heavy ion collision and the data cannot be used because of the lower typical temperature of CSs. In accelerators the typical energy scale is the strong interaction scale, $\Lambda_{QCD} \sim 200MeV$, that is at least three order of magnitude bigger than the typical temperature of compact objects. Furthermore, we mention that the numerical simulation of QCD in lattice QCD simulation have not been developed at such large baryonic density [106, 107].

2.4.1 Overview on Quantum Chromodynamics

The field theory of the strong interaction is the Quantum Chromodynamics (QCD). The gauge group of QCD is $SU(3)_c$, where the suffix c stands for color, and it is a non-Abelian quantum field theory [108–110]. The only particles that have non vanishing color charge are quarks and gluons. However, gluons are the mediators of strong interaction meaning that due to the non vanishing color charge they are self-interacting.

Quark Flavour	Electric Charge	Mass (MeV)
u	$2/3$	~ 2
d	$-1/3$	~ 5
s	$-1/3$	~ 100

Table 2.2: Light quarks' electric charge and masses.

What we know from observation of nature is that no color charged particles can be observed. All the particles that contains quarks and gluons, i.e. mesons and baryons, are in a color singlet state. This phenomenon called

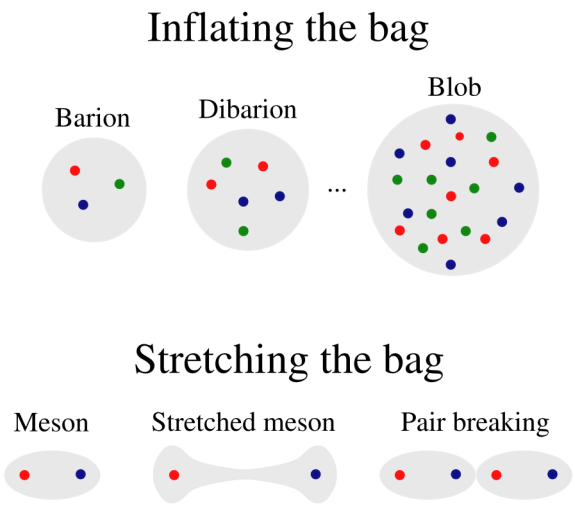

Figure 2.5: Cartoon of the MIT bag model. Inside the bag the quarks are almost free particles. However when one tries to separate the color charges, the pair production is favored and two mesons are finally created.

confinement is not well explained in standard model. However it is possible to describe the confinement through a phenomenological model: the MIT bag model [111, 112]. The bag, following this model, is a colorless zone in which quarks are almost free to move. The bag exerts a surface tension that acts as a negative pressure on the system. As one tries to separate two color charges, one stretches the bag that contains the quarks, which then breaks at least in two hadrons see Figure 2.5.

The other important characteristic of QCD can be explained making an analogy with electromagnetism. It is well known that the electromagnetic potential between two point charges in a dielectric medium is:

$$V_{QED}(r) = \frac{e^2}{4\pi\varepsilon r}, \tag{2.17}$$

where $\varepsilon > 1$ is the polarizability of the medium. The medium, in the case of electromagnetic field, screen the potential owing a reduction of the effective interaction. Making an analogy with QCD properties, let assume that we can define a potential:

$$V_{QCD} = \frac{q^2}{4\pi\varepsilon_s r}, \tag{2.18}$$

where where q is a charge associated with the strong interaction and ε_s is the analogue of the polarizability for strong interaction. In this case, the

behavior is the opposite respect to electromagnetism: deep inside an hadron the quarks behave like free particles meaning that $\varepsilon_s = 1$, i.e. the theory is *asymptotically free*, meanwhile at large distance the interactions becomes extremely strong, i.e. $\varepsilon_s \to 0$.

2.4.2 Quark Matter EoS

Due to their fermion nature, inside the Bag quarks are forced to occupy different energy levels, filling their Fermi spheres. In CSs the chemical potential of the light quarks (u and d) are much greater then the masses, but for the s quark the chemical potential and the mass are of the same order. That means that imposing the charge neutrality of the whole system, a large number of electrons are present in the star's interiors.

Let us consider a simplified model of quark matter assuming quarks as non interacting particles. The chemical equilibrium is guaranteed by the week processes:

$$\begin{aligned} u + e &\to d + \nu_e, \\ d &\to u + e + \bar{\nu_e}, \\ s &\to u + e + \nu_e, \\ u + e &\to s + \nu_e, \\ s + u &\leftrightarrow d + u. \end{aligned}$$

Since the neutrino chemical potential is zero (neutrino are not trapped), from the above processes we obtain the quark's chemical potential:

$$\mu_u = \mu - \frac{2}{3}\mu_e, \quad \mu_d = \mu + \frac{1}{3}\mu_e, \quad \mu_s = \mu + \frac{1}{3}\mu_e, \tag{2.19}$$

where μ is the mean quark chemical potential. Using the non vanishing mass of s quark, the Fermi momenta of the quarks are:

$$p_{F,u} = \mu_u, \quad p_{F,d} = \mu_d, \quad p_{F,s} = \sqrt{\mu_s^2 - m_s^2}. \tag{2.20}$$

From the last relations follows that the energy density ρ and the pressure p can be defined as [113]:

$$\sum_{i=u,d,s,e} \rho_i = \frac{3}{4\pi^2}(\mu_u^4 + \mu_d^4 + \mu_e^4) + \frac{3}{\pi^2}\int_0^{p_{F,s}} dp\, p^2\sqrt{p^2 - \mu_s^2}, \tag{2.21}$$

$$\sum_{i=u,d,s,e} P_i = \frac{1}{12\pi^2}(3\mu_u^4 + 3\mu_d^4 + \mu_e^4) + \frac{3}{\pi^2}\int_0^{p_{F,s}} dp\, p^2(\mu_s - \sqrt{p^2 - \mu_s^2}). \tag{2.22}$$

The electric charge neutrality of the system implies that:

$$0 = \frac{\partial}{\partial \mu_e} \sum_{i=u,d,s,e} P_i = -\frac{2}{3} n_u + \frac{1}{3} n_d + \frac{1}{3} n_s + n_e, \tag{2.23}$$

and expanding to the first order in the strange quark mass, we obtain:

$$\mu_e \simeq \frac{m_s^2}{4\mu},$$
$$p_{F,u} \simeq \mu - \frac{m_s^2}{6\mu},$$
$$p_{F,d} \simeq \mu + \frac{m_s^2}{12\mu},$$
$$p_{F,s} \simeq \mu - \frac{5m_s^2}{12\mu}.$$

Using the previous relation in the Eqs.(2.21) e (2.22) we obtain the EoS:

$$P \simeq \frac{3}{4\pi^2}\mu^4 - \frac{3m_s^2}{4\pi^2}\mu^2 - B. \tag{2.24}$$

where B is called the Bag constant. This equation of state have been derived neglecting the interactions. Including the interaction between quarks, it is possible to define an EoS for the strange quark matter [114]:

$$P \simeq \frac{3a_4}{4\pi^2}\mu^4 - \frac{3a_2}{4\pi^2}\mu^2 - B_{eff}. \tag{2.25}$$

The terms a_4 and a_2 in the Eq.(2.25) are two coefficients that do not depend on the quark chemical potential, and B_{eff} is a modified bag constant. The idea is that it is possible to describe with these three parameters the interaction between quarks. Perturbative calculations gives typical values for the parameters: $a_4 \simeq 0.7$ and $a_2 \simeq m_s^2 - 4\Delta$ where Δ is the energy gap associated to Cooper pairs of quarks. Quark matter at densities typical of CS is supposed to be in color superconducting phase. Several color superconducting phase have been proposed, see for instance [116–121].

Using this EoS it is possible to study the solution of TOV equation for stars with or made of deconfined quarks. Two theoretical model have been proposed: *Hybrid stars* and *Strange Stars*.

2.5 Hybrid Stars

Hybrid stars are CSs with a core formed of deconfined quark matter, see Figure 2.2. It is assumed that when the central density of a CS reaches

$\rho \simeq 2-3\,\rho_s$ there is a transition from standard nuclear matter to deconfined quark matter. The onion structure of Hybrid stars is similar to those of NS: the external layers are the same, then there is a coexistence phase and lastly a phase made of quarks and electrons.

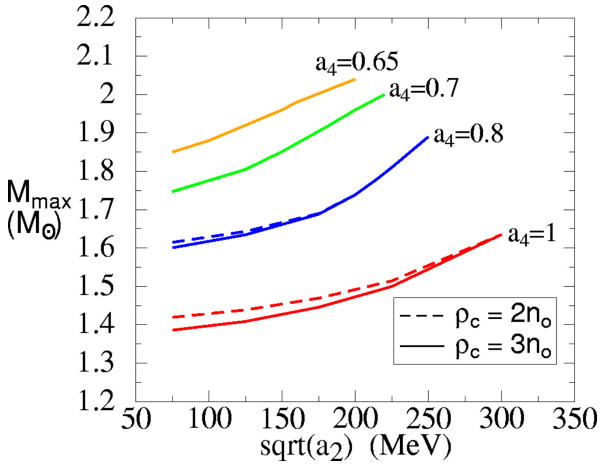

Figure 2.6: Maximum mass for a hybrid star model. The model is built assuming the APR nuclear EoS [115] and quark matter described by the EoS in Eq. (2.25). Figure taken from [114]

In general the presence of a quark phase softens the EoS of matter, so the observed maximum mass of a CS could be not reachable. However as shown in [114] the maximum mass for an Hybrid stars depends strongly on the parameters of the EoS. Using the Eq.(2.25) it is possible to study the effects of the parameters on maximum mass. Choosing B_{eff} in way to obtain a continuous transition between quark matter and nuclear matter for $\rho_t = 2\rho_s$ (solid lines in Figure 2.6) and for $\rho_t = 3\rho_s$ (dashed lines in Figure 2.6) we obtain the maximum mass as a function of the values of $\sqrt{a_2}$ and a_4. As can be seen from Figure 2.6, it is possible to obtain configurations with mass higher than $2M_\odot$ reproducing the experimental observations with an accurate choice of parameters.

There are two main scenarios for the formation of hybrid stars. The first scenario is that the conversion between nuclear matter and quark matter is an adiabatic phenomenon. This hypothesis implies that at certain densities the nuclear matter is so squeezed that the neutrons lost their identity and quarks degrees of freedom are liberated. The second possibility is that NS and hybrid stars are in different branches, i.e. NSs can be metastable stars. NSs could eventually turn into hybrid stars by an abrupt first order phase transition. The transition from one type of star to the other should be accompanied by a shrinking of the star and thus by the liberation of a huge amount

of energy eventually released by photons and neutrinos. This phenomenon could be associated to some astrophysical observations but, at present, no astrophysical evidence has been found.

2.6 Strange Stars

The existence of Strange Stars (SSs) is based on the hypothesis of Bodmer [122] and Witten [123] that standard nuclei are in a metastable state. According to this hypothesis, the real ground state of hadronic matter is a configuration that corresponds to an hypothetical short range free-energy minimum of the strong interaction. This configuration is a *collapsed state* of matter and thus we can imagine a strange star as a huge collapsed hadron. In the collapsed phase u, d, and s quarks are deconfined and a small fraction of electrons is present to guarantee the charge neutrality [124–127].

The interaction that binds the star is the strong interaction, i.e. SS is a self bound object. Gravity plays a role only for very massive stars. A characteristic of Self-Bound object is that SS mass can be arbitrarily small. More in detail with increasing baryon number A the size of the star grows as $R \sim A^{1/3}$. Looking at Figure 2.7, it is possible to see the different behavior of SSs (green dashed curve) from hybrid and NS.

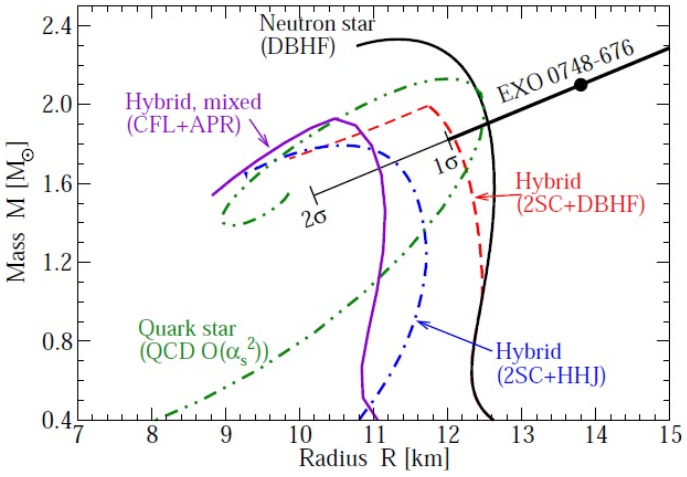

Figure 2.7: MR relations for different EoSs. Figure taken from [128]. In violet it is shown an Hybrid Star model with a the phenomenological EoS for quark matter joined with the APR EoS for the external layers. In blue and red two Hybrid Stars model with different EoSs both for quark matter and for Nuclear Matter. In black a NS with the EoS obtained using the Dirac-Brueckner-Hartree-Fock theory. In green a Strange star with EoS calculated utilizing a perturbative model of QCD. For more information on these EoSs see [128]

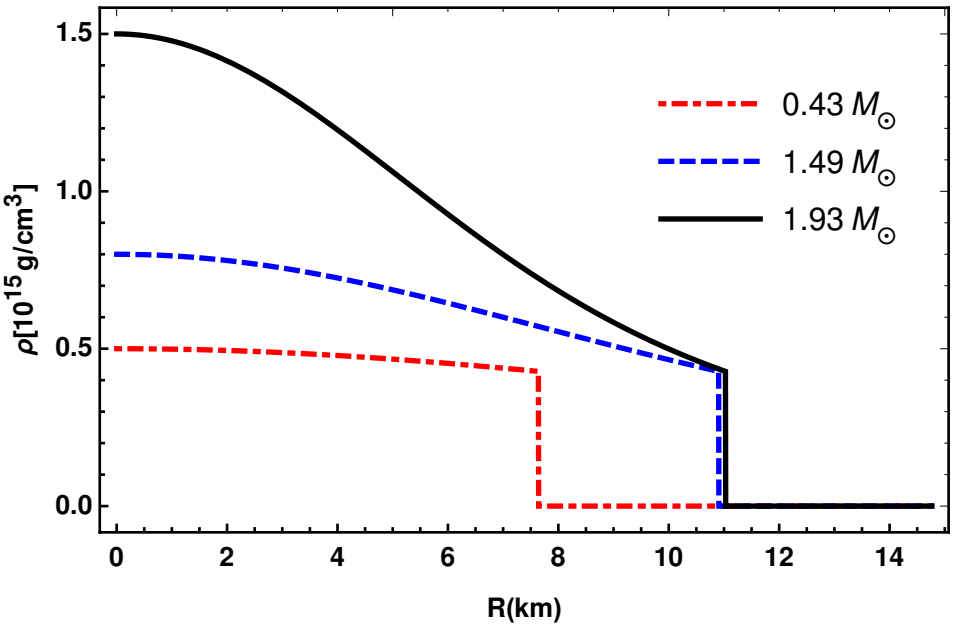

Figure 2.8: Typical density profiles for bare strange stars. Despite the sharp boundary, it is possible to note that density varies slowly inside the star. Even in the more massive case, solid black line, density varies less then one magnitude order inside a star with radius of about 10 km.

Another intriguing aspect of SSs is the surface behavior. To better understand the features of the surface let us define a simple EoS:

$$P = c_s^2(\rho - 4B) \tag{2.26}$$

where c_s is the speed of sound. This EoS corresponds to the simplest version of the MIT bag model [129]. Remembering that the surface of a star has a vanishing pressure, the energy density at the surface is: $\rho_{surf} = 4B$. The non vanishing surface density implies that the energy density abruptly changes on the typical distance of the strong interaction, i.e. 1 fm. In Figure 2.8 some typical energy density profiles of bare strange stars are shown.

From Figure 2.8 it is possible to note that in the inner layers of a SS the energy density varies less than one order of magnitude. This feature is typical of SSs. The region of the star in which quarks are confined by the Bag is called the *Quark Sphere*. Electrons are not bounded by the strong interaction so they can escape from the Quark Sphere. However, to guarantee the total charge neutrality of the star, electrons are distribuited outside the Quark Sphere in a layer of few hundreds of Fermi [124, 130]. This region is called *Electrosphere*. As a result, the quark sphere has a positive net charge. In fact into the Quark sphere, the number of strange quark is less than the other

flavors due to the non vanishing strange mass. The distribution of electrons and the positive charge of Quark Sphere generates a dipolar potential that has been estimated as $V \sim 5 \times 10^{17} V/cm$ [130].

Remarkably a SS could have a thin crust made of nuclear matter [131]. It should be suspended on the top of the Electrosphere by the dipole potential: the ions when approaches this potential are repelled. Furthermore the crust has the maximum density equal to neutron drip, because neutrons do not interact with the dipole field and so they could fall into the quark sphere and eventually being transformed. This could give upper limit on the nuclear crust. It is possible to demonstrate that for stars with $M > 1.7 M_{\odot}$ the ionic crust has a thickness of about 300 m and a mass of about $1.7 \times 10^{-5} M_{\odot}$ [2].

Chapter 3

Gravitational Wave Echoes from Compact Stars

The first prediction of the existence of gravitational radiation was made by Einstein, when he saw that the linearized weak-field equations admit solutions in form of waves traveling at the speed of light [132]. Several indirect detections of Gravitational Waves (GWs) were made studying their effect on the timing of pulsars in binary systems [132–136]. In 2015, one century after the publication of Einstein field equation [137], the first GW signal was directly observed by the LIGO-VIRGO Collaborations [138–140]. The Event was denoted as GW150914 and it was due to the coalescence of a Black Holes (BH) binary system. The waveform observed in GW150914 matches the one predicted from General Relativity [141–143], providing an important proof on the validity of the theory. Three further observation of BHs binary system coalescence have been done in the following years [144–146]. At the time of writing the present thesis about 10 BH binary system have been observed, see GWTC-1 catalog.

In 17th of August 2017 the LIGO-VIRGO Collaboration announced the detection of GW signal, denoted as GW170817 [147]. This signal, originated at a luminosity distance of 40^{+8}_{-14} Mpc, has a chirp mass:

$$\mathcal{M} = (m_1 m_2)^{3/5}/M^{1/5} = 1.188^{+0.004}_{-0.002} M_\odot, \tag{3.1}$$

where m_1 and m_2 are the masses of the binary merging objects and M is the total mass of the system. The chirp mass is a parameter that determines the orbital evolution of the system. It is related to the energy loss from the emission of GWs during the inspiral phase and it determines the frequency of the emitted GWs. From the Eq. (3.1) it is possible to extract the total estimated mass. The total mass is in the range $M = (2.73 - 3.29)M_\odot$ and the lowest value $M = 2.73 M_\odot$ corresponds to equal-mass components case:

$m_1 = m_2 = 1.365 M_\odot$. The GW170817 is consistent, for the first time, with a merging of NSs.

As expected from theoretical models [148–152], the GW170817 event has been associated with a short gamma ray burst (sGRB) observed on the Fermi satellite [153, 154]. Moreover after few hours an optical -infrared-ultraviolet astrophysical transient, associated to a "kilonova", have been observed [155–158]. Even though the electromagnetic counterparts are very interesting and GW170817 is a breakthrough in Multimessanger Astronomy, in this Chapter we focus on the GW signal, in particular on the possibility and on the consequence of the presence of GW echo. For more details on Electromagnetic counterpart see for instance [153–158].

The possibility that the merging of compact stars can lead to the emission of GW echoes have been investigated by several authors [188, 194, 195], but it remains a controversial topic, see for instance [159, 160]. The mechanism of the GW echoes relies on the existence of a very massive post-merger object leading to partial GWs trapping [161, 162]. However, the emission of GW echoes from BHs require a second reflection surface to avoid the GWs' absorption. This surface is related to to quantum effects close to the BH horizon, see for instance [165]. As discussed in [166], GW echoes can also be produced by ultracompact stars and there is no need of an internal reflection surface because, unlike BHs, an ultracompact star is not capable of absorbing a sizable fraction of GWs. In the following section we will discuss how the trapping of GWs is possible.

3.1 Theoretical aspects on GW Echoes

The perturbation of the metric tensor produce small fluctuation of both metric function and fluid variables. It is possible to study the dynamics of this fluctuations coupling Einstein's equation with hydrodynamical equation and conservation of baryon number. Expanding the perturbed equation in spherical harmonics two different modes are recognizable: polar and axial modes (modes with even and odd parity, respectively). However, BHs and CSs presents different features in these perturbations. For BHs polar and axial perturbation are isospectral while for non rotating CSs polar modes describe hydrodynamical perturbations and axial modes spacetime perturbations [170, 177–179]. In this context we focus on the spacetime perturbations of CSs, so we shall focus on axial modes. The first approach to spacetime modes, studied in GR is due to Kokkotas and Schutz in [175]. They developed a very simple toy model [175] founding that the spacetime modes are fastly damping [174]. This new family of modes, denoted as *w-mode* [176],

was found to have high frequencies (on the order of tens KHz) and fast damping time. This damping time decrease both with the order of the mode and with the compactness:

$$C = \frac{M}{R} \tag{3.2}$$

of the star [174].

A very interesting feature of w-modes is their possibility of be trapped [174]. Trapping modes are present when the compactness of the star is higher than 1/3. Objects that have a compactness $C \geq 1/3$ feature a *Photon sphere*, i.e. a region of the space in which circular orbit of photons and GWs are possible. The bound of Photon Sphere is located at $R = 3M$, where M is in unit of Scharzschild's radius. Thus, Photon Sphere is featured both by BHs [3] and by ultracompact stars [163, 164]. For instance, BHs (the most compact objects known) have a compactness $C = 1/2$ and the BH's Photon Sphere is responsible of the BH's shadow, the luminous region in Figure (3.1).

Figure 3.1: First photography of a BH captureb by Event Horizons Collaborations. Figure taken by https://eventhorizontelescope.org

Different kind of objects present a Photon Sphere, for example stars with compactness between $1/3 \leq C \leq 4/9$. The limit $C = 4/9$ is the fundamental *Buchdal's Limit* [180]. To understand the importance of Buchdal's Limit, let us to derive an analytical solution of the TOV equation at constant energy density. In this case integrating the Eq. (2.9), we obtain:

$$m(R) = 4/3\pi\rho R^3, \tag{3.3}$$

and integrating the Eq. (2.10) we obtain [5]:

$$p = \rho \frac{\sqrt{1-2Mr^2/R^3} - \sqrt{1-2M/R}}{3\sqrt{1-2M/R} - \sqrt{1-2Mr^2/R^3}}. \tag{3.4}$$

Taking $r = 0$ it is easy to show the relation between central pressure and energy density:

$$\frac{p_c}{\rho} = \frac{1 - \sqrt{1 - 2M/R}}{3\sqrt{1 - 2M/R} - 1}. \tag{3.5}$$

A star that reaches the Buchdal limit is a star whose central pressure diverges. Moreover, at the Buchdahl's limit, also the gravitational potential is not well defined, indeed for $M/R > 4/9$ the potential becomes imaginary at small values of r. This signals that the system is becoming unstable before reaching the Schwarzschild radius $R = M/2$. So Buchdahl's limit gives us the maximum compact configuration for an ultracompact star. However, there are more exotic objects with compactness $1/2 < C < 4/9$, the so called BH-mimick. The BH-mimick include object like gravstars [181, 182], Lorentzian wormholes [183], matter-bumpy BHs [184, 185], Kerr-like wormoholes [186] and Fuzzballs [187]. All this objects present a Photon-sphere, and trapped w-mode can be observed as GW echoes. Anyway the existence of these compact objects remains controversial.

The trapping of w-modes inside a star with compactness $C > 1/3$ is due to an angular potential barrier. For axial modes it is possible to define an effective potential [169, 170]:

$$V_{eff}(r) = e^{\nu(r)}\left[\frac{l(l+1)}{r^2} - \frac{6m(r)}{r^3} - 4\pi(P - \rho)\right], \tag{3.6}$$

that, as discussed for instance in [5, 169, 170], in the case of $s = l = 1$ corresponding to the case of massless photons, has a maximum at $r \simeq 3M$. The Photosphere represent the unstable circular null geodesic and has actually the same position for BHs and for CSs . However the potentials for BHs and for ultracompact stars differs significantly, see Figure 3.2 [169], where the effective radial potential in Eq. (3.6) is shown as a function of the tortoise coordinate:

$$z = r + 2M\log\left(\frac{r}{2M} - 1\right). \tag{3.7}$$

The BH effective potential vanishes at the horizons that corresponds to $z \to -\infty$ while the potential of a ultracompact star diverges at $r = 0$ because of the centrifugal term $l(l+1)/r^2$ [169, 170]. That means that effective potential of ultracompact stars behave like a potential well and gravitational and electromagnetic waves can be trapped. Following [169, 170], it is possible to describe the null geodesic as a Schröedinger-like equation [169, 170]:

$$\frac{d^2\psi}{dz^2} + (\omega^2 - V_{eff})\psi = 0. \tag{3.8}$$

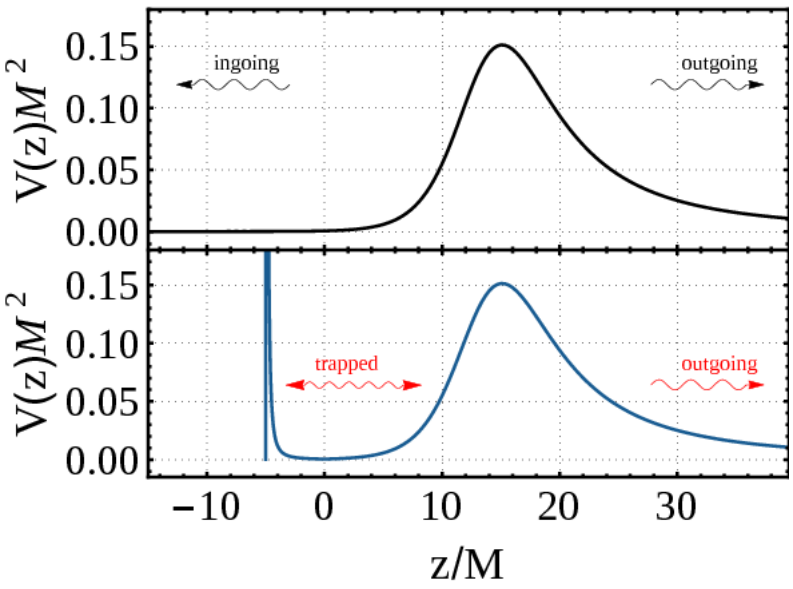

Figure 3.2: Effective potential for spacetime perturbations in function of tortoise coordinate (see Eq. 3.7) over the total mass. On the top we show the effective potential for a Schwarzschild BH. The w-modes propagates outgoing ($z \to \infty$) and ingoing ($z \to \infty$). For the generation of GW echo from BHs, a second reflective surface is needed close to horizons. On the bottom we show the effective potential for an ultracompact object. At the center of the star the centrifugal term of the the effective potential diverges. Thus, a ultracompact star support the quasi-trapped, long-lived modes, because the effective potential behaves like a potential well. Figure taken from [169].

where ψ is the wavefunction associated to the null geodesic motion. This equation must be solved by imposing the right boundary condition. It is simple to show that imposing $M = l = 0$, Eq. (3.8) is the wave equation governing a string [169]. Imposing Dirichlet boundary condition one finds that $\omega = n\pi/L$, where L is the thick of the cavity, i.e. in the case of ultracompact star is the stellar radius. This is actually the frequency of the w-mode standing wave as defined in [174]. In the case of BHs or BHs mimick the situations is slightly different. Infact, as it is possible to see from Figure 3.2 the partial trapping of GW and photons is possible if a second reflective surface located near the BH's horizon and related to quantum effects, is present (see for instance [165]).

One may indeed conceive the photon sphere as a trap for GWs, with characteristic frequencies on the order of the inverse of the length scale of the trap. Thus, the smaller the trap, i.e., the closer the stellar solution to the photon-sphere line, the larger the GW echo frequency. The typical echo time can be evaluated as the light time from the center of the star to the photon sphere, see [209], corresponding to:

$$\tau_{echo} = \int_0^{3M} \frac{dr}{\sqrt{e^{2\phi}(1 - \frac{2m(r)}{r})}}. \tag{3.9}$$

From the calculation of the typical echo time, GW echo frequency can be approximated by $\omega_{echo} = \pi/\tau_{echo}$. The argument underlying this approximation is that the echo frequency corresponds to that of standing waves inside the photon sphere, see for example the discussion in [174, 213]. Thus, it is assumed that during the merger of the NSs these modes are excited and partially trapped inside the photon sphere. After some time, they leak outside with approximately the same frequency of the standing waves. The frequency of the GW echo is therefore determined by the eigenmodes of the photon-sphere trap, and is not related to the frequency of the GW emission during the inspiral.

3.2 GW Echo observation

Several tentative evidence of repeating GW echoes have been found in LIGO/VIRGO observation of BH merger [188–190]. However, the significance of these observation is low, and the origin of this signal remains controversial [190, 191, 194, 195]. With the first observation of a Binary neutron star coalescence new tentative observations of GW echoes have been reported by Abedi in [195]. One particular aspect of this event is that the nature of

final object is unclear. Indeed, as told in [195], the final object of GW170817 event has a mass in the $2-3\,M_{\odot}$ range, so it could be a BH [192], an Hypermassive NS that in $\lesssim 1$ sec collapses into a BH [192], supramassive NS that collapses into a BH on timescale of $10-10^4$ seconds [192] or a stable NS (or SS) [147].

Abedi at al. developed a model-agnostic search of GW echo correlating the two detectors (Stanford and Livingstone), for more details see [195]. They estimate the time retardation of the GW echo as twice the tortoise coordinate distance between the photosphere and the BH membrane [195]:

$$\Delta t_{echo} = 8M\log M. \tag{3.10}$$

That means that, since the final mass of the binary merger is in the $2-3\,M_{\odot}$ range, the lowest frequency of the GW echo, defined as $f_{\rm echo} = 1/\Delta t_{\rm echo}$ ($\sim 80Hz$), is in the LIGO sensitivity and can be detected [195]. So they developed a model-agnostic strategy to find the lowest GW echoes harmonics [147, 195]. Furthermore, they estimated that in the merging process about the 5% of the energy is lost [193] constraining $\Delta t_{\rm echo}$ to be within [195]:

$$0.0109\,{\rm s} < \Delta t_{\rm echo} < 0.0159\,{\rm s}, \tag{3.11}$$

that corresponds to echo frequency of

$$63{\rm Hz} \leq f_{\rm echo} \leq 92{\rm Hz}. \tag{3.12}$$

After defining the lowest harmonic expected frequency, they search for a echo signal in the range $t - t_{merger} \leq 1$ sec. Furthermore, they obtained the amplitude spectral density, as discussed in [196], and they whitened the data, see for more details [195]. After the cross correlation of the resulting spectrograms (one from Livingston and the one from Hanford) they define the cross power spectrum $X(t,f)$, i.e. the Fourier transform of the cross correlation function, in function of time and frequency, see for more details [195].

The obtained results, in the postmerger spectrum, are shown in Figure 3.3 [195]. Abedi et al, claimed that a signal at $t - t_{\rm merger} \simeq 1.0$ sec after the merger and at $f_{\rm echo} \simeq 72$ Hz is present, green squares in Figure 3.3 [195]. They interpreted it as the evidence of the formation of an hypermassive NS that after 1 s collapses in a BH. The estimated significance is at $4.2\,\sigma$ that correspond to a false detection probability of 1.6×10^{-5}.

3.3 GW echo from Strange Stars

This section is based on our paper *Gravitational wave echoes from strange stars* [197], in which we examine the possibility that the ultracompact object

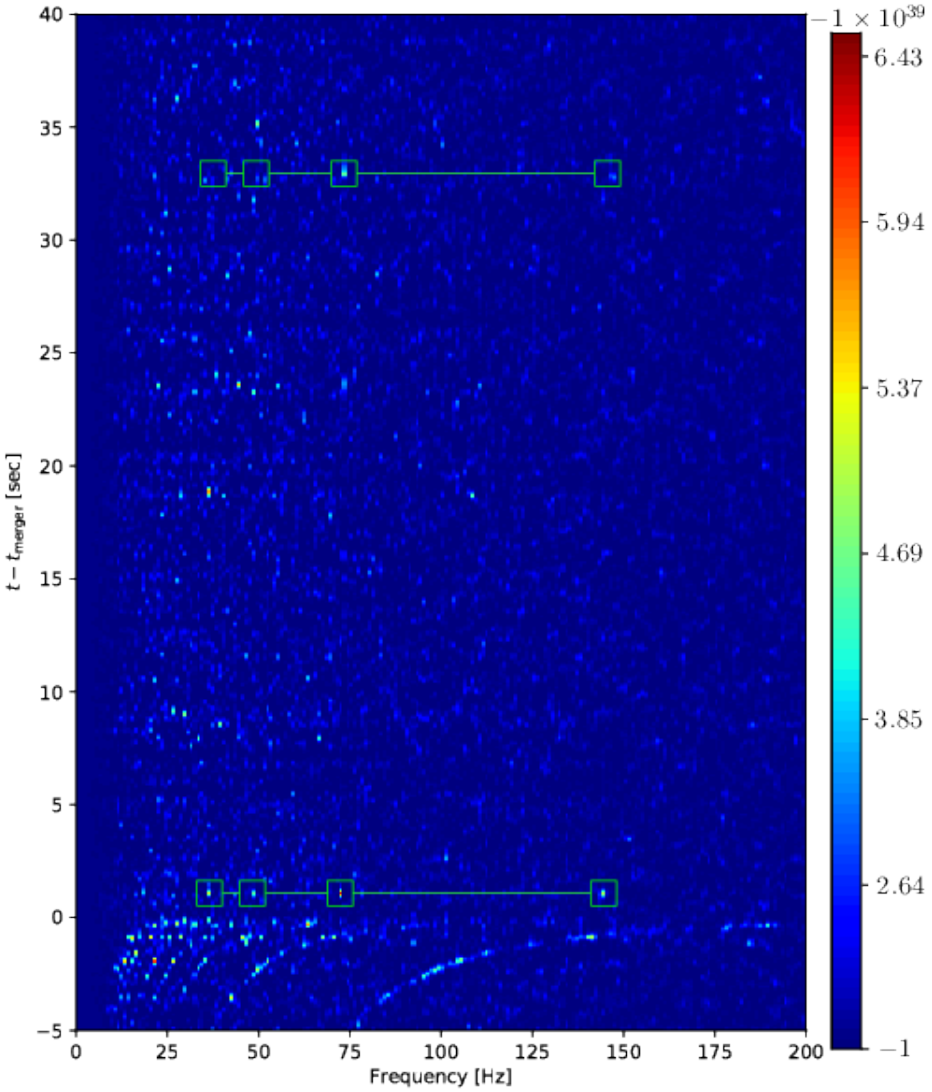

Figure 3.3: Time-frequency representation of $X(t, f)$ before and after the GW170817 event. In figure the possible peaks of echoes found are marked with green squares. Two tentative peaks have been found. The first one at $f_{peak} = 72 \pm 0.5$ Hz, 1 second after the merger. The second at the same frequency but 32.9 seconds after the merging [195]

produced during the GW170817 event is a SS, and we evaluate the frequency of GW echo. An interpretation of this echo signal from an ultracompact star was first proposed in [209]. This preliminar analysis, conducted by a simplified incompressible EoS, has shown that to produce a signal at such a low frequency, the stellar object formed in the coalescence of the NSs should be very compact, close to the Buchdal's limit. Thus the radius of this object shold be $R \simeq 9/4M$. However, as told before, this situation is unphysical because no stellar object can be so compact. Moreover, an incompressible EoS implies a diverging speed of sound. Since SSs are known to be very compact [2, 124], we studied whether SSs may have a photon sphere, approach the Buchdal's limit and eventually emit GW echo that reproduce the experimental result found in [195].

In the development of our model, different simplifying hypotheses have been done. First, we assume that the conversion of nuclear matter into quark matter happens by compression during the NS merging. This is justified by the analysis of GW170817 tidal deformability. Indeed both GW170817 tidal deformability by GW signals [147,198–200] and the electromagnetic counterpart observations [201] suggest that the EoS of the merging NSs cannot be too stiff (nor too soft),and from these analyses it follows that the merging stellar object can be two standard NSs or a NS and a hybrid star [202, 203]. The formation of a SS would certainly be accompained by a release of energy, as discussed in the framework of supernova explosions, see for instace [204–206], possibly affecting the gamma and neutrino emissions associated with the merging of NSs. The GW postmerger emission could also be different, but we are not aware of any simulation of merging of NSs leading to the formation of a SS. In this thesis we limit our analysis to the postmerger GW echo signal [197].

Furthermore we neglect both the effect of temperature and of stellar spinning, despite the SS is initially hot and presumably in a highly excited state, rotating at high frequency. Thus we consider a static configuration of cold quark matter, arguing that the effects of temperature and spin are negligible in this context, see below. However, it may be of interest that the excited SS could relax also emitting radio waves at kHz frequencies (or smaller) [130, 131, 207]

In principle, our study could lead to interesting information on quark matter EoS. For instance, whether the realization of the Bodmer and Witten hypothesis [122] that standard nuclei are not the ground state of matter is true. As argued before, the current astrophysical observation of masses and radii of NSs can in principle constrain the EoS of matter at suprasaturation densities. However, a strong constraint would only result from a simultaneous mass and radius observations which are difficult, meaning that at present

several different model of EoS can describe the known astrophysical data.

As told in the first chapter, the observation of NSs with gravitational mass $M \simeq 2M_\odot$ [52, 208] has challenged nuclear EoSs excluding too soft ones. If a compact star with an even larger mass, say of about $2.5M_\odot$ is the final stellar object resulting in the NSs merging associated with the GW170817 event, although compatible with extreme nuclear matter EoSs, it would certainly exclude a large number of models, possibly challenging the present understanding of core-collapse neutron star formation [50]. As we will see, requiring that this compact object emits GW echoes further constrains the model EoSs, excluding the known nuclear EoSs, as already shown in [163, 209], and constraining the quark matter EoS to be very stiff.

3.3.1 The Model

Our model is based on the stiffest EoS for quark matter, a simple bag model EoS as defined in Chapter 2, see Eq. (2.26):

$$\rho = p + 4B \tag{3.13}$$

where we set the speed of sound equal to 1 and we recall that p and ρ are the pressure and the energy density respectively. In Figure 3.4 we show the obtained mass-radius relation for two different values of the bag constant: $B_1 = (145\text{MeV}^4)$ (a typical bag model value) and $B_2 = (185\text{MeV}^4)$, corresponding to the curves SS1 and SS2, respectively. With this extreme EoS, the $M(R)$ curves cross the photon-sphere line $M = R/3$, but do not approach the Buchdahl's limit line. The reason is that for small masses and radii, the stellar mass is expected to grow as R^3, because strange quark matter is self-bound. Therefore, for small radii the $M(R)$ curve of SSs stands below the photon-sphere radius. It can only approach it when the $M(R)$ curve bends, which happens for sufficiently large masses. For large masses the gravitational pull helps to compress the structure, however it eventually leads to an unstable branch, when a central density increase leads to a gravitational mass reduction [3]. The last stable configurations, the ones with the largest masses, correspond to the tips of the $M(R)$ curves in the mass-radius diagram of Figure 3.4. These are as well the most compact stable configurations.

For the considered values of the bag constant we obtain maximum masses $M_{max} \approx 2M_\odot$, for SS2, and $M_{max} \approx 3.3M_\odot$ for SS1. Intermediate maximum masses can be obtained for values of the bag constant in the range $B_1 < B < B_2$, which can be easily inferred considering that the maximum mass scales as [123]:

$$M_{max} \propto B^{-1/2}. \tag{3.14}$$

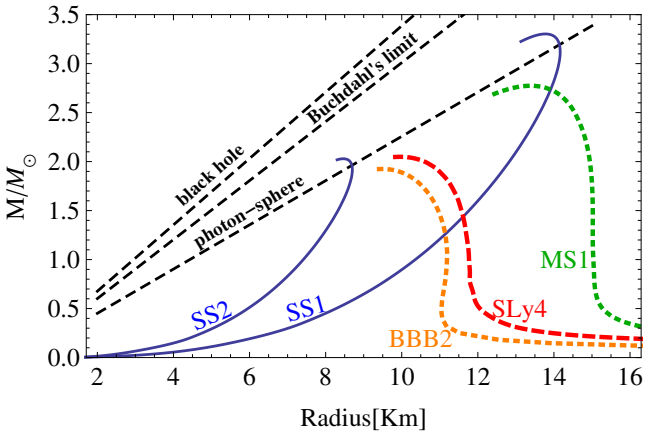

Figure 3.4: Mass-radius relations for different CS models. The emission of GW echo can only happen for those stellar models that cross the photon-sphere line. Standard NSs do not seem to be possible candidates. SS with a maximally stiff EoS are marginally compatible with this requirement.

Thus, for values of the bag constant in the above range, one spans maximum masses compatible with the $2M_\odot$ observations [52, 208] and the GW170817 estimated total mass of $2.7M_\odot$ [147]. To make clear how extreme these cases are, consider that the central baryonic densities of these SSs are about 25 times the nuclear saturation density. Actually, such extreme values of the baryonic densities are in agreement with the results obtained by simple models of NS collapse [210] and by numerical simulations including rotation, see for example [211, 212]. In these works, polytropic EoSs are used to mimic nuclear matter. Instead, in our approach we assume, maybe more reasonably, that at such large densities quark matter is liberated [102] and thus the collapse of two NSs leads to the formation of a SS. Whether the SS is the final stellar object or whether it collapses to a BH depends, in our very simple model, on the value of the bag constant. Small values of the bag constant do indeed allow us to have SSs with a large mass.

One may expect that a different quark matter EoS could provide a structure approaching the Buchdahl's limit line in Figure 3.4. A very general parametrization of the quark matter EoS was defined in the previous chapter in the Eq. (2.25), that we report here [114]:

$$P = \frac{3}{4\pi^2} a_4 \mu^4 - \frac{3}{4\pi^2} a_2 \mu^2 - B$$

Varying the various parameters we obtain last stable SSs that are less compact than those reported in Figure 3.4, basically because the EoS in Eq. (3.3.1) is less stiff than the simple parametrization Eq. (3.13). Regarding

standard nuclear matter, as already noted in [163, 209], the $M(R)$ curves obtained by the nuclear EoSs approach the photon-sphere line from below, but do not cross it. As representative examples we consider in Figure 3.4, the BBB2 [99], the SLy4 [98] and the MS1 [100] EoSs, which at the largest possible mass values have a speed of sound in the central region close to 1, but nonetheless are not sufficiently compact to cross the photon-sphere line.

Using the considered models of SS, we estimate the τ_{echo} as defined in Eq. (3.9) and considering the relation $\omega_{echo} = \pi/\tau_{echo}$, as told before, we obtain the lowest frequencies for our studied configurations. We obtain that the lower frequencies are of the order of tens of kilohertz. In particular, for the last stable massive stars, corresponding to the tips of the SS1 and SS2 curves in Figure (3.4), we obtain $\omega_{1,echo} \simeq 17$ kHz and $\omega_{2,echo} \simeq 27$ kHz, respectively. Values of the bag constant in between B_1 and B_2 lead to intermediate values of the echo frequency. The basic reason for the discrepancy between our results and those found in [209] is that strange quark matter is self-bound, but is not incompressible. Incompressible matter is characterized by a superluminal (actually infinite) speed of sound. In our approach we have instead assumed a speed of sound equal to the speed of light. In this case it is still possible to cross the photon-sphere line, but the star cannot be too compact because at that point gravitational effects are large, and then further increasing the central density the star gravitationally collapses.

We have neglected the stellar rotation and possible temperature effects on the EoS. Regarding the stellar rotation, although we have solved the TOV equations assuming a static stellar model including rotation is expected to slightly change the GW echo frequency, see for example the estimates reported in [209]. Those estimates apply to the present model for the basic reason that SSs are hardly deformable. Regarding the temperature effects, one should compare the expected temperatures produced in the NSs merging with the corresponding quark chemical potentials. Since in SSs the quark chemical potential is on the order of hundreds of MeV, it seems unlikely that such a high temperature scale is produced in the merging or in the postmerger environment.

An interesting possibility is that the SS produced by the merging of NSs is in the unstable branch. Since stars in the unstable branch are more compact than stable stars, they may lead to GW echoes at lower frequencies. In this case the star would quickly collapse to a BH, but it might have enough time to produce a GW echo signal. The estimated time for NS collapse to BH is on the order of a millisecond [210–212] and it strongly depends on how far from equilibrium the initial stellar configuration is. A delayed collapse, on timescales of $10 - 100$ ms, is obtained for differentially rotating stars, see for example [214], and for stiff EoSs [215]. We are not aware of any simulation

of merging NSs with the formation of an unstable SS, however, since the EoS in Eq. (3.13) is extremely stiff, it may have collapsing times of the order of 100 ms or more. In this case, the collapsing time could be longer than τ_{echo} , thus allowing, at least in principle, the emission of GW echoes at lower frequencies than those obtained in the present work. Note that for realistic estimates of the echo timescale one should evaluate τ_{echo} considering that the density and the pressure of the collapsing ultracompact star changes with time.

Chapter 4

The Neutron-Mirror Neutron mixing in Neutron Stars

4.1 Mirror World

In 1956 Lee and Yang proposed that the weak interactions of the fundamental particles are not invariant under mirror reflection of the coordinate system, or equivalently they are not invariant under Parity transformation [216]. Experiments confirmed that the parity is violated by the weak interaction. This interaction is left-chiral, i.e. it has the V-A form [217]. Nowadays, the fundamental interactions of particles are described by the Standard Model of Particle Physics. The Standard Model is a gauge theory whose symmetry is $G = SU(3)_c \times SU(2) \times U(1)$ [217, 218]. For a brief discussion on the representation of the $SU(3)$ group, see Chapter 2. The left-handed fermions transform as doublets of the electroweak $SU(2) \times U(1)$ subgroup, while the the right-handed fermions as singlet:

$$q_L = \begin{pmatrix} u_L \\ d_L \end{pmatrix}, \;\; l_L = \begin{pmatrix} \nu_L \\ e_L \end{pmatrix}, \;\; u_R, \;\; d_R, \;\; e_R, \tag{4.1}$$

where we denote with q the quark, u and d are respectively the up and down quark component of the doublet, l are the leptons, e is the electron and ν the neutrino. We are omitting in this discussion the family index because the representations are the same for all the three families. We can define the antiparticles fields by the transformation:

$$\bar{\psi}_L = C\gamma_0\psi_R^*, \tag{4.2}$$

and applying this transformation to the particles representations, the representations of antiparticles are:

$$\bar{q}_R = \begin{pmatrix} \bar{u}_R \\ \bar{d}_R \end{pmatrix}, \ \bar{l}_L = \begin{pmatrix} \bar{\nu}_L \\ \bar{e}_l \end{pmatrix}, \ \bar{u}_R, \ \bar{d}_R, \ \bar{e}_R. \tag{4.3}$$

Moreover, we define a global charge called the baryon number B, that is equal to $B = 1/3$ for all the quark field (and $B = -1/3$ for anti quark field), and a global charge denoted with L, that is the lepton number. It is equal to $L = 1$ for l_L and e_R and $L = -1$ for the respective antiparticles. The antiparticles weak interactions are right-handed, i.e. are of the V+A form. However, due to the baryon asymmetry of the Universe, particles are dominant and we observe V-A weak interaction.

There is an old idea, suggested by Li and Yang [219–221] that there can exist a hidden sector of particles which is an exact replica of the observable particle sector, however with right-handed interactions. This sector is the sector of mirror particles and it could be a non conventional candidate for Dark Matter. Then all the ordinary (O) particles, the electron e, the proton p, the neutron n, the photon γ, the neutrinos ν have invisible twins: e', p', n', γ', ν'. These twin particles are sterile to our standard interactions $SU(3) \times SU(2) \times U(1)$ but have their own gauge interactions $SU(3)' \times SU(2)' \times U(1)'$ and are called Mirror (M) particles [236]. So the M sector has the field content [246]:

$$q'_L = \begin{pmatrix} u'_L \\ d'_l \end{pmatrix}, \ l'_L = \begin{pmatrix} \nu'_L \\ e'_l \end{pmatrix}, \ u'_R, \ d'_R, \ e'_R, \tag{4.4}$$

and:

$$\bar{q}'_R = \begin{pmatrix} \bar{u}'_R \\ \bar{d}'_R \end{pmatrix}, \ \bar{l}'_L = \begin{pmatrix} \bar{\nu}'_L \\ \bar{e}'_l \end{pmatrix}, \ \bar{u}'_R, \ \bar{d}'_R, \ \bar{e}'_R. \tag{4.5}$$

For definiteness, let us define M fermion numbers: M baryon number B' is equal to 1/3 for M quarks u' and d' (whatever the parity they have), and M lepton number L' is equal to 1 for left handed M leptons and for right handed M electron. Similarly to what happens for O particles, M antiquarks have $B' = -1/3$ and M antilepton have $L' = -1$ [246]. For a hystorical overview and references on the M world see [222].

If the M particles exist in nature, one could think that they are the partners of standard particles obtained by a "mirror" symmetry. This symmetry, called M parity , is an exact symmetry and one could consider a theory based on the product $G \times G'$ of two identical gauge group with O particles belonging to G and M particles to G', i.e. the parallel M sector. The total Lagrangian of the system should be:

$$\mathcal{L}_{\text{tot}} = \mathcal{L} + \mathcal{L}' + \mathcal{L}_{\text{mix}}, \tag{4.6}$$

with the $\mathcal{L}$, $\mathcal{L}'$ Lagrangians of O and M particles respectively. $\mathcal{L}_{\rm mix}$ stands for possible interactions between the particles of two sectors. The identical forms of the Lagrangians $\mathcal{L}$ and $\mathcal{L}'$ is ensured by a discrete Z_2 symmetry $G \leftrightarrow G'$ when particles of G sector (fermions, Higgses and gauge fields) are exchanged with their twins from G'-sector (primed fermions, Higgses and gauge fields). Moreover the M parity implies that not only all the particles have their own M counterpart, but also all the coupling constant (gauge, Yukawa and Higgs) have the same pattern. That means that the microphysics of the two parallel sector are the same [236]. The case of spontaneously broken Z_2 symmetry when the weak scales in two sectors can be different was also discussed in the literature [231].

M particles can exist without violating any known experiment, or conversely the known experiments do not demonstrate the existence of M particles nor that M symmetry is broken in nature: they have only shown that the O particles are transparent to M interactions (whether M world exist) [223]. Assuming the existence of M particles, we need to understand the experimental implications and find out whether the existence of a parallel sector could be relevant for our Universe [223]. In the last years, several works have taken into account the existence of the M world, being motivated by the problems of flavour and CP violation [224, 225], neutrino physics [227–230], gravitational microlensing [231–233], ultra-high energy cosmic rays [234], etc..

M atoms, invisible in terms of ordinary photons but gravitationally coupled to our matter, can constitute some reasonable fraction of dark matter, or could even represent its entire amount (for reviews, see e.g. Refs. [235, 236]). M matter is an asymmetric type of dark matter, with an abundance related to the mirror baryon asymmetry. Its collisional and dissipative character can have specific implications for the cosmological evolution, formation and structure of galaxies and stars, etc. [237–240]. One could naively think that the O and M particles, because of the M symmetry, should have the same cosmological abundance and have the same cosmological evolution. However, this would be in contrast with the Big Bang nucleosynthesis bound on effective number of extra light degrees of freedom [223, 241]. The way out is that in the early universe the M world has a lower temperature then the O universe, $T' < T$. In particular, the Big Bang nucleosynthesis bounds require $T'/T < 0.5$ or so whereas a stronger limit $T'/T < 0.3$ emerges from the cosmological data on the large scale structure and cosmic microwave background [237–239]. This can be realized if after inflation O and M sectors are (re)heated in non-symmetric way and then both systems evolve adiabatically, without significant entropy production, with T'/T remaining nearly constant in all epochs until today [237–239]. In addition, all possible particle interactions between two sectors included in $\mathcal{L}_{\rm mix}$ should be out-of-equilibrium,

otherwise they would equilibrate temperatures between two sectors and one would have $T'/T \approx 1$. Remarkably, the baryon asymmetries in both O and M worlds can be co-generated in comparable amounts,

$$\Omega'_{\rm B}/\Omega_{\rm B} \geq 1$$

via $B-L$ violating interactions between the particles of two sectors [242–246].

The same B and L violating interactions that can be at the origin of the co-baryogenesis between the O and M sectors, can induce the mixing phenomena between O and M particles. In fact any neutral particle, elementary (as e.g. neutrinos) or composite (as e.g. the neutron or hydrogen atom) can have mixing with its mirror twin and thus can transform into the latter. In particular, effective L-violating operators:

$$\frac{1}{M}\ell\phi\ell'\phi', \tag{4.7}$$

where ℓ and ℓ' are the O and M lepton doublets and ϕ and ϕ' O and M Higgs doublets, induce active-sterile mixing between our neutrinos $\nu_{e,\mu,\tau}$ and mirror neutrinos $\nu'_{e,\mu,\tau}$ [227–230]. On the other hand, they give rise to co-leptogenesis mechanism which induces baryon asymmetries in both O and M worlds [242–246].

4.2 Mirror neutron-neutron mixing

We shall concentrate on the mixing between the neutron n and mirror neutron n' [247, 248]. This phenomenon is similar to neutron-antineutron mixing [249, 250] (for a recent review, see [251]). However, differently from the latter, $n - n'$ mixing is not restricted by strong experimental bounds and can be rather effective for free neutrons. Implications of $n - n'$ oscillation for the propagation of ultra-high energy cosmic rays, for neutrons from solar flares and for the Big Bang nucleosynthesis were discussed respectively in [252–254] and [255]. Experimental sensitivities for searching $n - n'$ transition at different neutron facilities were discussed in [256]. Several dedicated experiments for its search were already performed [257–261] (some of them show deviations from the null-hypothesis [263]), and new experiments are also planned [264, 265].

The mass mixing term $\epsilon nn'+$ h.c., violates ordinary and mirror baryon numbers by one unit, $\Delta B = 1$ and $\Delta B' = -1$, but it conserves the combination $B_T = B + B'$. The mixing can be induced by effective operators:

$$\frac{1}{\mathcal{M}^5}(\bar{u}\bar{d}\bar{d})(u'd'd') + h.c. \tag{4.8}$$

involving ordinary quarks u, d and mirror quarks u', d', where $\mathcal{M}$ is a cutoff scale. This operators in turn can be induced via a see-saw like mechanism involving e.g. heavy color triplets and neutral Dirac fermions [229, 247, 248]. Then, modulo $C = O(1)$ coefficients in the determination of the matrix element $\langle n|udd|0\rangle = C\Lambda^3_{\rm QCD}$, one has:

$$\epsilon = \frac{C^2\Lambda^6_{\rm QCD}}{\mathcal{M}^5} = 2.5\, C^2 \left(\frac{10{\rm TeV}}{\mathcal{M}}\right)^5 \times 10^{-15}{\rm eV} \tag{4.9}$$

where the Clebsch factor C depends on the Lorentz and isospin structure of Eq. (4.8). Therefore, for the cutoff scale $\mathcal{M}$ of few TeV, the underlying physics can be testable also at the LHC and future accelerators.

For free neutrons $n - n'$ conversion is affected by the presence of matter environment and magnetic fields [247, 248]. The $n - n'$ transition is kinematically forbidden for the neutrons bound in nuclei, and no limits on ϵ emerge from the nuclear stability bound [247,248]. For a comparison, the nuclear stability limits for $n - \bar{n}$ mixing are very stringent: $\epsilon_{n\bar{n}} < 2.5 \times 10^{-24}$ eV, in fact about 3 times stronger than the direct experimental limit $\epsilon_{n\bar{n}} < 7.7 \times 10^{-24}$ eV [251].

Altough the $n - n'$ transition is ineffective in nuclei, it is possible in NSs and we shall discuss this topic below. [247, 248].

4.3 Mirror neutron-neutron mixing in Neutron Stars

In general, evolution may play an important role in NSs, leading to a $0.2 - 0.3 M_\odot$ mass increase [51] due to matter fallback after the supernova explosion or accretion in recycled NSs. These mechanisms always imply a mass increase, thus it is generally believed that the mass of NS after their birth can only increase. As a consequence, those NSs in double NS binaries, which are thought to have received little or no accretion, should reflect the stellar mass at birth with a direct link to the supernova mechanism. The observed double NSs masses can be nicely fitted with a gaussian distribution with a mean value at $\mu \simeq 1.32 M_\odot$ and rather small dispersion, $\sigma \simeq 0.1 M_\odot$ see for example [51]. It is not clear why a general supernova explosion should lead to such a mass, and to a so peaked mass distribution.

Our goal is to challenge this paradigm, scrutinizing whether the double NSs might have followed a different evolution, with a larger initial mass followed by a gravitational mass decrease. In the proposed mechanism part of the standard hadronic content has been transformed in M matter, with a

gravitational mass (and radius) reduction during the stellar evolution. The transformation of O matter into M matter does indeed lead to a larger binding energy and is therefore energetically allowed. As discussed above, this cannot happen in standard nuclei, because a transition neutron-mirror neutron would lead to a decrease of the nuclear binding energy. The proposed mechanism also allows for more degenerate solutions: the EoS of standard nuclear matter allows NSs with similar radius but different gravitational masses. Including M matter, CSs with the same mass but different radii can exist: they correspond to stars with a different fraction of M matter. Recent analysis of NS masses in double NS systems suggest a bimodal distribution [267]. A possible interpretation is that the two distributions correspond to different type of stars with the low mass one corresponding to hybrid CS. i.e. with a deconfined quark matter core. Within the present approach, if the radii of some NS is found to be smaller than those of other NS with the same or smaller mass, they could correspond to stars with a large fraction of M matter inside.

4.3.1 Two fluid description

In order to calculate the equilibrium configuration, we assume that M matter and O nuclear matter can be described by the same EoS. Since the astrophysical observation of very massive NSs requires a stiff EoS, we consider the SLy EoS, which can indeed account for a mass $M \simeq 2M_\odot$ and a radius $R \approx 10$ km. The result of our analysis is that double NSs that have small masses could be old NSs in which a large fraction of O matter has been converted in M matter. As a second example we consider a polytropic EoS obtained, as described in Chapter 2, joining two polytropes $p = K\rho^\gamma$, with $\gamma = 3$ for the inner part of the NS and $\gamma = 4/3$ for its outer part, with the transition density chosen at $\rho_{\rm tr} = 1.33 \times 10^{14}$ g/cm^3. It allows larger maximal mass, $M_{\rm NS}^{\rm max} = 2.57\, M_\odot$. For typical masses of the NS $M \simeq 1.4\ M_\odot$ both of these EoS imply a radius of about 12 km.

A newborn NS formed after the gravitational collapse of the progenitor star consists only of O nuclear matter. However, $n \to n'$ transition starts to create in its interior M nuclear matter and hence the original NS should be gradually transformed into a mixed star (MS) partially consisting of O neutron matter and partially of M neutron matter, with the fraction of the latter increasing in time. We consider that the transformation process is adiabatic, with a conversion time much larger the the star cooling time, and described by Boltzmann equations:

$$\frac{dN_1}{dt} = -\Gamma N_1 + \Gamma' N_2\,, \qquad \frac{dN_2}{dt} = \Gamma N_1 - \Gamma' N_2\,, \tag{4.10}$$

where $N_1(t)$ and $N_2(t)$ are respectively the number of O and M baryons at the time t, Γ is $n \to n'$ transformation rate in the star which will be estimated in next section, and Γ' is the inverse $n' \to n$ transformation rate (which in fact is negligible, $\Gamma' \ll \Gamma$).

Hence, an initial NS consisting exclusively of O neutron matter (i.e. at $t = 0$ $N_1 = N_0$ and $N_2 = 0$), evolves into a MS with $N_1(t)$ decreasing and $N_2(t)$ increasing in time. However, the overall number of O and M baryons in the star is conserved, $N_1(t) + N_2(t) = N_0$. Therefore, Eqs. (4.10), neglecting the inverse reaction rate Γ', reduce to:

$$\frac{dx_2}{dt} = \Gamma\,(1 - x_2), \tag{4.11}$$

where $x_2 = N_2(t)/N_0$ is the fraction of M baryons at the time t. Asymptotically in time a MS may approach a final equilibrium configuration, $x_2 = x_1 = 1/2$. In the following we coin such a maximally MS as twin star (TS).

As far as the evolution is adiabatic, at any moment of time a MS can be described as a static concentric configuration of the O neutron matter and M neutron matter spheres respectively with the radii R_1 and R_2. Therefore, we consider a spherically symmetric system with the well known metric tensor $g_{\mu\nu} = \mathrm{diag}(-g_{tt},\, g_{rr},\, r^2, r^2 \sin^2\theta)$, which is determined by the total energy-momentum tensor:

$$T_{\mu\nu} = \mathrm{diag}(\rho e^{2\phi}, p e^{2\lambda}, p r^2, p r^2 \sin^2\theta)\,. \tag{4.12}$$

Note that we can write $T_{\mu\nu} = T^1_{\mu\nu} + T^2_{\mu\nu}$, where

$$T_{\alpha,\mu\nu} = \mathrm{diag}(\rho_\alpha e^{2\phi}, p_\alpha e^{2\lambda}, p_\alpha r^2, p_\alpha r^2 \sin^2\theta) \quad \text{where} \quad \alpha = 1, 2, \tag{4.13}$$

and where ρ_α, p_α are the energy density and the pressure of the two component respectively, but the functions ϕ and λ depend on the energy densities of both fluids. Hence, we can use a two-fluid description in which each component contributes separately to the energy density and pressure, i.e. $\rho = \rho_1 + \rho_2$ and $p = p_1 + p_2$.

We use the standard notations, defined in the previous chapters, $g_{tt} = e^{2\phi}$ and $g_{rr} = (1 - 2m/r)^{-1}$, $m(r)$ being the gravitational mass within the radius r. Retrieving the TOV equations, see Eq. (2.5,2.9,2.10) [15, 16] :

$$m' = 4\pi\rho r^2\,, \tag{4.14}$$

$$p' + (\rho + p)\phi' = 0\,, \tag{4.15}$$

$$\frac{p'}{\rho + p} + \frac{m + 4\pi p r^3}{r^2 - 2mr} = 0\,. \tag{4.16}$$

where the superscript $'$ stands for the radial gradients, i.e. for instance $m' = dm/dr$. We now denote with 1 the O matter component and with 2 the M matter the component respectively. The first equation is linear so we can split it between two components, $m(r) = m_1(r) + m_2(r)$:

$$m_1' = 4\pi\rho_1 r^2\,, \qquad m_2' = 4\pi\rho_2 r^2\,, \tag{4.17}$$

i.e. we have $m_\alpha(r) = 4\pi\int_0^r \rho_\alpha(r) r^2 dr$ $(\alpha = 1, 2)$. The gravitational mass of the mixed star is $M = M_1 + M_2$ where $M_\alpha = m_\alpha(R_\alpha) = 4\pi\int_0^{R_\alpha} \rho_\alpha r^2 dr$ (similarly to the one fluid description).

Once both components in the star are in hydrostatic equilibrium, $\dot{\rho}_\alpha, \dot{p}_\alpha = 0$, considering $\nabla_\mu T_\nu^{\mu(\alpha)} = 0$ for each of them separately give

$$\phi' = \frac{p_1'}{\rho_1 + p_1} = \frac{p_2'}{\rho_2 + p_2}\,. \tag{4.18}$$

As for the TOV equation, it in fact couples the pressures and energy densities of two fluids. Using Eqs. (4.17) and (4.18), it gives the coupled differential equations for the O neutron matter and M neutron matter components:

$$\frac{p_1'}{\rho_1 + p_1} = \frac{p_2'}{\rho_2 + p_2} = \frac{m_1 + m_2 + 4\pi(p_1 + p_2) r^3}{2(m_1 + m_2) r - r^2}\,. \tag{4.19}$$

In summary, the system of equations to be used for determining the structure of a MS is the following:

$$\begin{aligned}
\frac{dm_1}{dr} &= 4\pi\rho_1 r^2 \\
\frac{dm_2}{dr} &= 4\pi\rho_2 r^2 \quad \text{for} \qquad r \le R_2 \\
\frac{dp_1}{dr} &= (\rho_1 + p_1)\frac{m_1 + m_2 + 4\pi(p_1 + p_2) r^3}{2(m_1 + m_2) r - r^2} \\
\frac{dp_2}{dr} &= \frac{\rho_2 + p_2}{\rho_1 + p_1}\frac{dp_1}{dr} \qquad \text{for} \qquad r \le R_2\,,
\end{aligned} \tag{4.20}$$

where have assumed that $R_1 > R_2$.

Similarly to the case of one fluid description, we can solve the TOV equations once both central density, ρ_{1c} and ρ_{2c} are given. From this we can define the central masses and the central pressure of both the components and then one integrates towards the surface the differential equations (4.20). During the gradual conversion of the initial NS into the MS the O neutron matter component remains larger than the M neutron matter one, $N_1 > N_2$, so that at any position and any time $\rho_2(r) < \rho_1(r)$. Thus we should always

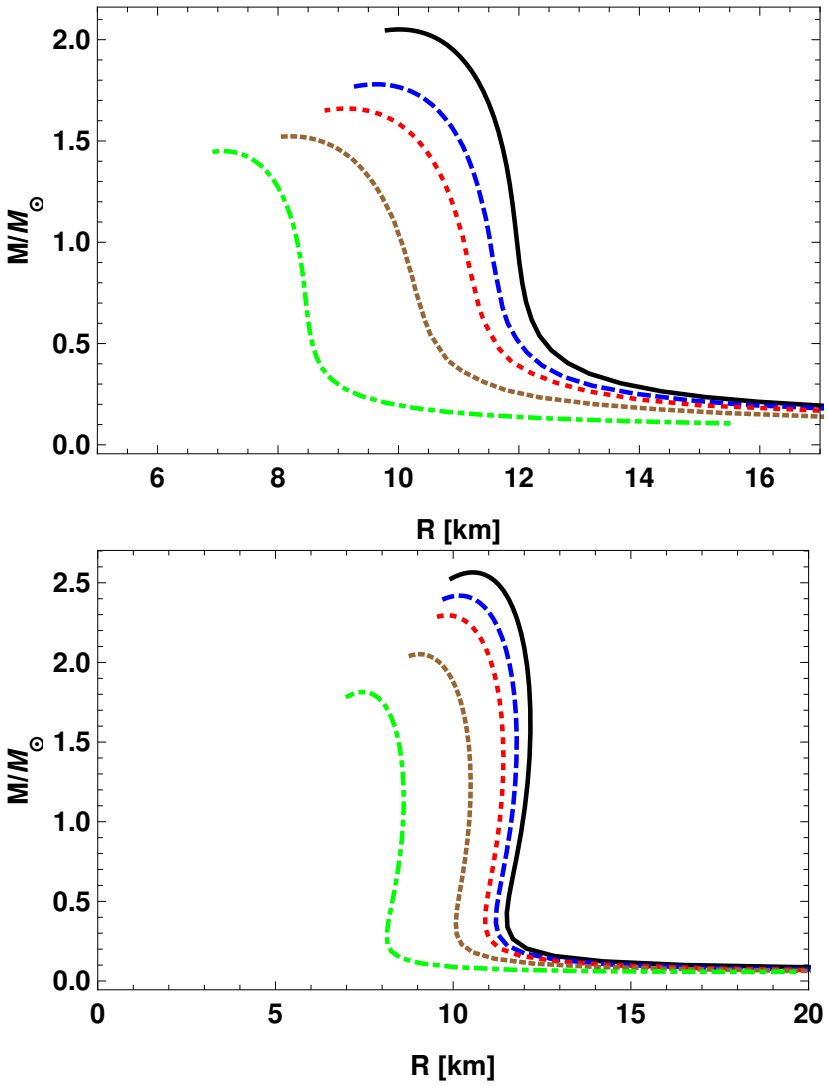

Figure 4.1: Mass-radius diagrams obtained with two different EoS: Sly (top panel) and joined Polytropic (bottom panel). Black solid curves correspond to initial configurations ($\chi = 0$) whereas blue, red, brown and green dashed curves correspond to mixed configurations respectively with $\chi = 0.5, 0.6, 0.75$ and 1. In the TS configuration mass and radius are rescaled from NS configuration by a factor $1/\sqrt{2}$.

have $R_2 < R_1$ and $M_2 < M_1$. At $r = R_2$, the mass of the mirror component saturates, $m_2(r > R_2) = M_2$, and one has to stop the integration for the M neutron matter component at the radius R_2 while continuing it for the O neutron matter component to the radius R_1. Therefore, the radius of the mixed star is $R = R_1$. However, in the asymptotic TS configuration with $\rho_1(r) = \rho_2(r)$, the density profiles of two components should be identical by

symmetry, $\rho_2(r) = \rho_1(r)$, and thus for the radius and mass of the TS we should have $R = R_1 = R_2$, $M = 2M_1 = 2M_2$.

In Figure 4.1 we show the mass-radius diagrams for mixed stars obtained for our choices of the EoS. We introduce the ratio of central densities $\chi = \rho_{2c}/\rho_{1c}$ as a relevant parameter that depends on the age of a star. In particular, for a newborn NS we have $\chi = 0$. But once it evolves as MS this parameter increases and for a TS configuration it can asymptotically approach the value $\chi = 1$.

For two identical compact stars we can set $\rho_{c1} = \rho_{c2}$, which for symmetry gives $R_1 = R_2$, $p = 2p_2$, $m = 2m_2$ etc. So we can focus on one of the two components. The corresponding TOV's equations become

$$\frac{dm_2}{dr} = 4\pi\rho_2 r^2\,, \tag{4.21}$$

$$\frac{dp_2}{dr} = (\rho_2 + p_2)\frac{m_2 + 4\pi p_2 r^3}{2m_2 r - r^2/2}\,, \tag{4.22}$$

where the first equation is the standard one but the second differential equation differs from the standard one for a factor of $1/2$ in one of the terms of the denominator. However, one can rewrite the above equations as a standard TOV's equations by the rescaling

$$r \to r/\sqrt{2} \qquad m_2 \to m_2/2\sqrt{2} \tag{4.23}$$

$$p_2 \to p_2 \qquad \rho_2 \to \rho_2\,, \tag{4.24}$$

which indeed leads to

$$\frac{dm_2}{dr} = 4\pi\rho_2 r^2\,, \tag{4.25}$$

$$\frac{dp_2}{dr} = (\rho_2 + p_2)\frac{m_2 + 4\pi p_2 r^3}{2m_2 r - r^2}\,, \tag{4.26}$$

meaning that the stellar radius and the total mass are rescaled by a $1/\sqrt{2}$ factor with respect to the standard NS case; note that the compactness M/R is invariant. In Table 4.1 we report the maximum mass and associated radius for different χ. The masses and the radius obtained for a TS follows the scale law expected.

4.3.2 Total Baryon Density Curves

As told in the previous section, in our model we suppose that the total baryon number, i.e. the sum of O baryons and M baryons, is constant. In order to

χ	$M_{max}/M_\odot$	$R[km]$
0	2.05	10.00
0.5	1.78	9.64
0.6	1.66	9.11
0.75	1.52	8.22
1	1.45	7.06

χ	$M_{max}/M_\odot$	$R[km]$
0	2.57	10.56
0.5	2.42	10.22
0.6	2.30	9.84
0.75	2.05	9.08
1	1.81	7.46

Table 4.1: Maximum Mass and the associated radius in function of χ for SLy EoS (left) and for Joined Polytropic EoS (right).

calculate the curves at constant baryon number we have to define the density number in function of the energy density. The problem has a very simple solution for the considered EoSs. Indeed in tables used for the definition of the EoS (for instance see http://www.ioffe.ru/astro/NSG/NSEOS/sly4.html) usually it is possible to find the values of baryon number density, and interpolating data it is possible to define the function $n(\rho)$, that is the number density of baryons as a function of the energy density.

For a polytropic EoS it is possible to find an analytical form of $n(\rho)$. In fact, considering the well known relation [3]:

$$n\frac{d\rho}{dn} = \rho + p, \tag{4.27}$$

and substituting a polytrope $p = K\rho^\gamma$ in (Eq. 4.27), we simply obtain:

$$\frac{d\rho}{\rho + K\rho^\gamma} = \frac{dn}{n}. \tag{4.28}$$

Integrating the last equation from nuclear saturation density, where $\rho_s \simeq 2.8 \times 10^1 4\mathrm{g/cm}^3$ and $n_s \simeq 0.16\mathrm{baryons/fm}^3$, we obtain:

$$\begin{aligned}
\int_{\rho_s}^{\rho} \frac{dx}{x + Kx^\gamma} &= ln(n/n_s), \\
\int_{\rho_s}^{\rho} \frac{dx}{x} - \int_{\rho_s}^{\rho} \frac{Kx^{\gamma-2}}{1 + Kx^{\gamma-1}} dx &= ln(n/n_s), \\
ln\left(\frac{n}{n_s}\right) = ln\left(\frac{\rho}{\rho_s}\right) - \frac{1}{\gamma - 1} ln\left(\frac{1 + K\rho^{\gamma-1}}{1 + K\rho_s^{\gamma-1}}\right) \\
ln\left(\frac{n}{n_s}\right) = ln\left(\frac{\rho}{\rho_s}\right) + ln\left(\frac{1 + K\rho_s^{\gamma-1}}{1 + K\rho^{\gamma-1}}\right)^{\frac{1}{\gamma-1}} \\
\Rightarrow \quad n = n_s \left(\frac{\rho}{\rho_s}\right) \left(\frac{1 + K\rho_s^{\gamma-1}}{1 + K\rho^{\gamma-1}}\right)^{\frac{1}{\gamma-1}}
\end{aligned} \tag{4.29}$$

Using the dependence of energy density obtained by TOV solutions, we have that the baryon density is actually a function of the radius, i.e. $n_b(\rho(r))$. So we can numerically integrate it:

$$N_\alpha = 4\pi \int_0^{R_\alpha} (1-2m/r)^{-1/2} n_\alpha r^2 dr, \tag{4.30}$$

where $n_1(r)$ and $n_2(r)$ are the O and M baryon number densities at the radius r and we define $N_T = N_1 + N_2$, the total number of baryons. In Figure (4.2) we show the dependence of total baryon number with the total energy density, i.e $\rho(r) = \rho_1(r) + \rho_2(r)$.

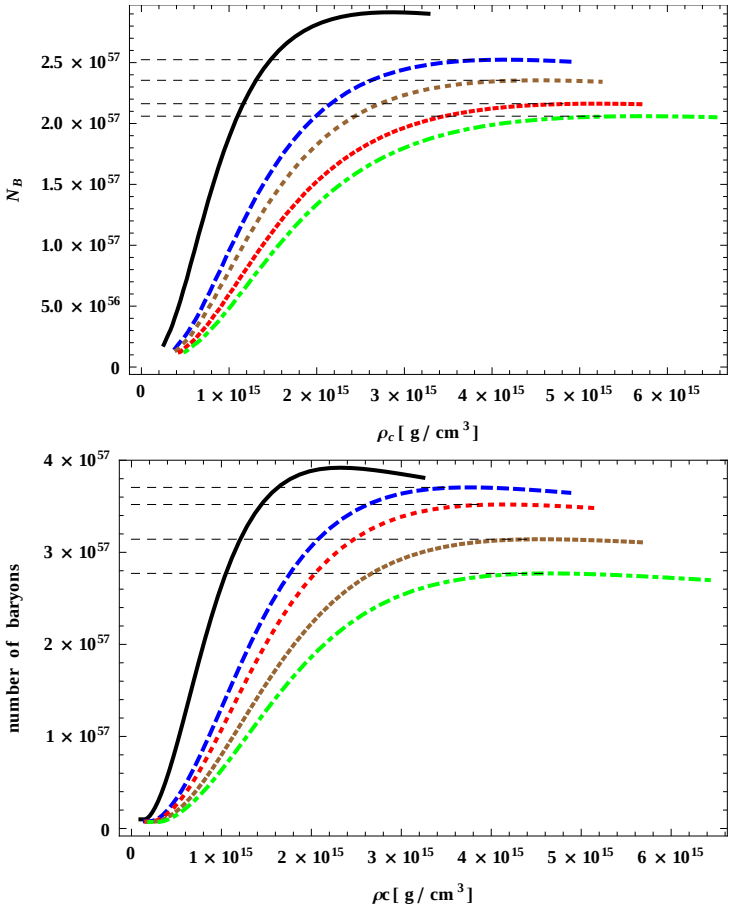

Figure 4.2: Total number of baryons (O+M) versus central energy density diagrams obtained with two different EoS: Sly (top panel) and joined polytrope (bottom panel). The colors follow the same "rule" of Figure (4.1). The horizontal black dashed lines in connect the configurations with different χ having the same overall baryon number $N_1 + N_2 = N_0$. In table 4.2 we show corresponding values of total baryonic number.

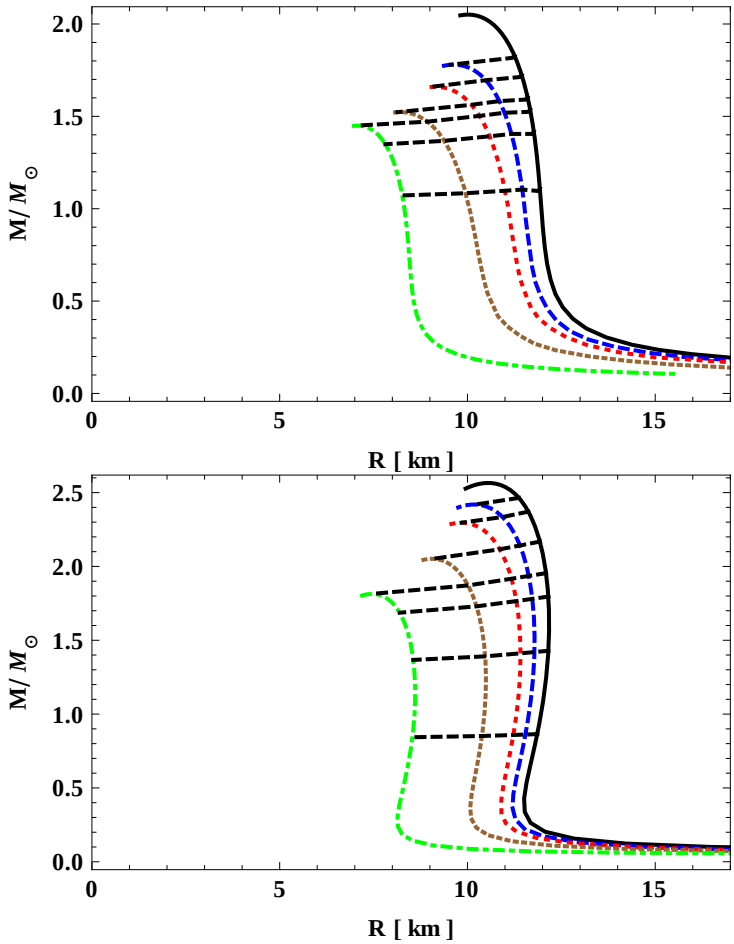

Figure 4.3: Solution of the TOV equation obtained and lines at constant total baryonic number. The dashed black line indicate the evolution of a given NS. The four higher curves have the same value shown in Table 4.2. All the curves with N_B fewer that the baryon number maximum for $\chi = 1$, are stable meaning that the asymptotic TS regime could be reached after some time. The stable black curve shown in the graph have $N_B = 1.88 \times 10^{57}$, $N_B = 1.43 \times 10^{57}$ for SLy EoS (top panel) and $N_B = 2.51 \times 10^{57}$, $N_B = 1.93 \times 10^{57}$ and $N_B = 1.12 \times 10^{57}$ for Polytropic EoS (bottom panel).

The horizontal black dashed lines in Figure 4.3 connect the configurations with different χ having the same overall baryon number $N_1 + N_2 = N_0$, Hence, they describe the evolution of a NS of a given initial mass entirely composed of O neutron matter ($\chi = 0$, i.e. $N_1 = N_0$, $N_2 = 0$, black curves), to a final TS ($\chi = 1$, i.e. $N_1 = N_2 = N_0/2$, green dashed curves), passing intermediate stages with different χ. Concluding this section, a young NS with a mass $M_{NS}(\rho_{1c})$ exclusively composed by O nuclear matter with an initial central density ρ_{1c} and zero initial density of M neutron matter ρ_{2c}, due to $n \to n'$

χ	N_{Bmax}
0.5	2.52×10^{57}
0.6	2.35×10^{57}
0.75	2.16×10^{57}
1	2.06×10^{57}

χ	N_{Bmax}
0.5	$3.71 \times 10^{57}2$
0.6	3.52×10^{57}
0.75	3.14×10^{57}
1	2.77×10^{57}

Table 4.2: Maximum total baryonic number as a function of χ for SLy EoS (left) and for Joined Polytropic EoS (right).

conversion should slowly evolve to a MS, with $\rho_{2c}(t)$ and $\chi(t) = \rho_{2c}(t)/\rho_{1c}(t)$ adiabatically increasing in time. In the conversion process the total baryonic number N_T is conserved. In this way the star would continuously convert gravitational energy in heat which will be emitted in presumably in terms of O and M neutrinos and photons. We assumed that the conversion process is slow, with the conversion time much exceeding the cooling time, and so at any stage the MS is in a equilibrium configuration.

The fate of a star depends on its initial mass. During the conversion the star becomes more compact, and in addition, its gravitational mass becomes somewhat smaller because of gain in the gravitational binding energy. Focusing on the constant baryon number trajectories, see Figure 4.3, the mass difference in between the initial and final states does not exceed 0.1 $M_\odot$ for both the considered EoS. This means that for the case of Sly, an NS with the initial mass $M_{\rm NS} < 1.5\ M_\odot$ and the radius of 12 km or so, can evolve into an asymptotic final configuration of a TS ($\chi = 1$) with a slightly smaller mass ($M < 1.45\ M_\odot$) but considerably more compact, with the radius of about 8.5 km or so. Therefore, whether any observations will find that two NSs with the typical mass of 1.4 $M_\odot$ having different radii, could be interpreted as observations of two objects with different values of χ, i.e. with "mixture" of the O neutron matter and M neutron matter components. In addition, the more compact star should be older.

Maybe an interesting aspect is that NS with larger initial mass, e.g. $M_{\rm NS} > 1.5\ M_\odot$ in the case of Sly EoS, cannot reach the final TS configuration. For example a NS with initial mass $M = 1.8\ M_\odot$ (or 1.6 $M_\odot$) will become unstable and collapse to a BH as soon as χ reaches the value of 0.5 (0.75) or so. So, it is important to understand how fast the NS transformation process is.

4.3.3 Transformation rate time

In a generic medium the evolution of a $n - \bar{n}'$ system, including two spin states for each of n and n', is described by the Schrödinger equation with the

effective Hamiltonian :

$$H = \begin{pmatrix} m + V - iW + \mu \mathbf{B}\sigma & \epsilon \\ \epsilon & m' + V' - iW' + \mu' \mathbf{B}'\sigma \end{pmatrix}, \tag{4.31}$$

where V, V' and W, W' stand respectively for the coherent scattering and absorption of n and n' in ordinary and mirror matter, $\mathbf{B}$ and $\mathbf{B}'$ are ordinary and mirror magnetic fields, $\sigma = (\sigma_x, \sigma_y, \sigma_z)$ are the Pauli matrices, $\mu = 6 \times 10^{-18}$ MeV/G is the neutron magnetic moment and μ' is that for mirror neutron.

In the NS medium we take the optical potential as proportional to the chemical potential of the neutron component, modulo some order 1 coefficient.[1] Let us assume that the $n - n'$ conversion time is much larger than the NS cooling time, and consider an enough old and cold NS, with the temperature much less than the chemical potential, $T \ll \mu$. Thus we take μ simply as the Fermi energy which, in the approximation of ideal non-relativistic Fermi gas is, $E_F \simeq \xi^{2/3} \times 60$ MeV, where $\xi = n_1/n_{\rm s}$ is the ordinary baryon number density in units of nuclear saturation density. The M Fermi energy E'_F has the same dependence on the M baryon number density $\xi' = n_2/n_{\rm s}$. The effect of the magnetic field is negligible, because $|\mu B| \ll 1$ MeV even for magnetars with a magnetic field B reaching 10^{16} G. Furthermore, the small mass difference $m' - m$, if any, can be also neglected.

The $n - n'$ oscillation results from the process $nn \to nn'$ with an average oscillation probability between the two neutron states:[2]

$$\begin{aligned} P_{nn'} &= \frac{1}{2} \sin^2 2\theta_{nn'} \simeq 2 \left(\frac{\epsilon}{E_F - E'_F} \right)^2 \\ &\simeq \left(\frac{\epsilon}{10^{-15}\ \text{eV}} \right)^2 \frac{6 \times 10^{-46}}{\xi^{4/3} \left[1 - (E'_F/E_F) \right]^2}, \end{aligned} \tag{4.32}$$

hence, in any nn collision n' can be produced with a mean probability $P_{nn'}\,\eta$. η is the Pauli blocking factor which takes into account that the final state n cannot have a momentum below the Fermi momentum $p_F = (2mE_F)^{1/2} \simeq \xi^{1/3} \times 340$ MeV while the momentum of produced n' should be above p'_F. This also tells that the inverse reaction rate Γ' in Eq. (4.10) is in fact suppressed. The shape of η as a function of E'_F/E_F is given in Figure 4.4. It has a maximum $\eta(0) \approx 0.18$ at $E'_F = 0$, then it quickly decreases with increasing E'_F/E_F and asymptotically vanishes for a twin star state when $E'_F = E_F$.

[1] In NSs the O neutron matter component consists dominantly of neutrons. It contains also some subdominant fraction of protons (and electrons) but for simplicity we neglect their effects.

[2] Obvioulsy, this expression is valid if $\epsilon \ll E_F - E'_F$ which condition is practically always satisfied in real situations as far as ϵ is very small.

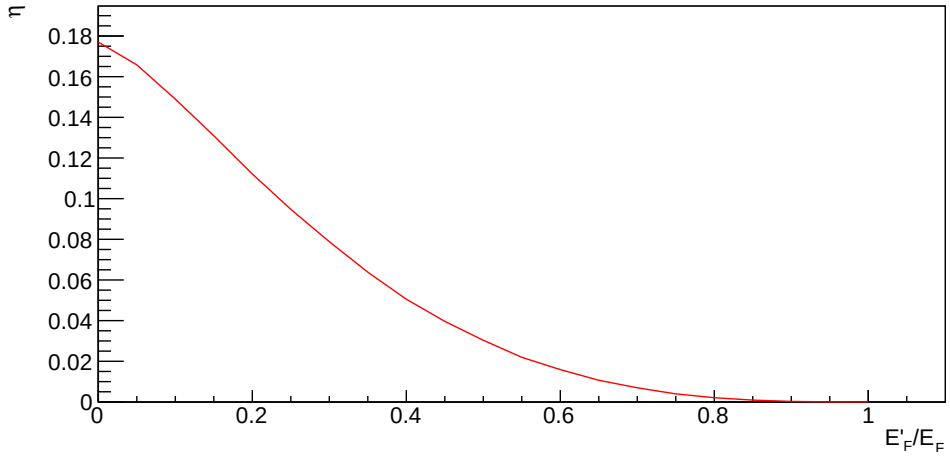

Figure 4.4: Pauli blocking factor η as a function of E'_F/E_F. Growing the Fermi energy of the M particles the conversion time abruptly grows.

Therefore, the rate of mirror neutron production inside a star is not constant in time and it depends on its actual composition, i.e. on the ratio N_2/N_1, at the time t. For an initial NS at $t = 0$ with $N_2 = 0$ and so $E'_F = 0$, it can be estimated as

$$\Gamma_0 = \langle \sigma v \rangle \, n_1 \, \eta(0) P_{nn'}(0) \simeq \left(\frac{a\epsilon}{10^{-15}\,\mathrm{eV}} \right)^2 \times 10^{-15}\ \mathrm{yr}^{-1}\,, \tag{4.33}$$

where we take $\sigma = 4a^2 \times 10^{-25}\,\mathrm{cm}^2$, a being the effective nn scattering length in the medium in units of $n_s^{-1/3} = 1.8$ fm, and $p_F/m \simeq 0.35\,\xi^{1/3}$ the average relative velocity.

So, we can define the characteristic transformation time of the NS as inverse of Eq. (4.33), i.e.

$$\tau_0 = \Gamma_0^{-1} \sim \left(\frac{10^{-15}\,\mathrm{eV}}{\epsilon} \right)^2 \times 10^{13}\mathrm{yr}, \tag{4.34}$$

where we have taken a scattering length for free neutrons $a \simeq 18$ fm, though in conditions of dense nuclear matter the scattering length can be considerably smaller. In particular, for the values $\epsilon < 10^{-15}$ eV or in other terms $\tau_{nn'} = \epsilon^{-1} > 1$ s (which is of experimental interest for search of $n - n'$ oscillation) in the case of exactly mass degeneration it is many orders of magnitude larger than the Universe lifetime, confirming the claim of original paper [247, 248]. (For latest update of the experimental limits on $\tau_{nn'} = \epsilon^{-1}$ see Ref. [261].)

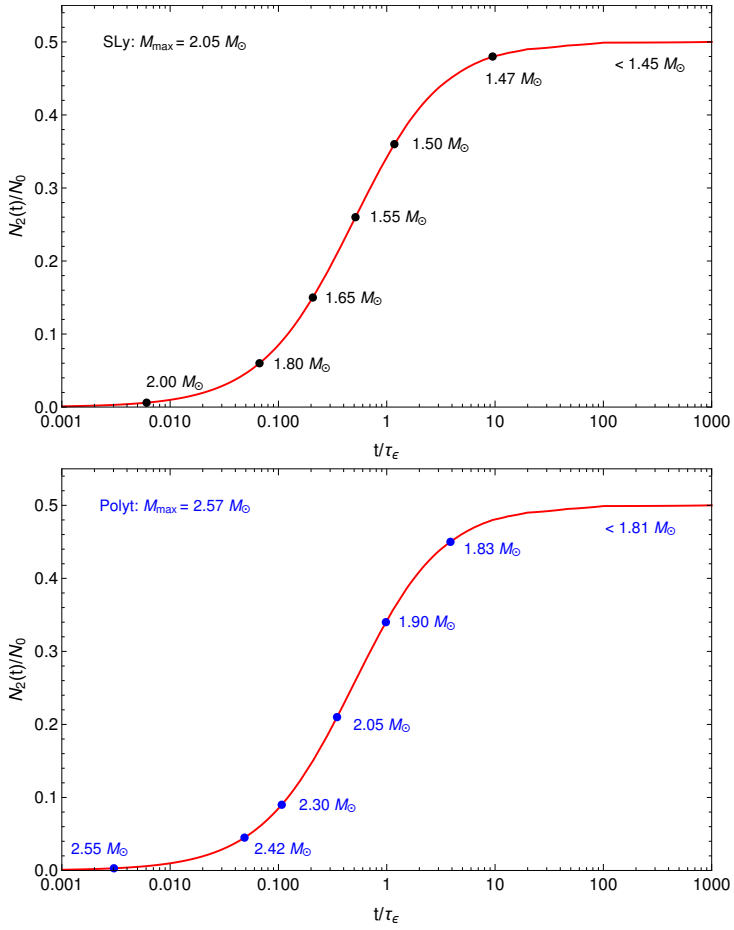

Figure 4.5: The time evolution of the M fraction N_2/N_0 in the NS composition, in units of characteristic transformation time $\tau_0 = \Gamma_0^{-1}$. The black points on the upper panel show the maximal possible mass of the mixed NS of the given age t in the case of the Sly EoS. The blue points on the bottom panel show the same for the polytropic EoS.

However, for larger values of ϵ and in particular for $\epsilon > 10^{-11}$ eV, in which the $n - n'$ conversion (with mass splitting $\Delta m > 10^3\epsilon$) can be of interest for the so-called neutron lifetime puzzle [262], we get $\tau_\epsilon < 10^7$ yr or so. For more mature NSs, with fraction $N_2/N_0 = x_2$ of M baryons becoming comparable to the O baryon fraction $N_1/N_0 = x_1 = 1 - x_2$, the transformation rate slows down. From Eq. (4.32) we get $\Gamma(x_2) = \Gamma_0\mathcal{F}(x_2)$ where $\mathcal{F}(x_2) = \left[1 - (E'_F/E_F)\right]^2 \times \eta(0)/\eta(E'_F/E_F)$. Then integrating Eq. (4.11) we get the time during which the M baryon fraction in the star reaches a given value $x_2 = N_2/N_0$:

$$t(x_2) = \int_0^{x_2} \frac{dx}{\Gamma(x)(1-x)} = \tau_0 \int_0^{x_2} dx \frac{\mathcal{F}(x)}{1-x} \tag{4.35}$$

Since in the evolution of a MS the mirror x_2 increases, an O NS should be gradually transformed into a TS with $x_2 = x_1 = 1/2$. We show in Figure 4.5 the time evolution of the M fraction.

4.3.4 TOY model for Mass distribution of Mixed Stars

An interesting aspect of the first example (Sly EoS) is that a pure NS can have a mass at most $M_{\rm NS}^{\rm max} \approx 2.05 M_\odot$ while maximal allowed mass of a TS is $M_{\rm NS}^{\rm max} \simeq 1.45 M_\odot$. Hence, in our picture the heaviest observed pulsars PSR J0348+0432 and J1614-2230, with masses respectively 2.01 $M_\odot$ [52] and 1.97(4) $M_\odot$ [208] should be considered as young NS almost exclusively composed of O nuclear matter, with M matter constituting no more than $5 \div 10$ per cent of its mass. In their further evolution, accumulating more M matter inside, at some moment they should collapse and transform into BHs.

In this section we show a simple toy model for the evolution of NS, assuming our hypotheses of $n - n'$ conversion. Our goal is to find a correlation between the presence of M matter inside a star and the observed mass distribution of NS. In this section we consider only double NS because, as discussed in the introduction of this section, we assume that double NS can not capture matter by accretion. In Figure 4.6 the histogram of the observed mass of known double NS are shown. The data are taken from [50] and are fitted with a gaussian distribution with $\mu = 1.32 M_\odot$ and $\sigma = 0.1 M_\odot$. Although the distribution is not gaussian, fitting with gaussian distribution gives us an estimation of the behavior of experimental masses and could be useful to compare the obtained results.

In order to develop a toy model of the mass distribution, we have to assume an initial NS distribution, hence we study the evolution of NS masses distribution in function of time. For this case we restrict our analysis to the SLy EoS, assuming that very massive stars are young and are evolving toward

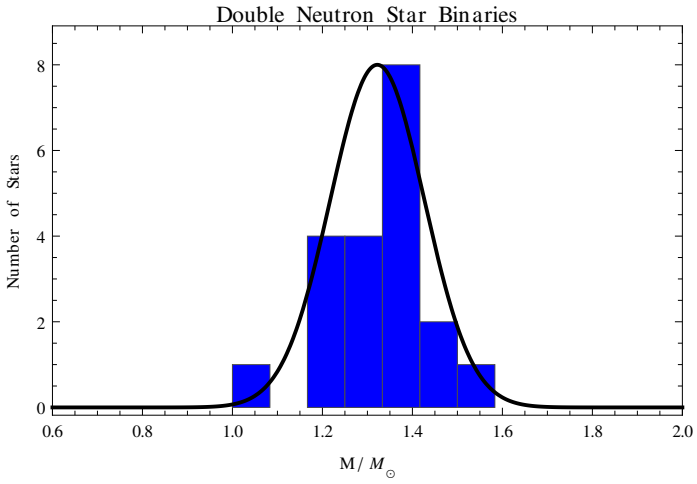

Figure 4.6: Histogram with the observed double NS masses. The histogram is fitted with a gaussian with mean value $\mu = 1.32 M_\odot$ and a $\sigma = 0.1 M_\odot$.

the TS configuration.

As told before, for the SLy EoS, NS with $M_{\rm NS} > 1.5\ M_\odot$ do not reach the asymptotic configuration. Thus, we calculate the maximum mass for several values of χ, and interpolating the data we derive the maximum fraction of M energy density sustainable by stars. Assuming that the relation between χ and time can be approximated as a quadratic function of some typical stellar time, we define the time laws of evolution. For a star that can reach the asymptotic configuration TS, the time law is:

$$m(t) = \begin{cases} m0 + (m1 - m0)(\chi)^2 & \text{for } \chi < 1 \\ m1 & \text{otherwise} \end{cases} \tag{4.36}$$

where we define as m_0 and m_1 the mass of NS and TS configurations. A star with a initial mass exceeding $1.5 M_\odot$, after some time decays in a BH. Thus, the mass temporal dependence can be schematized as:

$$m(t) = \begin{cases} m0 + (mc - m0)(\chi/\chi_c)^2 & \text{for } \chi < \chi_c \\ 0 & \text{otherwise} \end{cases} \tag{4.37}$$

where m_c and χ_c are the mass and the maximum fraction before the conversion of the star in a BH.

We assume a NS mass distribution peaked around $M \sim 1.5 M_\odot$ and slowly decreasing. The reasons are that we imagine that most of the NS born with a mass near the Chandrasekhar limit. However, the mass of NS have an experimental bound of $M \simeq 1.17 M_\odot$ [270] and we have the experimental

upper limit of $2.05M_{\odot}$ [52]. For this reason we decide to cut the tails of our distribution, assuming that NS could born with mass in the range $1 - 2M_{\odot}$, see Figure 4.7.

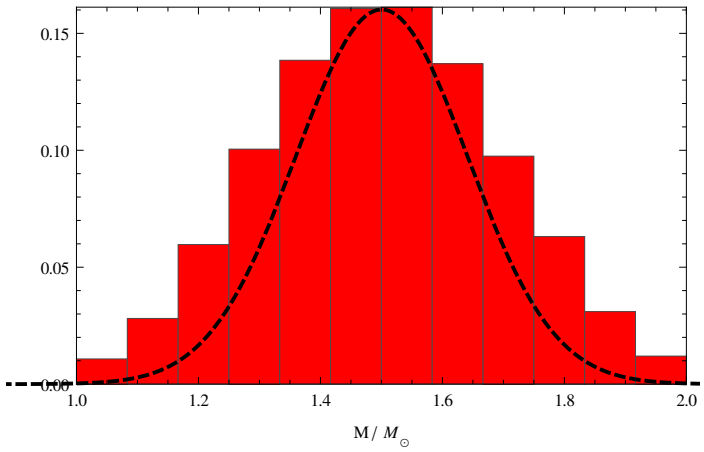

Figure 4.7: Histogram with the hypothesized mass of newly born NS. The distribution is a gaussian but with cutted tails. However it can be fitted with a gaussian with mean value $\mu = 1.5M_{\odot}$ and a $\sigma = 0.2M_{\odot}$.

Using the assumed temporal evolution of mass, we randomly generate stars at fixed rate time. For instance we show in Figure 4.8 the distribution after $5t_p$ and $10t_p$, where t_p is the time that a star last to reach the TS configuration, when the rate of generation of stars is of 10 stars per t_p. The column centered in zero shows the number of stars that after some times decays in BHs.

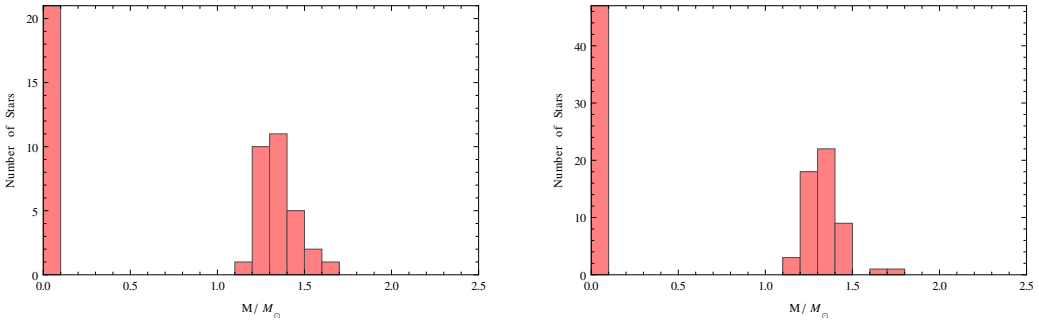

Figure 4.8: Distribution of Mass for stars randomly generated in time after $t_p = 5$(left) and $t_p = 10$ (right). The columns centered around zero shows the stars that have decayed in BH. It is possible to note that massive stars are present

With the rate time one order of magnitude bigger than the evolution time we are approximating what told in the previous section, i.e. the transition

time is slower than the cooling time of a NS, so the process of transformation could be considered as adiabatic, as theorized. It is very interesting to note that NS big masses state are populating when the process of generating NS is not finished. This is in agreement with our assumption that the observed NS with big masses observed in the present day, if it is no subject to accretion of matter, could be a young star and might decay during its evolution in a BH.

It is very interesting to note the distribution of star when we wait for a long time after the process of generations ends. We show our results in Figure 4.9. For asymptotically large times, only TS with mass smaller than

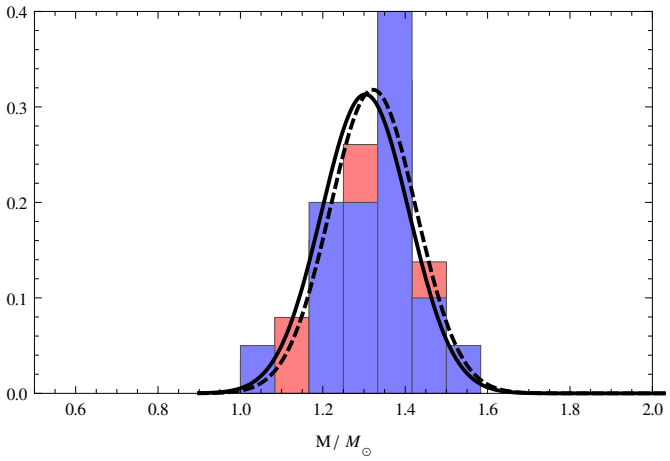

Figure 4.9: Asymptotic mass distribution for stars randomly generated in time (in red) and observed double NS masses (in blue). We have fitted the Asymptotic mass distribution with a gaussian(solid black line). The parameters of this gaussian are: $\mu = 1.30 M_\odot$ and $\sigma = 0.11 M_\odot$ in a good agreement with the parameters of gaussian distribution of observed double NS mass (dashed black line).

$(1/\sqrt{2})M_{\rm NS}^{\rm max}$ will survive. Let us stress, that radii of such stars should of about $\sqrt{2}$ times smaller than the radii of ordinary NS, as told before. Hence, for the sly EoS, the NSs with masses of about $2M_\odot$ should be still rather young but by the time they should collapse to BHs and only NS with mass less than 1.45 $M_\odot$ can survive, full $n - \bar{n}'$ conversion forming more compact objects, with radii reduced from initial 12 km to final 8.5 km. The compactness of these objects can have interesting implications for merger of NS binaries, in particular on the features of the GW signal induced by this merger which is also known as a main source of production of heavy elements (heavier than iron, and gold in particular) in the Universe. Moreover this mechanism produces BH with a mass of about $1.5 M_\odot$ without any violent explosion.

In Figure 4.9, we fitted the asymptotic mass distribution obtained with a gaussian. The parameters of the gaussian found are $\mu = 1.30 M_\odot$ and $\sigma = 0.11 M_\odot$. This is in qualitative agreement with the observed double NS mass distribution (whose values are as told before, $\mu = 1.32 M_\odot$ and $\sigma = 0.1 M_\odot$). However some discrepancies can be noted in Figure 4.9.

The source of these discrepancies can be different. First of all for this toy model the assumption that massive NS are young while double NS are old could be over simplistic. An estimation of the age of pulsars can be found on Pulsar Database [269] in which all the parameters known of several pulsars are reported. The estimation of Pulsar's age is the characteristic time, defined in the first Chapter in Eq. (1.9):

$$t_c = \frac{P}{2\dot{P}}. \tag{4.38}$$

Despite this estimation seems to be in qualitative agreement with Crab pulsar age, we cannot trust it for the other pulsars, due to the lack of information on the pulsar's history. Typical pulsar age are in between $10^9 - 10^{14}$ years but it seems that no correlation between type of NS, masses and age is present. Moreover, the estimate of the characteristic age has been obtained in the magnetic dipolar field limit. This is another possible source of error, because of the lack of information on the nature of the NS magnetic field. For all these reasons, it is very challenging to estimate with good accuracy the age of NS, so we can speculate that our assumption is reasonable. Another possible source of error in our model is the low statistic. Our distribution is obtained for a very long time and with the generation of thousand of stars. Differently, the known masses of double NS are only 20. Of course more statistic is needed to prove our results. Lastly, we have no information on the distribution of mass after supernovae explosion, so our assumption on newly born NS mass distribution can induce errors in the distribution of the temporal evolved masses.

Chapter 5

Radial Oscillations of Compact Stars

The radial oscillations of relativistic stars is an old problem. The equation governing the dynamical stability of the radial mode oscillations were derived by Chandrasekar [271, 272] by a linear response expansion. After this pioneristic study, radial modes of CS have been investigated by several authors [273, 276, 279, 281–283]. The relevance of radial oscillations is due to their stability implication: a star is stable if the fundamental eigenfrequency associated to radial oscillations, i.e. oscillations of pressure, is real. Indeed, the equations associated to radial oscillations form a Sturm-Liouville problem. One characteristic of Sturm-Liouville problem is the hierarchy of the eigenfrequencies. Indeed, the eigenfrequencies are real, following that $\omega_0 < \omega_1 < \cdots < \omega_n$. However, solutions in GR must be found numerically. Despite radial oscillations are not coupled with gravitational waves (see, Birkoff theorem [5]) we believe that they are responsible of energy transmission in supernovae explosion, so they could have a fundamental relevance in the matter expulsion from compact object [273]. Furthermore, as told in [274], the study of the instability through radial oscillation is of fundamental relevance in the constructions of quasar model.

Regarding the stability of CSs, a null eigenfrequency mode should be obtained at maximum of the mass-radius diagram, that is at the last stable configuration [3]. Our goal is to test a new numerical method to obtain the eigenfrequencies and the eigenfunctions of the radial oscillations and to test the paradigm that the last stable configuration corresponds to the maximum of the mass-radius diagram. In this chapter we briefly report some relevant literature results and than we enter into details of our method.

5.1 Radial oscillation in Newtonian Limit

A long discussion of radial oscillation in the Newtonian limit has been done in [3] and here we report the main passages. The hydrostatic equilibrium of a fluid is described by the equations:

$$\frac{\partial \rho}{\partial t} + \nabla \cdot (\rho \mathbf{v}) = 0, \tag{5.1}$$

$$\frac{d\mathbf{v}}{dt} = -\frac{1}{\rho}\nabla p - \nabla \phi, \tag{5.2}$$

i.e. the continuity equation and the Euler's Equation. The gravitational potential in the Newtonian theory is the solution of the Poisson's equation:

$$\nabla^2 \phi = 4\pi G \rho. \tag{5.3}$$

In order to study the perturbation of a fluid two possible descriptions are possible: the *Eulerian* and the *Lagrangian* ones. In the Eulerian description one studies the changes on the fluid variables in a particular point of space while Lagrangian description follows one element of fluid in its evolution. Following [3], if we define as $Q(\mathbf{x}, t)$ a generic attribute of the perturbed flow and $Q_0(\mathbf{x}, t)$ the relative function of unperturbed background, we can define the Eulerian perturbation as:

$$\delta Q \equiv Q(\mathbf{x}, t) - Q_0(\mathbf{x}, t). \tag{5.4}$$

While, defining a generic *Lagrangian displacement* $\xi(\mathbf{x}, t)$ which connects fluid element in the unperturbed state to the corresponding in the perturbed state, we can define the Lagrangian perturbation as [3]:

$$\Delta Q \equiv Q[\mathbf{x} + \xi(\mathbf{x}, t), t] - Q_0(\mathbf{x}, t). \tag{5.5}$$

So, it is possible to relate the Lagrangian and the Eulerian perturbation as:

$$\Delta = \delta + \xi \cdot \nabla. \tag{5.6}$$

The dynamics of the perturbation is governed by the perturbed Euler's Equation [3]:

$$\Delta \left(\frac{dv^i}{dt} + \frac{1}{\rho}\nabla_i p + \nabla_i \phi \right) = 0, \tag{5.7}$$

where i indicates the directional component. Using:

$$\Delta \mathbf{v} = \frac{d}{dt}(\mathbf{x} + \boldsymbol{\xi}) - \frac{d\mathbf{x}}{dt} = \frac{d\xi}{dt}, \tag{5.8}$$

and known relations between derivatives, see for details [3], we can obtain the perturbed Euler's Equation:

$$\frac{d^2\xi'}{dt^2} - \frac{\Delta\rho}{\rho^2}\nabla_i p + \frac{1}{\rho}\nabla_i \Delta p + \nabla_i \Delta\phi - \nabla_i \xi^j \left(\frac{1}{\rho}\nabla_j p + \nabla_j \phi\right) = 0. \tag{5.9}$$

This equation can be simplified multiplying it for ρ and considering v^i the only non vanishing component of velocity [3]:

$$\rho\frac{d^2\xi'}{dt^2} - \frac{\Delta\rho}{\rho}\nabla_i p + \nabla_i \Delta p + \rho\nabla_t \Delta\phi = 0. \tag{5.10}$$

The Eq. (5.10) is the dynamical equation of motion for the perturbations [3]. Supposing that we can factorize the time dependence of the perturbations:

$$\xi_i = e^{i\omega t} X_i(\mathbf{x}), \tag{5.11}$$

we can rewrite the Eq. (5.10), as [3]

$$-\omega^2 \rho \xi^i(\mathbf{x}) = L_{ij}\xi^j(\mathbf{x}), \tag{5.12}$$

where:

$$\begin{aligned} L_{ij}\xi^j = \quad & \nabla_i(\Gamma p \nabla_j \xi^j) - (\nabla_j \xi^j)\nabla_i p + (\nabla_i \xi^j)\nabla_j p - \\ & -\rho\xi^j \nabla_j \nabla_i \phi - \rho\nabla_i \delta\phi, \end{aligned}$$

and Γ is the adiabatic index:

$$\Gamma = \frac{\partial \ln p}{\partial \ln \rho}. \tag{5.13}$$

For a static spherical symmetric star this equation can be written as:

$$\frac{d}{dr}\left(\Gamma p \frac{1}{r^2}\frac{d}{dr}\left(r^2\xi\right)\right) - \frac{4}{r}\frac{dp}{dr}\xi + \omega^2\rho\xi = 0 \ . \tag{5.14}$$

which is a homogeneous second order differential equation with variable coefficient. The boundary condition for the radial perturbations are [3]:

$$\xi = 0 \text{ at } r = 0, \tag{5.15}$$

$$\Delta p = 0 \text{ at } r = R, \tag{5.16}$$

with R the radius of the star. While the first equation of Eq. (5.16) is quite obvious in spherical symmetry, the second tells us that an element lying at

the unperturbed surface is displaced of a non vanishing quantities. Since the variation of the pressure is [3]:

$$\Delta p = -\Gamma p \frac{1}{r^2}\frac{d}{dr}(r^2\xi), \tag{5.17}$$

the condition that Δp vanishes at $r = R$, implies that:

$$\xi \text{ finite at } r \sim R. \tag{5.18}$$

The Eq. (5.14), with the defined boundary condition is a *Sturm-Liouville* eigenvalue equation for ω^2 [3].

It is possible to find an analytic solution if we consider a spherical star with constant density, i.e. with an adiabatic index $\Gamma = \infty$ (incompressible gas). That means that we can define the total mass as:

$$m(r) = \frac{4}{3}\pi\rho r^3, \tag{5.19}$$

and the pressure is:

$$p(r) = \frac{2\pi G\rho^2}{3}(R^2 - r^2). \tag{5.20}$$

Using the last expression in the Eq.(5.14) and the prime for the derivative respect to $x = r/R$ we obtain [3]:

$$\left(1 - x^2\right)\xi'' + \left(\frac{2}{x} - 4x\right)\xi' + \left(\frac{8\alpha + \omega^2\rho - 2\Gamma_1\alpha}{\Gamma_1\alpha} - \frac{2}{x^2}\right)\xi = 0, \tag{5.21}$$

where Γ_1 is the adiabatic index governing the perturbation [3]. In general Γ_1 is not equal to Γ, where the latter is the adiabatic index governing the background pressure-density relation.

The solution to this equation is obtainable expanding the displacement as power series:

$$\xi = \sum_{n=0}^{\infty}(n+s)a_n x^{n+s} \quad \text{with } a_0 \neq 0. \tag{5.22}$$

Calculating the first and second derivative and substituting them into Eq. (5.21) we obtain the recursive relation for the coefficients of the series:

$$\frac{a_{n+2}}{a_n} = \frac{n^2 + 5n + 4 - A}{n^2 + 7n + 10}, \tag{5.23}$$

valid for even n, while $a_1 = a_3 = a_5 = ... = 0$ for odd n. The series is divergent, so in order to obtain solution we have to chose a suitable A:

$$A = n^2 + 5n + 4, \quad n = 0, 2, 4, ... \tag{5.24}$$

that implies:

$$\omega^2 = \frac{2\pi}{3} G\rho \left[\Gamma\left(n^2 + 5n + 6\right) - 8\right] \tag{5.25}$$

As discussed in [3], the star is unstable if $\Gamma < 4/3$. Furthermore in [3] is been demonstrated that the *turning point*, i.e. the point in which:

$$\frac{dm}{d\rho_c} = 0, \tag{5.26}$$

where ρ_c is the central density of the star, correspond to the last stable configuration. This result was obtained using a polytropic EoS but, as discussed before, any nuclear EoS can be described by properly joining polytropes. For that reason this result is generally accepted for all EoS of matter.

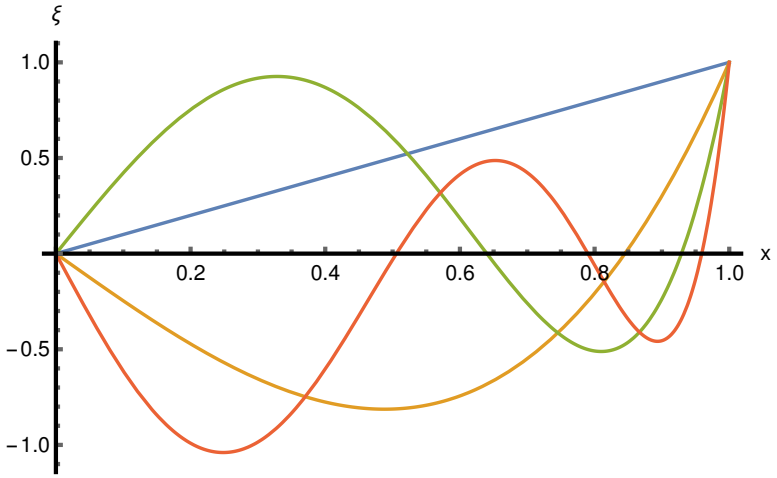

Figure 5.1: Normalized radial displacement $\xi(r)/\xi(R)$ in function of $x = r/R$ for the first four oscillations modes in the Newtonian limit using a constant density EoS. The mode with $n = 0$ is a straight line and do not have any nodes.

5.2 Radial oscillation in General Relativity

Let us now derive the equation that govern the radial perturbations in General relativity perturbing both the fluid and the metric variables. However, following the same approach used in [271,275] we assume that the radial oscillations are infinitesimal adiabatic perturbations. We are in the limit of *linear response theory* that means that metric and fluid functions are linearized.

We consider spherical symmetric and static stars described by the well known Schwarzschild Metric Eq.(2.2):

$$ds^2 = -e^{2\phi_0} dt^2 + e^{2\lambda_0} dr^2 + r^2 \left(d\theta^2 + \sin^2\theta d\phi^2\right),$$

where the subscript 0 specify the unperturbed quantities. Let us recall that for the Schwarschild solution we have:

$$\lambda_0' = \frac{1}{2r}\left(1 - e^{2\lambda_0}\right) + 4\pi r \rho_0 e^{2\lambda_0}, \tag{5.27}$$

and:

$$\phi_0' = -\frac{1}{2r}\left(1 - e^{2\lambda_0}\right) + 4\pi r p_0 e^{2\lambda_0} \quad . \tag{5.28}$$

From the TOV's equation we can relate the prime derivative of the pressure with the prime derivative of the gravitational potential as:

$$p_0' = -\left(\rho_0 + p_0\right)\phi_0'. \tag{5.29}$$

In order to perturb the metric functions, let us define the perturbed quantities $\phi(r)$ and $\lambda(r)$, thus we can write the metric function as:

$$ds^2 = -e^{2\phi}dt^2 + e^{2\lambda}dr^2 + r^2\left(d\theta^2 + \sin^2\theta d\phi^2\right). \tag{5.30}$$

Similarly to the Newtonian case, we can write the perturbations of the fluid and metric function as Eulerian perturbation:

$$\begin{aligned}
\phi(t,r) &= \phi_0(r) + \delta\phi(t,r) \\
\lambda(t,r) &= \lambda_0(r) + \delta\lambda(t,r) \\
p(t,r) &= p_0(r) + \delta p(t,r) \\
\rho(t,r) &= \rho_0(r) + \delta\rho(t,r) \\
n(t,r) &= n_0(r) + \delta n(t,r) \quad ,
\end{aligned}$$

or lagrangian perturbations:

$$\begin{aligned}
\Delta p(t,r) &= p[t, r + X(t,r)] - p_0(r) \approx \delta p + p_0' X \\
\Delta\rho(t,r) &= \rho[t, r + X(t,r)] - \rho_0(r) \approx \delta\rho + \rho_0' X \\
\Delta n(t,r) &= n[t, r + X(t,r)] - n_0(r) \approx \delta n + n_0' X \quad ,
\end{aligned}$$

with $X(r)$ displacement function.

Through the conservation of the baryon number, $\nabla \cdot (n\mathbf{u})$, where u is the four-vector associated to the velocity of perturbation, following [5], we can obtain:

$$\frac{dn}{d\tau} = -n(\nabla \cdot \mathbf{u}), \tag{5.31}$$

where this derivative is made along the fluid world line. In term of Lagrangian perturbation we obtain:

$$\frac{d\Delta n}{d\tau} = -n(\nabla \cdot \boldsymbol{u}). \tag{5.32}$$

Supposing that the only non vanishing component are the temporal and the radial component of the four-velocity we can obtain:

$$\frac{u^r}{u^t} = \left(\frac{dr/d\tau}{dt/d\tau}\right) = \left(\frac{dr}{dt}\right) = \frac{\partial X}{\partial t} \equiv \dot{X} \tag{5.33}$$

Using this relation in the metric function, and dividing for $d\tau^2$, we obtain:

$$\left(u^t\right)^2 e^{2\phi} - \left(u^r\right)^2 e^{2\lambda} = 1. \tag{5.34}$$

Let us now get the result to the first order of X:

$$u^t = e^{-\phi} = e^{-\phi_0}(1 - \delta\phi) \qquad u^r = \dot{X} e^{-\phi_0} \tag{5.35}$$

Using the explicit form of the components of four-velocity and simple relations of the metric, see [5] for more details, we obtain the perturbation of the baryon number:

$$\Delta n = -n_0 \left[r^{-2} e^{-\lambda_0} \frac{d}{dr}\left(r^2 e^{\lambda_0} X\right) + \delta\lambda \right] \quad . \tag{5.36}$$

Using the adiabatic limit, i.e. considering that negligible heat are transferred during the radial vibrations, it is possible to relate the Lagrangian perturbation of number density with the Lagrangian perturbation of pressure:

$$\left(\frac{\partial \ln p}{\partial \ln n}\right)_s \equiv \Gamma = \frac{n}{p}\frac{\Delta p}{\Delta n}, \tag{5.37}$$

where Γ is GR analogous of the Newtonian adiabatic index. Combining this equation with Eq. (5.36), one obtains the Eulerian perturbation of pressure [5]:

$$\delta p = -\Gamma p_0 \left[r^{-2} e^{-\lambda_0 \left(r^2 e^{\lambda_0} X\right)'} + \delta\lambda \right] - X p_0' \quad . \tag{5.38}$$

In order to calculate the perturbation of energy density, as shown in [5], we can use the energy conservation: $\mathbf{u} \cdot (\nabla \cdot \mathbf{T}) = \mathbf{0}$. From this relation follows that:

$$\frac{d\rho}{d\tau} = \frac{\rho + p}{n}\frac{dn}{d\tau}. \tag{5.39}$$

This equation can be rewrite in terms of Lagrangian perturbation:

$$\frac{d\Delta\rho}{d\tau} = \frac{\rho + p}{n}\frac{d\Delta n}{d\tau} \quad , \tag{5.40}$$

and can be integrating in time, assuming an expansion to the first order of all the perturbed variables:

$$\Delta\rho = \frac{\rho_0 + p_0}{n_0}\Delta n, \tag{5.41}$$

where we are using that the constant of integration is zero because when $\Delta n = 0$, $\Delta\rho = 0$ as well. From the last equation, using Eq. (5.38) and writing the Eulerian perturbation of energy density $\delta\rho$ in function of its Lagrangian perturbation, we obtain [5]:

$$\delta\rho = -\left(\rho_0 + p_0\right)\left[r^{-2}e^{-\lambda_0}\left(r^2 e^{\lambda_0}X\right)' + \delta\lambda\right] - X\rho_0' \quad . \tag{5.42}$$

Let us now linearize the Einstein field equation, in particular the component $G_{\hat{r}\hat{r}}$ and $G_{\hat{t}\hat{r}}$. The Einstein field equations in a orthonormal frame, (see [5] for more details on the calculation), can be write as:

$$\begin{aligned} G_{\hat{r}\hat{t}} &= 2(\dot{\lambda}/r)e^{-(\lambda+\phi)} \simeq 2r^{-1}e^{-(\lambda_0+\phi_0)}\delta\dot{\lambda} \\ G_{\hat{r}\hat{r}} &= 2\left(\phi'/r\right)e^{-2\lambda} + r^{-2}\left(e^{-2\lambda} - 1\right) \\ &\simeq \left(G_{\hat{r}\hat{r}}\right)_0 + 2r^{-1}e^{-2\lambda_0}\delta\phi' - 2e^{-2\lambda_0}\left(2r^{-1}\phi_0' + r^{-2}\right)\delta\lambda \end{aligned} \quad , \tag{5.43}$$

where the dot indicates the time derivative, and prime indicates the radial derivative as usual. Remembering that the stress-energy tensor is:

$$T_{\hat{\alpha}\hat{\beta}} = (p+\rho)u_{\hat{\alpha}}u_{\hat{\beta}} + p\eta_{\alpha\beta}, \tag{5.44}$$

with the component of the four velocities obtained, using the Eqs. (5.38) and (5.42), we obtain [5]:

$$T_{\hat{r}\hat{t}} = -(\rho_0 + p_0)e^{\lambda_0-\phi_0}\dot{X} \qquad T_{\hat{r}\hat{r}} = p_0 + \delta p. \tag{5.45}$$

So, integrating the Einstein equation with respect to time and choice the constant of integration so $\delta\lambda = 0$ when $X = 0$ we obtain:

$$\delta\lambda = -4\pi\left(\rho_0 + p_0\right)re^{2\lambda_0}X = -\left(\lambda_0' + \phi_0'\right)X \tag{5.46}$$

and:

$$\delta\phi' = -4\pi\Gamma p_0 r^{-1}e^{2\lambda_0+\phi_0}\left(r^2e^{-\phi_0}X\right)' + \left[4\pi p_0' r - 4\pi\left(\rho_0 + p_0\right)\right]e^{2\lambda_0}X \quad . \tag{5.47}$$

The dynamic evolution of the fluid displacement $X(t,r)$ is governed by the Euler equation [5]:

$$(\rho + p)\mathbf{a} = -\left[\nabla\mathbf{p} + \left(\nabla_{\mathbf{u}}\mathbf{p}\right)\mathbf{u}\right] \tag{5.48}$$

where $\mathbf{a}$ is the four-acceleration, that as shown in [5]:

$$a_r = \phi_0' + \delta\phi' + e^{2(\lambda_0-\phi_0)}\ddot{X}. \tag{5.49}$$

This equation, combined with pressure and energy density expanded at the first order gives the Euler equation gives:

$$(\rho_0 + p_0)\, e^{2(\Lambda_0 - \phi_0)} \ddot{X} = -\delta p' - (\delta\rho + \delta p)\phi_0' - (\rho_0 + p_0)\, \delta\phi' \quad . \tag{5.50}$$

Consider the harmonic dependence on time of X, i.e. considering as for Newtonian perturbation that:

$$X(r,t) = e^{i\omega t} X(r), \tag{5.51}$$

we obtain the dynamic equation describing the radial oscillations of a star [5, 275]:

$$-\omega^2 W \ddot{\xi} = (P\xi')' + Q\xi, \tag{5.52}$$

with:

$$\xi = r^2 e^{-\phi} X(r) \tag{5.53}$$

$$W r^2 = (\rho + p)\, e^{3\lambda + \phi} \tag{5.54}$$

$$P r^2 = \gamma p e^{\lambda + 3\phi} \tag{5.55}$$

$$Q r^2 = e^{\lambda + 3\phi}(\rho + p)\left((\phi')^2 + \frac{4\phi'}{r} - 8\pi e^{2\lambda} p\right) \tag{5.56}$$

so ξ is a renormalized displacement and the functions P, Q, W are determined by the equilibrium structure of the star. The function $\gamma = (p + \rho)/p \;\; dp/d\rho$ is the adiabatic index. In the last equation, and as for the following of this chapter, we omit the subscript 0 because of all the quantities used refer to the equilibrium configuration.

The Eq. (5.60) defines a *Sturm-Liouville* problem as in the Newtonian case. Our goal is to find a simple way to find eigenvalues and eigenvectors for different EoS of the nuclear matter. For any Sturmian system that the eigenvalues ω_n^2 are ordered:

$$\omega_n^2 < \omega_{n+1}^2 \tag{5.57}$$

meaning that the fundamental $0th$ mode has the lowest frequency. From this follows that whether $\omega_0^2 > 0$ the frequency of the lowest mode is real and the solution is purely oscillatory. While, if $\omega_0^2 < 0$ the frequency of the lowest mode have a non vanishing imaginary part, and this situation correspond to an exponentially growing solution leading to a instability [275]. It is believed that the fundamental mode ω_0 becomes imaginary when the central density becomes larger then the critical value for which the mass of the star is maximal and the star should collapse into a BH. When the central density is equal to the critical value (that depends on EoS of the matter),

the lowest frequency might be zero. Using these properties for known EoS is an affordable and strong test of validity of our method.

In order to solve the radial oscillation problem two boundary condition are required. The boundary condition at the center of the star is:

$$\xi(r) = 0, \tag{5.58}$$

that means obviously that the radial perturbation must vanish at $r = 0$. Moreover, similarly to the Newtonian case at the surface the Lagrangian variation of the pressure must vanish:

$$\Delta p = 0, \qquad \text{meaning that} \quad \gamma\, p\, \xi' = 0. \tag{5.59}$$

As in the Newtonian case, from the last boundary conditions follows that a fluid element lying at the surface is displaced of a non vanishing quantities.

Eq. (5.52)can be written in another way [275]:

$$\begin{aligned} &c_{\mathrm{s}}^2 \xi'' + \left((c_{\mathrm{s}}^2)' - Z + 4\pi r \gamma p \mathrm{e}^{2\lambda} - \phi' \right) \xi' \\ &+ \left[2\left(\phi'\right)^2 + \tfrac{2m}{r^3} \mathrm{e}^{2\lambda} - Z' - 4\pi(\rho + p) Z r \mathrm{e}^{2\lambda} + \omega^2 \mathrm{e}^{2\lambda - 2\phi} \right] \xi = 0 \end{aligned} \tag{5.60}$$

where the square of the speed of sound c_s is calclulated from the unperturbed background for a specific EoS [275]:

$$c_{\mathrm{s}}^2 = \frac{\mathrm{d}p}{\mathrm{d}\rho} \tag{5.61}$$

and:

$$Z(r) = c_{\mathrm{s}}^2 \left(\phi' - \frac{2}{r} \right) \quad . \tag{5.62}$$

Eq. (5.60) shows that the Sturmian problem is dependent on the behavior of speed of sound. In the following chapter we describe our general method to solve the eigenvalue problem, while in the last chapter we focus on star models constructed with non continuous speed of sound in order to scrutinize whether a discontinuity could lead to new stability condition.

5.3 Numerical Method

Several numerical methods have been developed for solving the differential Eq. (5.52). [276,277]. We based our model on the method proposed by *Glass and Harpaz* (also used by Kokkotas [275]), referred as *Numerov Method*. It is based on the discretization of the radial coordinate in N steps, transforming

the Sturm-Liouville differential equation in an eigenvalue problem. A correct implementation of the boundary conditions is extremely important, as the frequencies are quantized and therefore strongly depend on the behavior of the radial displacement at $r = 0$ and $r = R$. Thus we require that the left boundary condition correctly reproduces the known behavior close to the stellar center. Regarding the right boundary condition, we do not impose it, but we renormalize the obtained eigenfunction to 1

More in details, the equations Eq. (5.52) (or equivalently Eq. (5.60)) can be written as:

$$A_1\xi(r)'' + A_2\xi(r)' + A_3\xi(r) = \omega^2\xi(r), \tag{5.63}$$

where of course we define from Eq. (5.52):

$$A_1(r) = \frac{P(r)}{W(r)}, \quad A_2(r) = \frac{P'(r)}{W(r)} \quad A_3(r) = \frac{Q(r)}{W(r)}. \tag{5.64}$$

We discretize the radial coordinate as:

$$r_n = n\alpha \tag{5.65}$$

with $\alpha = R/N$ and N the total number of steps. Using finite difference schemes for derivatives of the displacement, as done in [276], we obtain the discretized derivatives of the displacement:

$$\xi'(r_n) = \frac{\xi(r_{n+1})-\xi(r_{n-1})}{2h} + \mathcal{O}(h^2), \tag{5.66}$$

$$\xi''(r_n) = \frac{\xi(r_{n-1})+\xi(r_{n+1})-2\xi(r_n)}{h^2} + \mathcal{O}(h^2), \tag{5.67}$$

where we assume $h = r_{n+1} - r_n$ the discretization step. Then the Eq. (5.63) turns to:

$$\begin{aligned}\xi(r_{n+1})\left(\frac{A_1(r_n)}{h^2} + \frac{A_2(r_n)}{2h}\right) + \xi(r_{n-1})\left(\frac{A_1(r_n)}{h^2} - \frac{A_2(r_i)}{2h}\right) + \\ +\xi(r_i)\left(A_3(r_i) - \frac{2A_1(r_i)}{h^2}\right) = \omega^2\xi(r_i) \quad ,\end{aligned} \tag{5.68}$$

or in more compact form:

$$\xi(r_{n+1})f_i + \xi(r_{n-1})g_i + \xi(r_n)h_i = \omega^2\xi(r_n) \quad . \tag{5.69}$$

From the last relations it is possible to construct a tridiagonal matrix A, with

dimension $N \times N$:

$$A = \begin{pmatrix} h_0 & f_0 & 0 & 0 & \cdots & 0 & 0 & 0 \\ g_1 & h_1 & f_1 & 0 & \cdots & 0 & 0 & 0 \\ 0 & g_2 & h_2 & f_2 & \cdots & 0 & 0 & 0 \\ \vdots & & & & \ddots & & & \vdots \\ 0 & 0 & 0 & \cdots & g_{N-2} & h_{N-2} & f_{N-2} & 0 \\ 0 & 0 & 0 & \cdots & 0 & g_{N-1} & h_{N-1} & f_{N-1} \\ 0 & 0 & 0 & \cdots & 0 & 0 & g_N & h_N \end{pmatrix}. \tag{5.70}$$

From the matrix A we find the associated eigenvalues solving the characteristic equation:

$$(A - \omega_n^2 I)\xi = 0, \tag{5.71}$$

where $\xi^T = \begin{pmatrix} \xi(r_0) & \xi(r_1) & \xi(r_2) & \cdots & \xi(r_{N-2}) & \xi(r_{N-1}) & \xi(r_N) \end{pmatrix}$.

It is interesting to note that the matrix A is nearly symmetric. In fact two generic matrix element A_{nn+1} and A_{n+1n} are:

$$A_{n,n+1} = f(r_n) = \left(\frac{A_1(r_n)}{h^2} + \frac{A_2(r_n)}{2h} \right), \tag{5.72}$$

$$A_{n+1,n} = g(r_{n+1}) = \left(\frac{A_1(r_{n+1})}{h^2} - \frac{A_2(r_{n+1})}{2h} \right). \tag{5.73}$$

Even taking a very large number of steps so $r_n \approx r_{n+1}$, the different signs in the definition of the functions f and g yields a non symmetric matrix. Despite is not symmetric, it is possible to show that the eigenvalues of this matrix are reals if the product of the terms $A_{n+1,n}A_{n,n+1} > 0$ [278].

We tested this method studying the eigenfrequencies of stars with a polytropic EoS. Despite the very fast computational speed, the eigenvalues was strongly dependent on the number N of discretization steps. Furthermore we have compared our results with the Kokkotas' [275] results obtaining relevant discrepancies even taking an high number of steps ($N = 1000$ or even more). For instance, for central density of about $1. \times 10^{15}\mathrm{g/cm}^3$ and using a polytrope EoS with $\gamma = 2$, we obtained discrepancies of the order of 10%. Increasing central density the difference between the results is bigger. Moreover, differently from what we expect, we do not obtain that null eigenvalues correspond to the maximum stellar mass. Thus, this model give us some errors. The source of our errors come from the fact that using the method of Glass we are not correctly imposing the boundary condition of the problem.

Since the thermodynamic quantities are not defined for $r < 0$ and for $r > R$ we have to define the numerical derivatives close to the border. To

give the right behavior at surface of the star, we decided to change the last row of the matrix A using a backward finite difference scheme:

$$\xi'(r_N) = \frac{\xi(r_N - 2h) - 4\xi(r_N - h) + 3\xi(r_N)}{2h} \tag{5.74}$$

$$\xi''(r_N) = \frac{\xi(r_N - 2h) - 2\xi(r_N - h) + \xi(r_N)}{2h} \tag{5.75}$$

For the left boundary condition we have a similar problem. However, in this case we decided to use the known behavior of the solution close to the stellar center [275]:

$$\xi(r) = \xi_0 r^3 e^{-\phi} + \mathcal{O}(r^5). \tag{5.76}$$

To implement this condition we use a simple trick. In agreement with Eq. (5.76), close to the stellar center the first two discretized values of any eigenmode should be:

$$\xi_1 = C_1 r_{\rm min}^3 \qquad \text{and} \qquad \xi_2 = C_1 (r_{\rm min} + \epsilon)^3 \,. \tag{5.77}$$

where r_{min} is the minimum value considered in the numerical integration of the TOV equation. We set to 0 the terms $A_{1,1}$ and $A_{2,2}$, meaning that the only non vanishing terms of the first two rows of A are the terms $A_{1,2}$ and $A_{2,1}$, that we denoted with a_{12} and a_{21}. Thus, the matrix A has a 2×2 block:

$$\begin{pmatrix} 0 & a_{12} \\ a_{21} & 0 \end{pmatrix}. \tag{5.78}$$

From this assumption it follows that:

$$\begin{aligned} \omega^2 \xi_1 &= a_{12} \xi_2 \,, \\ \omega^2 \xi_2 &= a_{21} \xi_1 \,, \end{aligned} \tag{5.79}$$

which is the simplest way to link the first two values of the displacement close to the stellar center. Obviously, we do not know ω, therefore it seems that we cannot fix the values of a_{12} and a_{21}. However, from the previous equations we obtain that $a_{12} a_{21} = \omega^4$, and

$$\frac{a_{12}}{a_{21}} = \left(\frac{r_{\rm min}}{r_{\rm min} + \epsilon} \right)^6 \,, \tag{5.80}$$

which determines the ratio between these two matrix elements. Fixing the eigenmode for simplicity to $\omega^4 = 1$, we obtain that:

$$a_{12} = \frac{1}{a_{21}} = \left(\frac{r_{\rm min}}{r_{\rm min} + \epsilon} \right)^3 \,, \tag{5.81}$$

ρ_{cent}	R_K	R	M_K	M	ν_{KR}	ν_0
$(10^{15}\ g/cm^3)$	(km)	(km)	$(M_\odot)$	$(M_\odot)$	(kHz)	(kHz)
3.500	8.604	8.602	2.120	2.120	0.32*	0.63i
3.450	8.629	8.632	2.120	2.121	0.244	0.40i
3.400	8.655	8.653	2.120	2.121	0.620	0.134
3.200	8.763	8.761	2.118	1.126	1.140	0.963
3.000	8.881	8.879	2.111	2.112	1.519	1.385
2.600	9.140	9.138	2.075	2.076	2.151	2.052
2.200	9.419	9.417	1.988	1.989	2.716	2.636
1.800	9.672	9.670	1.809	1.810	3.235	3.166
1.400	9.784	9.782	1.484	1.484	3.665	3.601
1.000	9.491	9.489	0.977	0.978	3.870	3.813

Table 5.1: Comparison of the frequency of fundamental mode between the results of Kokkotas [275] and our result for a polytropic EoS with $\Gamma = 3$. Our results are of the order of the 5% lower than our result and as a consequence we find that the instability modes is reached for lower central densities.

and thus these matrix elements are now fixed. This will result in two spurious eigenvalues $\omega^2 = \pm 1$ in the spectrum. In the end, since we know the values of these two spurious eigenvalues, we can easily identify and remove them as well as the corresponding eigenvectors.

Using this trick we obtained very precise results. For instance, we show in Table 5.1 the frequencies of the first mode obtained using a polytropic EoS with $\Gamma = 3$ and $N = 500$. We compare our result with the ones obtained by Kokkotas in [275]. It is possible to note discrepancies of the order of few percent in the obtained results. The source of this error seems to be in the solution of TOV equation. Indeed, it seems that fixing a central energy density we obtain slightly different masses and radii.

We have developed several checks for state the reliability of our method. First of all we note that the results obtained are nearly independent from the number N of discretization step. For instance, in Table 5.2 we show the results obtained varying N with the same EoS used in Tab. 5.1. It is clear from Table 5.2 that using $N = 500$ is a good compromise between convergence speed and accuracy. Furthermore, we study the dependence of the lowest mode in function of the mass and on the central energy density. In Figure 5.2 we show this dependence choosing $N = 500$. As we expected the null mode coincides with the maximum mass. The same analysis have been done with several EoS, see Appendix A, obtaining similar result.

Regarding the radial eigenfunctionwe checked that the interpolated eigenvectors and the corresponding eigenfrequencies are solutions of the differen-

ρ_{cent}	ν_0	N
$(10^{15}\ g/cm^3)$	(kHz)	
1.000	3.816	300
1.000	3.817	400
1.000	3.813	500
1.000	3.813	1000
1.000	3.813	2000

Table 5.2: Dependence of fundamental eigenfrequency from the number of steps N. In table we show the results obtained with a polytropic EoS and adiabatic index $\Gamma = 3$.

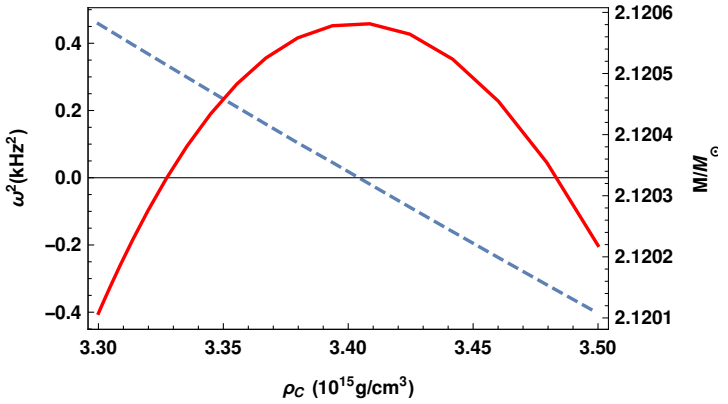

Figure 5.2: Fundamental frequency (dashed blue line) and mass (red solid line) dependence on the central energy density for a polytropic EoS with $\Gamma = 3$.

tial equation governing the radial fluctuations with an error of the order of few percent. An important nontrivial check is that the numerically obtained radial displacements have the correct behavior at the stellar center. Sufficiently close to the stellar center the radial displacement of any mode should behave as

$$X_n(r) = r^{-2}\xi_n(r)e^{\phi} \propto r\,, \tag{5.82}$$

which follows from Eq. (5.76). Since in the numerical procedure we impose this dependence, this is a test that we correctly implemented this condition; in other words, that adding the block matrix to the top-left corner of the matrix A does provide the correct behavior close to the stellar center. In Figure 5.3 we show the first four modes normalized with the respective value at the surface. All the shown eigenvectors follows the behavior desired providing reliability to our method.

So far, we solved the problem for relatively simple EoS (polytropic, interpolated and EoS for SSs). As already dissussed, from the Eq. (5.60) we

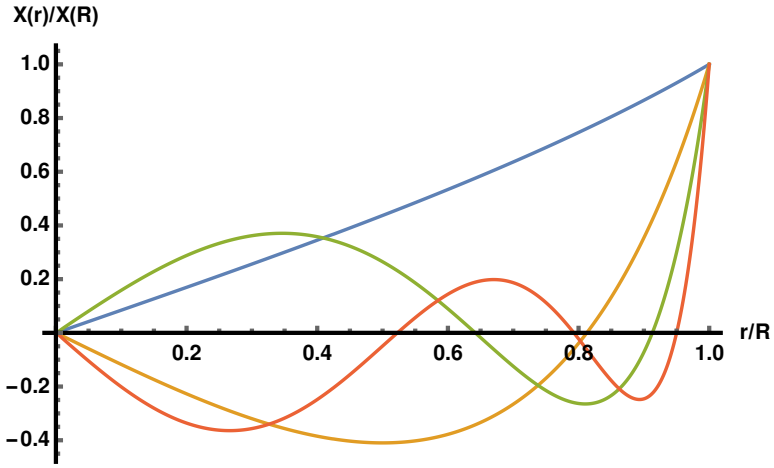

Figure 5.3: First four modes of normalized radial displacement as a function of the radial coordinate obtained for a polytropic EoS with $\Gamma = 3$ for $\rho_c = 1.10^{15}\text{g/cm}^3$. The normalization have been done dividing the radial displacement for its value at the surface of the star

immediately see that the problem is dependent on the speed of sound inside the star, thus the next step is the study of radial oscillation for stars with discontinuous speed of sound.

5.4 Radial Oscillation with a Phase transition

Looking at Eq. (5.60) a discontinuity of the c_s^2 function means that the coefficient of the second derivative of the displacement function is discontinuous. Moreover, in the A_2 term it is present the spatial derivative of c_s^2 that is a delta function. So assuming that the derivation of Eq. (5.60) is valid also for discontinuous coefficients, we could approximate the behavior of the discontinuity imposing an extra boundary condition.

For a static star one imposes that the pressure is a continuous function. Thus for the same reason we assume that $p = p_0 + \Delta p$ must be a continuous functions, meaning that Δp is continuous. Looking at the behavior of Δp, we have a boundary condition at the interface between two different phases:

$$c_s^2(\bar{r}_-)\xi(\bar{r}_-) = c_s^2(\bar{r}_+)\xi(\bar{r}_+) \tag{5.83}$$

where we have defined $\bar{r}$ the radius at which transition happens, $\bar{r}_-$ and $\bar{r}_+$ two points near the interface with $\bar{r}_- < \bar{r} < \bar{r}_+$.

In the neighborhood of $\bar{r}$ is not possible to define a Taylor expansion. However, we can use this trick: we expand backward the function $\xi(\bar{r}_-)$ and

forward the function $\xi(\bar{r}_+)$ meaning that:

$$\xi(\bar{r}_- - \varepsilon) = \xi(\bar{r}_-) - \varepsilon\xi'(\bar{r}_-), \tag{5.84}$$
$$\xi(\bar{r}_+ + \varepsilon) = \xi(\bar{r}_+) - \varepsilon\xi'(\bar{r}_+) \tag{5.85}$$

Let us now multiply the first for $c_s^2(\bar{r}_-)$ and the second for $c_s^2(\bar{r}_-)$ obtaining:

$$c_s^2(\bar{r}_-)\xi(\bar{r}_- - \varepsilon) = c_s^2(\bar{r}_-)\xi(\bar{r}_-) - \varepsilon c_s^2(\bar{r}_-)\xi'(\bar{r}_-), \tag{5.86}$$
$$c_s^2(\bar{r}_+)\xi(\bar{r}_+ + \varepsilon) = c_s^2(\bar{r}_+)\xi(\bar{r}_+) + \varepsilon c_s^2(\bar{r}_+)\xi'(\bar{r}_+). \tag{5.87}$$

Using the continuity of the function Δp we can define:

$$c_s^2(\bar{r}_-)\xi(\bar{r}_-) = c_s^2(\bar{r}_+)\xi(\bar{r}_+) = c_s^2(\bar{r})\xi(\bar{r}) \tag{5.88}$$

for $\bar{r}_- \approx \bar{r}_+$. Thus, subtracting the first equation to the second, we obtain:

$$\xi'(r)c_s^2(r) = \frac{1}{2\varepsilon}\left[c_s^2(\bar{r}_+)\big(\xi(\bar{r}_+ + \varepsilon) - \xi(\bar{r})\big) - c_s^2(\bar{r}_-)\big(\xi(\bar{r}_- - \varepsilon) - \xi(\bar{r}_-)\big)\right], \tag{5.89}$$

thus:

$$\xi'(\bar{r}_-) = \frac{1}{2\varepsilon}\left[\frac{c_s^2(\bar{r}_+)}{c_s^2(\bar{r}_-)}\big(\xi(\bar{r}_+ + \varepsilon) - \xi(\bar{r})\big) - \big(\xi(\bar{r}_- - \varepsilon) - \xi(\bar{r}_-)\big)\right], \tag{5.90}$$
$$\xi'(\bar{r}_+) = \frac{1}{2\varepsilon}\left[\big(\xi(\bar{r}_+ + \varepsilon) - \xi(\bar{r})\big) - \frac{c_s^2(\bar{r}_-)}{c_s^2(\bar{r}_+)}\big(\xi(\bar{r}_- - \varepsilon) - \xi(\bar{r}_-)\big)\right] \tag{5.91}$$

For the second derivative we use again the Taylor expansion up to the second order:

$$\xi(\bar{r}_- - \varepsilon) = \xi(\bar{r}_-) - \varepsilon\xi'(\bar{r}_-) + \frac{\varepsilon^2}{2}\xi''(\bar{r}_-), \tag{5.92}$$
$$\xi(\bar{r}_+ + \varepsilon) = \xi(\bar{r}_+) + \varepsilon\xi'(\bar{r}_+) + \frac{\varepsilon^2}{2}\xi''(\bar{r}_+). \tag{5.93}$$

Similarly for the first derivative, we multiply the first equation for $c_s^2(\bar{r}_-)$ and the second for $c_s^2((\bar{r}_+)$, obtaining:

$$c_s^2(\bar{r}_-)\xi(\bar{r}_- - \varepsilon) = c_s^2(\bar{r}_-)\xi(\bar{r}_-) - \varepsilon c_s^2(\bar{r}_-)\xi'(\bar{r}_-) + \frac{\varepsilon^2}{2}c_s^2(\bar{r}_-)\xi''(\bar{r}_-), \tag{5.94}$$
$$c_s^2(\bar{r}_+)\xi(\bar{r}_+ + \varepsilon) = c_s^2(\bar{r}_+)\xi(\bar{r}_+) + \varepsilon c_s^2(\bar{r}_+)\xi'(\bar{r}_+) + \frac{\varepsilon^2}{2}c_s^2(\bar{r}_+)\xi''(\bar{r}_+). \tag{5.95}$$

Thus applying the relation for the first derivative to the last equations we obtain:

$$\xi''(\bar{r}_-) = \frac{1}{\varepsilon^2 c_s^2(\bar{r}_-)}\left[c_s^2(\bar{r}_+)(\xi(\bar{r}_+ + \varepsilon) - \xi(\bar{r}_+) - c_s^2(\bar{r}_-)(\xi(\bar{r}_-) - \xi(\bar{r}_- - \varepsilon)\right] \tag{5.96}$$

$$\xi''(\bar{r}_+) = \frac{1}{\varepsilon^2 c_s^2(\bar{r}_+)}\left[c_s^2(\bar{r}_+)(\xi(\bar{r}_+ + \varepsilon) - \xi(\bar{r}_+) - c_s^2(\bar{r}_-)(\xi(\bar{r}_-) - \xi(\bar{r}_- - \varepsilon)\right] \tag{5.97}$$

We show the results of our method applying it to a star with a core made of deconfined quark joined with a polytrope for the external part. This kind of EoS can schematize an Hybrid star. For the description of the quark matter we use the EoS developed in [114], i.e. a parametrization of the pressure in function of the chemical potential:

$$p = \frac{3a_4}{4\pi^2}\mu^4 - \frac{3a_2}{4\pi^2}\mu^2 - B_{eff},$$

for the external part we use a polytropic EoS with $\Gamma = 3$. We chose the parameters in order to have

$$p_i(\bar{r}) = p_e(\bar{r}), \tag{5.98}$$

$$\rho_i(\bar{r}) = \rho_e(\bar{r}), \tag{5.99}$$

where p_i, p_e, ρ_i, ρ_e are the pressure and energy density of the internal and external part respectively. The used parameters are $a_4 = 0.7$, $a_2 = (200MeV)^2$ and $B_{eff} = (165MeV)^4$. We obtain a transition when the density is $\rho_{tr} = 3.52961 \times 10^{14}$. In Figure 5.4 we show the dependence of the fundamental eigenfrequency and of the mass on the central density of the star. It is very interesting to note that the maximum of the mass corresponds to the null fundamental eigenfrequency as in the previous cases.

Another test of reliability has been done looking at the Lagrangian perturbation of the pressure. In Figure 5.5 is shown the dependence of the Lagrangian perturbation of the pressure in function of the normalized radius of the star for a particular solution of the TOV obtained with $\rho_c = 1. \times 10^{15}\mathrm{g/cm}^3$. This function, as expected, is a continuous function so the total pressure, i.e. $p = p_0 + \Delta p$ is continuous, preserving the hydrostatic equilibrium. This condition have been imposed, so our method is working as desired. Despite this EoS is quite not reasonable (a_2 is too small and $\Gamma = 3$ is not a good approximation for the external part of an Hybrid star), it is an instructive good test of reliability of our method.

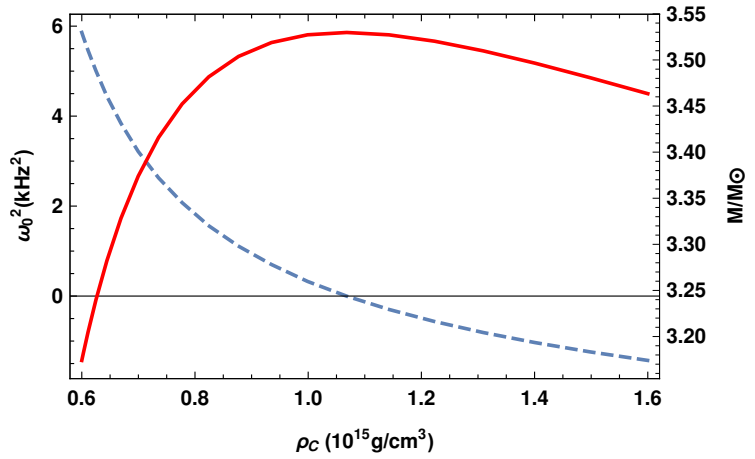

Figure 5.4: Fundamental eigenfrequency (dashed blue line) and mass (red solid line) dependence on the central energy density for a star with discontinuous speed of sound. The EoS is obtained joining a parametrized EoS for quark matter at the center and a polytrope with $\Gamma = 3$ for the external part

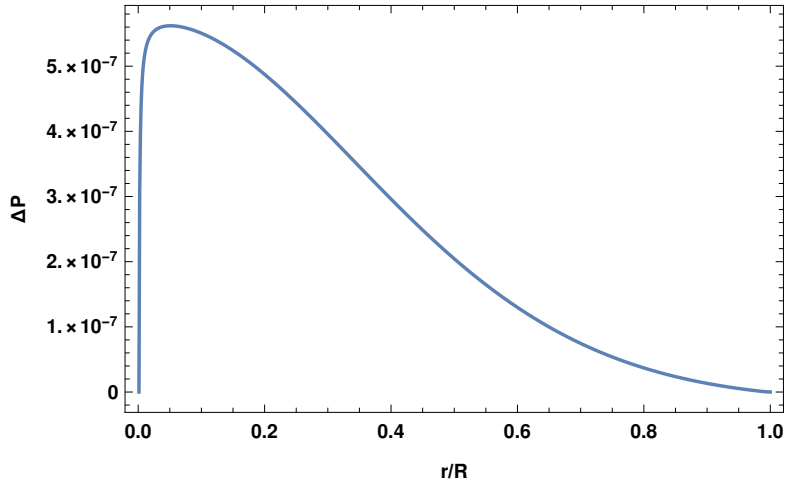

Figure 5.5: Lagrangian perturbation of the pressure for star with discontinuous speed of sound in function of the normalized radius As expected the function is a continuous function, meaning that no jumps of the pressure are present in the star, so the hydrostatic equilibrium is preserved.

We verify that when Δp is not a continuous function, for instance when we do not impose the continuity of the function $\xi(r)c_s^2(r)$, the null eigenfrequency appears at central matter density exceeding the central density of the maximum star. This could lead to a new mechanism of instability that needs further investigation.

Chapter 6

Conclusions

In this thesis we have examined three different aspects on Compact Stars stability.

The first aspect is the possible emission of Gravitational Wave Echoes from Strange Stars. Event GW170817 is a Gravitational Waves detection event occurred the 17th of August 2017 [147] with a total estimated mass $M = 2.73 M_{\odot}$ meaning that in the equal component mass limit the masses of the components are $m_1 = m_2 = 1.365 M_{\odot}$. Thus, the GW170817 is the first Gravitational Waves detection consistent with a merging of Neutron Stars. However, the total mass do not allow us to determine the nature of the final object: it could be either a Black Hole or an ultracompact Star. Moreover, it has been recently claimed by *Abedi et al.* [195] that a Gravitational Wave Echo signal at a frequency of 72 Hz and with a significance level of 4.2σ is present in the postmerger spectrum of the event GW170817.

An object with a compactness factor $C = M/R$ greater than 1/3 can emit Gravitational Wave Echoes [188, 194, 195]. The phenomenon responsible of the emission of Gravitational Waves Echoes is the partial trapping of Gravitational Waves due to an angular potential barrier. Pani and Ferrari [209] showed that an ultracompact star approaching the Buchdal's limit can emit Gravitational Waves Echoes at a frequency compatible with the tentative experimental observation. They obtained this result considering a simplified incompressible Equation of State. However, due to the divergent speed of sound, this case is unphysical and any realistic Neutron Star model is not enough compact to trap Gravitational Waves.

Since Strange Stars are more compact than ordinary Neutron Star, we have analyzed the possible emission of Gravitational Wave Echoes from a Strange Star described by the stiffest Equation of State possible: a simple Bag model $p = c_s^2(\rho - 4B)$ with speed of sound equal to 1 . We have found that even using this Equation of State the maximum stable configuration of

a Strange Star has a compactness slightly greater then 1/3 meaning that it does not approach the Buchdal's limit. As a consequence, the obtained Gravitational Waves Echo frequencies are of the order of tens of kilohertz. Thus, Strange Stars can emit Gravitational Waves Echoes but with frequencies at least two order of magnitude bigger than the experimental observation. This could be a signature that the remnant object is a Black Hole.

The second aspect is the possible mixing of Neutrons and Mirror neutrons in a Neutron Star. Mirror matter is a non conventional Dark matter candidate formed by particles that are identical copies of standard model particles but with right-handed interactions [219–221]. It has been supposed that Mirror particles have the same content, the same interactions, and the same coupling constants of ordinary particles. Thus, Mirror symmetry allow us to consider that Mirror particles and ordinary particles have also the same thermodynamic behavior. For this reason we have considered that Mirror matter is described by the same Equation of State of the ordinary matter.

Knowing that Mirror content and ordinary particles interact only through gravity, we have used a two fluid description. We have split the TOV equations into four coupled differential equations. In order to solve this system we have defined boundary conditions for ordinary and Mirror content and we have defined the parameter χ, that is the ratio between Mirror matter energy density and ordinary matter energy density. We have assumed that the transition between Mirror and ordinary matter is an adiabatic process with time scale much bigger than the Neutron Star cooling. For this reason we have decided to use standard Equation of State, in particular SLy and polytropic Equation of State. We have assumed that the mixing neutron-Mirror neutron is more efficient in the center of the star due to the larger baryon density. Hence we have considered a two concentric stars model with the one made of ordinary matter having larger mass, larger energy density and larger radius.

Stars acquire binding energy transforming ordinary matter into Mirror matter, thus this phenomenon should be energetically favored. In principle the fraction of Mirror matter could grow until it reaches the fraction of ordinary neutron matter. We have denoted this asymptotic configuration as Twin Stars. In a Twin Star all the quantities like radius, mass, pressure and energy density of the two content are equal. We have showed with simple arguments that using the same Equation of State the maximum mass of a Twin Star is $\sqrt{2}$ times smaller than the Neutron Star one. In addition, the respective radii are rescaled by the same factor meaning that the compactness factor of the maximum configuration is conserved. Whether radius determination become more precise it would be possible to observe stars with equal masses but different radii. This could be a signature of the presence of Mirror matter

in Neutron Stars and could have some implication on Gravitational Waves emission.

We have supposed that χ is dependent on time and we have assumed that the fraction of energy density due to the mirror matter is monotonically increasing. This assumption is justified because of the negligible transition rate mirror-ordinary matter. Thus, we have speculated that very massive Neutron Stars could be young stars exclusively composed of ordinary matter. We have assumed that the conversion occurs at constant baryon number meaning that not all Neutron Stars could reach the Twin Star configuration. Indeed, there exist a critical central density and any Neutron Star born with higher central energy density at some point decades into a Black Hole. This phenomenon should occur without any violent explosion. Since we have never observed it before, if any observation will be possible it could be a signature of the presence of Mirror matter in Neutron Stars. Assuming that a star could reach the Twin Star configuration, we have estimated the transformation rate obtaining a characteristic transformation time some order of magnitude bigger than the Universe lifetime. As a consequence this results could justify the observation of very massive Neutron Stars.

The mean value of the observed mass of double Neutron Star in binary system is $1.32M_{\odot}$. This value is not so far from the maximum mass of a Twin Star described by SLy equation, i.e. $1.45M_{\odot}$. For this reason we have developed a toy model to reproduce the observed Neutron Star masses distribution assuming that stars are described by SLy Equation of State. Furthermore, we have supposed that Neutron Star are generated with a gaussian mass distribution with mean value of $1.5M_{\odot}$ and $\sigma = 0.2M_{\odot}$. In this picture stars born with mass greater than $1.5M_{\odot}$ have a total number of baryons too high to reach a stable configuration and after some times collapse in a Black Hole. After some evolution time we have obtained a distribution in qualitative agreement with the observed double Neutron Star mass distribution.

The last aspect is the radial oscillation of stars. This problem was first analyzed by Chandrasekar [271, 272] by linear response theory. It turns that the equation governing the radial oscillation of stars is a Sturm-Liouville problem and our goal has been to solve it for spherical static stars. In this analysis the typical assumption is that the radial oscillations are infinitesimal adiabatic perturbations of the stellar configuration and can be described with the same Equation of State of the background.

Our numerical method is an extension of the Numerov's method that takes into account the boundary conditions properly. Numerov method consists in discretizing the stellar radius coordinate in N steps transforming the Sturm-Liouville problem in an eigenvalue problem [276]. We have developed an algorithm to quickly determine the eigenfrequency and the eigenmodes of

the stellar radial oscillation imposing the correct behavior of the eigenmodes at the stellar center. We have tested the extended Numerov's method for many different stellar model confirming the paradigm that the last stable configuration, corresponding to the null mode, coincide with the maximum mass. Several further tests have been proposed and all of them confirm the reliability of our novel numerical method.

An important aspect is that in any considered case we have found that the algorithm is very fast and the results are extremely stable even for $N = 500$ discretized points. Doubling the number of discretized points we have not found any appreciable change in the eigenfrequencies or in the eigenmodes meaning that we are able to drastically reduce the computational times without reducing accuracy.

An important role in the radial oscillation problem is played by interface discontinuity. In this thesis we have focused on the radial oscillation of stars described by an Equation of State with discontinuous speed of sound. In order to deal with this problem we have treated the interface discontinuity as an additional boundary condition and we have imposed that the total pressure, i.e. the background pressure plus its perturbation, must be continuous to preserve hydrostatic equilibrium. Even in this case, we have found that the fundamental mode is associated to the maximum mass unless we consider discontinuous pressure perturbation. Whether this condition is possible, the null eigenfrequency appears at central matter density exceeding the central density of the maximum star. This could lead to new instability condition that could be explored in future studies. Moreover, having a reliable numerical method for the radial oscillation of Compact Stars it is possible to explore some other aspect like density discontinuity and test new Equation of State.

Bibliography

[1] N.K. Glendenning, *Compact Stars. Nuclear Physics, Particle Physics, and General Relativity.* Springer (1996)

[2] P. Haensel, A.Y. Potekhin, and D.G. Yakovlev, *Neutron Stars 1. Equation of State and Structure.* Springer (2007)

[3] S.L. Shapiro, S.A. Teukolsky, *Black Holes, White Dwarfs, and Neutron Stars. The Physics of Compact Objects.* John Wiley & Sons (1983)

[4] F. Weber, *Pulsars as Astrophysical Laboratories for Nuclear and Particle Physics.* IoP (1999)

[5] C. W. Misner,K.S. Thorne,J.A. Wheeler,*Gravitation.* W. H. Freeman. (1973)

[6] S. Carroll, *Spacetime and Geometry. An introduction to General Relativity.* Addison Wisley. (1990)

[7] R. Feynman, *Feynman Lectures on Gravitation.* Addison Wisley. (1995)

[8] S. Weinberg, *Gravitation and Cosmology: Principles and Applications of the General Theory of Relativity.* John Wiley and Sons Inc. (1972)

[9] B. Schutz, *Gravity from the ground up.* Cambridge University Press. (2003).

[10] S. W. Hawking and G. F. R. Ellis, *The Large Scale Structure of Space-Time.* Cambridge University Press. (1973).

[11] J. Chadwick, *Possible existence of a neutron*, Nature **129**, 312 (1932).

[12] L. D. Landau, *On the theory of stars*, Phys. Z. Sowjetunion **1** (1932).

[13] W. Baade,F. Zwicky, *Supernovae and cosmic rays*, Phys. Rev. **45**, 138 (1934).

[14] W. Baade, F. Zwicky, *On Super-novae*. Proceedings of the National Academy of Sciences **20**, (5): 254-259. (1934)

[15] J. R. Oppenheimer, G. M. Volkoff, *On Massive Neutron Cores*. Phys. Rev. **55**, (4): 374-381 (1939).

[16] Richard C. Tolman,*Static Solutions of Einstein's Field Equations for Spheres of Fluid*, Physical Review **55**, 374 (1939).

[17] G. Gamow,*Structure of Atomic Nuclei and Nuclear Transformations*. Oxford: Oxford University Press (1937).

[18] L. D. Landau, 1937, *Origin of stellar energy*, Doklady Akad. Nauk SSSR **17**, 301-302 (in Russian) (1937); Nature, **141**, 333-334 (1938).

[19] H. A. Bethe, C. L. Critchfield, *The formation of deuterons by proton combination*, Phys. Rev. **54**, 248-254 (1938).

[20] B. K. Harrison , M. Wakano, J.A. Wheeler, *Matter-energy at high density: end point of thermonuclear evolution*, La structure et évolution de l'univers (Brussells: R. Stoops), 124-140 (1958).

[21] A.G.W. Cameron, *Pycnonuclear reactions and nova explosions*, Astrophys. J. **130**, 916-940 (1959).

[22] E.E. Salpeter, *Matter at high densities*, Ann. Phys. (N.Y.) **11**, 393-413 (1960).

[23] V. A. Ambartsumyan , G. S. Saakyan G.S., *The degenerate superdense gas of elementary particles*, Astron. Zh. **37**, 193-209 (1960).

[24] D. Ivanenko, D.F. Kurdgelaidze, *Hypothesis on quark stars*, Astrofizika **1**, 479-482 (1965).

[25] D. Ivanenko, D.F. Kurdgelaidze, *Remarks on quark stars*, Lett. Nuovo Cimento **2**, 13-16 (1969).

[26] H.Y. Chiu and E.E Salpeter, *Surface X-Ray Emission from Neutron Stars*, Phys. Rev. Lett. **12**, 413 (1964).

[27] R. Giacconi, H. Gursky, F. R. Paolini and B. B. Rossi, *Evidence for X-Rays from Sources outside the Solar System*, Phys. Rev. Lett. **9**, 439 (1962).

[28] A. Hewish, S. J. Bell, J. D. H. Pilkington, P. F. Scott and R. A. Collins, *Observation of a Rapidly Pulsating Radio Source*, Nature **217**, 709-713 (1968).

[29] T. Gold, *Rotating Neutron Stars as the Origin of the Pulsating Radio Sources*, In: Pulsating Stars. Springer, Boston, MA (1967).

[30] F. Pacini, *Energy Emission from a Neutron Star*, Nature **216**, 567 (1967).

[31] D. H. Staelin and E. C. Reifenstein, III *Pulsating radio sources near the Crab Nebula*, Science, **162**, 3861 (1968).

[32] E. C. Reifenstein, III, D. H. Staelin and W. D. Brundage, *Crab Nebula Pulsar NPO527*, Phys. Rev. Lett. **22**, 311 (1969).

[33] R. A. Hulse and J. H. Taylor, *Discovery of a pulsar in a binary system*, ApJ **195**, L51-L53 (1975).

[34] D. C. Backer *et al.*, *A millisecond pulsar*, Nature **300**, 615 (1982).

[35] F. D. Seward, F. R. Harnden Jr. and D. J. Helfand, *Discovery of a 50 millisecond pulsar in the Large Magellanic Cloud*,ApJ **287**, L19 (1984).

[36] A. G. Lyne, A. Brinklow, J. Middleditch, S. R. Kulkarni, D. C. Backer and T. R. Clifton, *The discovery of a millisecond pulsar in the globular cluster M28*, Nature **328**, 399-401 (1987).

[37] M. Burgay *et al.*, *An increased estimate of the merger rate of double neutron stars from observations of a highly relativistic system*, Nature, **426**, 531-533 (2003).

[38] A. G. Lyne *et al.*, *A Double-Pulsar System-A Rare Laboratory forRelativistic Gravity and Plasma Physics*, Science **303**, 1153-1157 (2004).

[39] J. W.T. Hessels *et al.*, *A Radio Pulsar Spinning at 716 Hz*, Science **311**, 1901 (2006).

[40] A. Lépine-Szily and Pierre Descouvemont, *Nuclear astrophysics: nucleosynthesis in the Universe*, International Journal of Astrobiology **11**, Issue 4 (2012).

[41] W.S.C.Williams, *Nuclear and Particle Physics*. Oxford Science Publications (1991)

[42] A. Burrows, J. Hayes, B. A. Fryxell, *On the nature of core collapse supernova explosions*, Astrophys. J. **450**, 830 (1995).

[43] P.W. Anderson, N. Itoh, *Pulsar glitches and restlessness as hard superfluidity phenomenon.* Nature **256**, 25-27 (1975).

[44] D. Pines, A. Alpar, *Superfluidity in neutron stars.* Nature **316**, 27-32 (1985).

[45] B. Link, R. I. Epstein and Kenneth A. Van Riper, *Pulsar glitches as probes of neutron star interiors*, Nature **359**, 616-618 (1992).

[46] W. C. G. Ho, C. M. Espinoza, D. Antonopoulou and N. Anderson, *Pinning down the superfluid and measuring masses using pulsar glitches*, Science Advances **1**, 9 (2015).

[47] J. P. Ostriker and J. E. Gunn, *On the Nature of Pulsars. I. Theory*, ApJ **157**, 1395 (1969).

[48] D. Pines, R. Tamagaki, S. Tsuruta, *Structure and Evolution of Neutron Stars.* Addison Wisley. (1992)

[49] A. G. Lyne, F. Graham-Smith, *Pulsar astronomy*, Cambridge University Press. (2005)

[50] J. M. Lattimer, *The Nuclear Equation of State and Neutron Star Masses.* Annu.Rev.Nucl.Part.Sci., 62: 485-515 (2012).

[51] F. Ozel, P. Freire, *Masses, Radii, and Equation of State of Neutron Stars.* Annual Review of Astronomy and Astrophysics **54**, 401-440 (2016).

[52] J. Antoniadis et al., *A Massive Pulsar in a Compact Relativistic Binary* , Science **340** (2013).

[53] M. H. van Kerkwijk, R. P. Breton, and S. R. Kulkarni, *Evidence for a Massive Neutron Star from a Radial-velocity Study of the Companion to the Black-widow Pulsar PSR B1957+ 20*, ApJ **728** (2011).

[54] S. Mereghetti, *In high-Energy Emission from Pulsars and Their Systems*, Springer (2011)

[55] J. M. Lattimer, K. A. van Riper, M. Prakash, M. Prakash, *Rapid Cooling and the Structure of Neutron Stars*, Astrophys. J, **425**, 802 (1994).

[56] O. Y. Gnedin, D. G. Yakovlev, A. Y. Potekhin, *Thermal relaxation in young neutron stars*, Mon. Not. R. Aston. Soc. **324** (3), 725-736 (2001).

[57] P. Haensel, *Apparent radii of neutron stars and equationof state of dense matter*, Astron. Astrophys. **380**, 186-189 (2001).

[58] J. M. Lattimer, *Neutron Star Mass and Radius Measurements*, Universe **5**, 159 (2019).

[59] S. Guillot, M. Servillat, N. A. Webb, and R. E. Rutledge1,*Measurement of the radius of Neutron Stars with high signal-to-noise quiescient low-mass X-RAY Binaries in Globular Clusters.* The Astrophysical Journal **772**, 7 (2013).

[60] C. A. Raithel, F. Ozel and D. Psaltis, *Tidal Deformability from GW170817 as a Direct Probe of the Neutron Star Radius* ApJ. L. **857**, 2 (2018).

[61] S. Bose, K. Chakravarti, L. Rezzolla, B. S. Sathyaprakash, and K. Takami, *Neutron-Star Radius from a Population of Binary Neutron Star Mergers*, Phys. Rev. Lett. **120**, 031102 (2018).

[62] V. E. Zavlin, G. G. Pavlov, *Modeling Neutron Star Atmospheres* Proc. of the 270-th Heraeus Seminar on Neutron Stars, Pulsars and Supernova Remnants, W. Becker, H. Lesch and J. Truemper (eds.), 2002, MPE Reports **278**, p. 273 (2002).

[63] W. C. Ho, D. L. Kaplan, P. Chang, M. Van Adelsberg, A. Y. Potekhin, *Magnetic hydrogen atmosphere models and the neutron star RX J1856.5-3754*, Month. Not. R. Astro. Soc. **375**, 3 (2007).

[64] V. F. Suleimanov, A. Y. Potekhin and K. Werner,*Models of magnetized neutron star atmospheres: thin atmospheres and partially ionized hydrogen atmospheres with vacuum polarization*, A&A **500**, 891-899 (2009).

[65] K. Mori, C. J. Hailey, *Detailed Atmosphere Modeling for the Neutron Star 1E1207.4-5209: Evidence of Oxygen/Neon Atmosphere*, ApJ **648**, 2 (2006).

[66] V. Suleimanov, J. Poutanen and K. Werner, *X-ray bursting neutron star atmosphere models using an exact relativistic kinetic equation for Compton scattering*, A&A **545**, A120 (2012).

[67] N.Chamel, P.Haensel, *Neutron Star Crust.*Living Rev. Relativity **11**, 10 (2008).

[68] D. A. Baiko, A. I. Chugunov, *Breaking properties of neutron star crust*, MNRAS **480**, 5511-5516 (2018).

[69] S. B. Ruster, M. Hempel, J. Schaffner-Bielich, *The outer crust of non-accreting cold neutron stars*, Phys. Rev. C **73**, 035804 (2006).

[70] G.Baym, C.J. Pethick and P. Sutherland, *The Ground State of Matter at High Densities: Equation of State and Stellar Models.* Astrophys. J. **170**, 299-317 (1971).

[71] J. W. Negele, and D. Vautherin, *Neutron star matter at sub-nuclear densities*, Nucl. Phys. **298** A207 (1973).

[72] D. G. Ravenhall, C. J. Pethick and J.R. Wilson, *Structure of Matter below Nuclear Saturation Density*, Phys. Rev. Lett. **50**, 2066 (1983).

[73] D. N. Kobyakov and C. J. Pethick, *Superfluid Liquid Crystals: Pasta Phases in Neutron Star Crusts*, J. Exp. Theor. Phys. **127**, 851-859 (2018).

[74] G. Watanabe, K. Iida and K. Sato, *Thermodynamic properties of nuclear "pasta" in neutron star crusts*, Nucl. Phys. A **676**, 455-473 (2000).

[75] J. A. Sauls, *Superfluidity in the Interiors of Neutron Stars*, NATO ASI Series C **262**, 457-490 (1989).

[76] B. Haskell, A. Sedrakian, *Superfluidity and Superconductivity in Neutron Stars*, Eur. Phys. J. A 55, 167 (2019).

[77] F. Weber, R. Negreiros, P. Rosenfield, *Neutron Star Interiors and the Equation of State of Superdense Matter*, In: Becker W. (eds) Neutron Stars and Pulsars. Astrophysics and Space Science Library **357**. Springer

[78] P. Haensel and M. Proszynski, *Pion Condensation in cold dense matter and neutron stars*, ApJ **258**, 306-320 (1982).

[79] G. Baym, E. Flowers, *Pion condensation in neutron star matter: Equilibrium conditions and model calculations*, Nucl.Phys. A **222**, 29-64 (1974).

[80] A. Ramos, J. Schaffner-Bielich, J. Wambach, *Kaon Condensation in Neutron Stars*, Lect.Notes Phys. **578**, 175-202 (2001).

[81] Y. Lim, K. Kwak, C. H. Hyun, C. H. Lee, *Kaon condensation in neutron stars with Skyrme-Hartree-Fock models*, Phys. Rev. C **89**, 055804 (2014).

[82] N.Itoh, *Hydrostatic Equilibrium of Hypothetical Quark Stars*. Prog. Theor. Phys. **44**, 291 (1970).

[83] G. Baym, S.A. Chin, *Can a Neutron Star Be a Giant MIT Bag?*. Phys. Lett. B **62**, 241-244 (1976).

[84] G. Lugones and I. Bombaci, *Deconfinement and color superconductivity in cold neutron stars*, Phys. Rev. D **72**, 065021 (2005).

[85] R. Rajamaran and H. A. Bethe, *Three-Body Problem in Nuclear Matter*, Rev. Mod. Phys. **39**, 745 (1967).

[86] H. A. Bethe, *Theory of Nuclear Matter*, Ann. Rev, Nucl. Sc. **21**:93-244 (1971).

[87] B. D. Day, *Elements of the Brueckner-Goldston Theory of Nuclear Matter*, Rev. Mod. Phys. **39**, 719 (1967).

[88] M. Baldo, G. F. Burgio, H. J. Schulze, *Hyperon stars in the Brueckner-Bethe-Goldstone theory*, Phys.Rev.C **61**, 055801 (2000).

[89] M. Baldo, A. Fiasconaro, H. Q. Song, G. Giansiracusa, and U. Lombardo, *High density symmetric nuclear matter in the Bethe-Brueckner-Goldstone approach*, Phys. Rev. C **65**, 017303 (2001).

[90] M. Baldo, I. Bombaci, L. S. Ferreira, G. Giansiracusa, U.Lombardo, *Nuclear matter equation of state with single particle correlations*, Phys. Lett. B **255**, 1 (1988).

[91] M. Baldo, I. Bombaci, G. Giansiracusa, U. Lombardo, C. Mahaux, and R. Sartor, *Nuclear matter properties from a separable representation of the Paris interaction*, Phys. Rev. C **41**, 1748 (1990).

[92] P. C. Martin, J. S. Schwinger, *Theory of many particle systems. 1.*, Phys.Rev. **115**, 1342-1373 (1959).

[93] W. H. Dickhoff and C. Barbieri, *Self-consistent Green's function method for nuclei and nuclear matter*, Progress in Particle and Nuclear Physics **52**, 377-496 (2004).

[94] H. Müther A. Polls, *Two-Body Correlations in Nuclear Systems*, Progress in Particle and Nuclear Physics **45**, 243-334 (2000).

[95] G. F. Burgio, A. F. Fantina, *Nuclear Equation of state for Compact Stars and Supernovae*, The Physics and Astrophysics of Neutron Stars (Astrophysics and Space Science Library Book 457), Springer (2018)

[96] J. M. Lattimer, M. Prakash, *Neutron Star Structure and the Equation of State.* The Astrophysical Journal **550**: 426-442 (2001).

[97] J. M. Lattimer, M. Prakash, *Neutron star observations: Prognosis for equation of state constraints.* Phys. Rep. **442**, Issue 1-6, 109-165 (2007).

[98] F. Douchin and P. Haensel, *A unified equation of state of dense matter and neutron star structure.* Astron. Astrophys. 380, 151 (2001).

[99] M. Baldo, I. Bombaci, and G.F. Burgio, *Microscopic nuclear equation of state with three-body forces and neutron star structure.* A&A **328**, 274 (1997).

[100] H. Muller and B. D. Serot, *Relativistic mean field theory and the high density nuclear equation of state.* Nucl. Phys. A 606, 508 (1996).

[101] M. Prakash, J. R. Cooke, and J. M. Lattimer, *Quark-hadron phase transition in protoneutron stars* Phys. Rev. D **52**, 661 (1995).

[102] N. Cabibbo and G. Parisi, *Exponential hadronic spectrum and quark liberation.* Phys. Lett. B **59**, 67-69 (1975).

[103] R. C. Hwa and X. N. Wang, *Quark-gluon plasma 4*, Singapore, World Scientific Publishing Co. Pte. Ltd. (2010)

[104] L. S. Kisslinger and D. Das, *Review of QCD, Quark-Gluon Plasma, Heavy Quark Hybrids, and Heavy Quark State production in p-p and A-A collisions*, Int. J. Mod. Phys. A **31**, 1630010 (2016).

[105] R. Pasechnik, M. Šumbera, *Phenomenological Review on Quark-Gluon Plasma: Concepts vs. Observations*, Universe **3**, 7 (2017).

[106] S. Muroya, A. Nakamura, C. Nonaka, T. Takaishi, *Lattice QCD at finite density: an introductory review*, Prog. Theor. Phys. **110**, 616-668 (2003).

[107] O. Philipsen, *Lattice QCD at finite temperature and density*, Eur. Phys. J. ST **152**: 29-60 (2007).

[108] H.Halzen, Martin,*Quark and Leptons: An Introductory Course in Modern Particle Physics.* John Wiley and Sons (1984)

[109] K. Nakamura, et all., *Review of Particle Physics.* Journal of Physics **G37**, 075021 (2010).

[110] M. Seymour *Quantum ChromoDynamics.* arXiv:hep-ph/0505192

[111] A.Chodos, R. L. Jaffe, K. Johnson, C. B. Thorne and V. F. Weisskopf, *New extended model of hadrons*, Phys.Rev.D **9** 3471 (1974).

[112] A. Chodos, R. L. Jaffe, K. Johnson and C. B. Thorn,*Baryon Structure In The Bag Theory*, Phys. Rev. D **10**, 2599 (1974).

[113] A. Schmitt, *Dense matter in compact stars. A pedagogical introduction.*Lect.Notes Phys. **811**:1-111 2010.

[114] M.Alford, M. Braby, M. Paris, S. Reddy, *Hybrid stars that masquerade as neutron stars* Astrophys.J. **629** 969-978 (2005).

[115] A. Akmal, V. R. Pandharipande, and D. G. Ravenhall, *Equation of state of nucleon matter and neutron star structure*, Phys. Rev. C **58**, 1804 (1998).

[116] M.Mannarelli, K.Rajagopal, R. Sharma, *The rigidity of crystalline colour superconducting quark matter* Phys. Rev. D **76**, 074026 (2007).

[117] K. Rajagopal, F. Wilczek *The Condensed Matter Physics of QCD* At The Frontier of Particle Physics, pp. 2061-2151 (2001).

[118] M. Alford, A. Schmitt, K. Rajagopal, T. Sch afer, *Color superconductivity in dense quark matter.* Rev. Mod. Phys. **80**:1455-1515 (2008).

[119] M. Alford, K. Rajagopal, F. Wilczek, *Color-Flavor Locking and Chiral Symmetry Breaking in High Density QCD* Nucl. Phys. B **537**, 443 (1999).

[120] M. Alford, K. Rajagopal, *Absence of two flavor color superconductivity in compact stars*, JHEP 0206, 031 (2002).

[121] R. Anglani, R. Casalbuoni, M. Ciminale, N. Ippolito, R. Gatto, M. Mannarelli, M. Ruggieri, *Crystalline color superconductors:A review* Rev.Mod.Phys. **86**, 509-561 (2014).

[122] A.R. Bodmer, *Collapsed Nuclei.*Phys. Rev. D **4**, 1601 (1971).

[123] E. Witten, *Cosmic separation of phases.* Phys. Rev. D. **30**, 272 (1984).

[124] C. Alcock, E. Farhi, A. Olinto, *Strange Stars.* The Astrophysical Journal, **310**: 261-272 (1986).

[125] J. Madsen, *Physics and Astrophysics of Strange Quark Matter* Hadrons in dense matter and hadrosynthesis, Springer (1999).

[126] F.Weber, *Strange Quark Matter and Compact Stars* Progress in Particle and Nuclear Physics, Elsevier (2005).

[127] P. Haensel, J. Zdunik and R. Schaeffer, *Strange quark stars*, Astron. Astrophys. **160**, 121 (1986).

[128] M. Alford, D. Blaschke, A. Drago, T. Klähn, G. Pagliara & J. Schaffner-Bielich, *Quark matter in compact stars?.* Nature **445**, E7-E8 (2007).

[129] E. Farhi and R.L. Jaffe, *Strange matter*, Phys.Rev. D, **30**, 11 (1984).

[130] M. Mannarelli, G. Pagliaroli, A. Parisi, L. Pilo, *Electromagnetic signals from bare strange stars.* Phys. Rev. D **89**, 103014 (2014).

[131] M. Mannarelli, G. Pagliaroli, A. Parisi, L. Pilo, F. Tonelli, *Torsional oscillation of non bare strange stars*, ApJ, **815**:81 (2015).

[132] A. Dirkes, - *Gravitational Waves - A Review on the Conceptual Foundations of Gravitational Radiation*, Int. J. Mod. Phys. A, **33**, 1830013 (2018).

[133] R. A. Hulse, J. H. Taylor, *Discovery of a pulsar in a binary-system*, Astrophys. J. **195**:L51-L53 (1975).

[134] M. Burgay et al., *An increased estimate of the merger rate of double neutron stars from observations of a highly relativistic system*, Nature **426**, 531-533 (2003).

[135] I. H. Stairs, *Testing General Relativity with Pulsar Timing*, LivingRev.Rel. **6**:5 (2003).

[136] K. Liu, R.P. Eatough, N. Wex, M. Kramer, *Pulsar-black hole binaries: prospects for new gravity tests with future radio telescopes*, Mon.Not.Roy.Astron.Soc. **445**, 3, 3115-3132 (2014).

[137] A. Einstein, *Die Feldgleichungen der Gravitation*, Sitzungsberichte der Königlich Preussischen Akademie der Wissenschaften (1915).

[138] B. P. Abbott et al. (LIGO Scientific Collaboration and Virgo Collaboration), *Observation of Gravitational Waves from a Binary Black Hole Merger*, Phys. Rev. Lett **116**, 061102 (2016).

[139] B. P. Abbott et al. (LIGO Scientific Collaboration and Virgo Collaboration), *GW150914: The Advanced LIGO Detectors in the Era of First Discoveries*, Phys. Rev. Lett. **116**, 131103 (2016).

[140] B. P. Abbott et al. (LIGO Scientific Collaboration and Virgo Collaboration), *GW150914: First results from the search for binary black hole coalescence with Advanced LIGO*, Phys. Rev. D **93**, 122003 (2016).

[141] F. Pretorius, *Evolution of Binary Black Hole Spacetimes*, Physical Review Letters **95**, (12): 121101 (2005).

[142] M. Campanelli, C. O. Lousto, P. Marronetti, Y. Zlochower, *Accurate Evolutions of Orbiting Black-Hole Binaries Without Excision*, Phys.Rev.Lett. **96**: 111101 (2006).

[143] John G. Baker, Joan Centrella, Dae-Il Choi, Michael Koppitz, James van Meter, *Gravitational wave extraction from an inspiraling configuration of merging black holes*, Phys.Rev.Lett. **96**: 111102 (2006).

[144] B. P. Abbott et al. (LIGO Scientific Collaboration and Virgo Collaboration), *GW151226: Observation of Gravitational Waves from a 22-Solar-Mass Binary Black Hole Coalescence*, Phys. Rev. Lett. **116**, 241103 (2016).

[145] B. P. Abbott et al. (LIGO Scientific Collaboration and Virgo Collaboration), *GW170104: Observation of a 50-Solar-Mass Binary Black Hole Coalescence at Redshift 0.2*, Phys. Rev. Lett., **118** (22): 221101 (2017).

[146] B. P. Abott et al. (LIGO Scientific Collaboration and Virgo Collaboration), *GW170814: A Three-Detector Observation of Gravitational Waves from a Binary Black Hole Coalescence*, Phys. Rev. Lett. **119**, 141101 (2017).

[147] B.P. Abbott, R. Abbott, T.D. Abbott, F. Acernese, K. Ackley, C. Adams et al., *GW170817: Observation of Gravitational Waves from a Binary Neutron Star Inspiral*, Phys. Rev. Lett. **119**, 161101 (2017).

[148] J. Goodman, *Are gamma-ray bursts optically thick?*, Astroph. J. **308**, L47 (1986).

[149] B. Paczynski, *Gamma-ray bursters at cosmological distances*, Astroph. J. **308**, L43-L46 (1986).

[150] D. Eichler, M. Livio, T. Piran and D. N. Schramm, *Nucleosynthesis, neutrino bursts and gamma-rays from coalescing neutron stars*, Nature **340**, 126-128 (1989).

[151] R. Narayan, T. Piran and A. Shemi, *Neutron star and black hole binaries in the Galaxy*, Astroph. J. **379**, L17-L20 (1979).

[152] R. Narayan, B. Paczynski and T. Piran, *Gamma-ray bursts as the death throes of massive binary stars*, Astroph. J. **395**, L83-L86 (1992).

[153] B. P. Abbott, R. Abbott, T. D. Abbott, F. Acernese, K. Ackley, C. Adams et al, *Gravitational Waves and Gamma-Rays from a Binary Neutron Star Merger: GW170817 and GRB 170817A*, Astroph. J. **848**, L13 (2017).

[154] A. Goldstein, P. Veres, E. Burns, M. S. Briggs, R. Hamburg, D. Kocevski et al., *An Ordinary Short Gamma-Ray Burst with Extraordinary Implications: Fermi-GBM Detection of GRB 170817A*, Astroph. J. **848**, L14 (2017).

[155] D. A. Coulter, R. J. Foley, C. D. Kilpatrick, M. R. Drout, A. L. Piro, B. J. Shappee et al., *Swope Supernova Survey 2017a (SSS17a), the optical counterpart to a gravitational wave source*, Science **358**, 1556-1558 (2017).

[156] I. Arcavi, G. Hosseinzadeh, D. A. Howell, C. McCully, D. Poznanski, D. Kasen et al., *Optical emission from a kilonova following a gravitational-wave-detected neutron-star merger*, Nature **551**, 64-66 (2017).

[157] P. S. Cowperthwaite, E. Berger, V. A. Villar, B. D. Metzger, M. Nicholl, R. Chornock et al., *The Electromagnetic Counterpart of the Binary Neutron Star Merger LIGO/Virgo GW170817. II. UV, Optical, and Near-infrared Light Curves and Comparison to Kilonova Models*, Astrophys. J. **848**, L 17 (2017).

[158] M. Nicholl, E. Berger, D. Kasen, B. D. Metzger, J. Elias, C. Briceño et al, *The Electromagnetic Counterpart of the Binary Neutron Star Merger LIGO/Virgo GW170817. III. Optical and UV Spectra of a Blue Kilonova from Fast Polar Ejecta*, Astroph. J. **848**, L18 (2017).

[159] G. Ashton, O. Birnholtz, M. Cabero, C. Capano, T. Dent, B. Krishnan, G. D. Meadors, A. B. Nielsen, A. Nitz, and J. Westerweck, *Comments on: "Echoes from the abyss: Evidence for Planck-scale structure at black hole horizons"*, arXiv:1612.05625 (2016).

[160] J. Westerweck, A. B. Nielsen, O. Fischer-Birnholtz, M. Cabero, C. Capano, T. Dent, B. Krishnan, G. Meadors, and A. H. Nitz,*Low significance of evidence for black hole echoes in gravitational wave data*, Phys. Rev. D **97**, 124037 (2018).

[161] C.-M. Claudel, K. S. Virbhadra and G. F. R. Ellis, *The geometry of photon surfaces*, J. Math. Phys **42**, 818 (2001).

[162] K. S. Virbhadra and G. F. R. Ellis, *Schwarzschild black hole lensing*, Phys. Rev. D **62**, 084003 (2000).

[163] B. R. Iyer, C. V. Vishveshwara and S. V. Dhurandhar, *Ultracompact ($R < 3M$) objects in general relativity*, Classical Quantum Gravity **2**, 219 (1985).

[164] R. J. Nemiroff, P. A. Becker, and K. S. Wood, *Properties of Ultracompact neutron stars*, Astrophys. J. **406**, 590 (1993).

[165] C. Barcelò, R. Carballo-Rubio, and L. J. Garay, *Gravitational wave echoes from macroscopic quantum gravity effects*, J. High Energy Phys. 05, 054 (2017).

[166] V. Ferrari and K. D. Kokkotas *Scattering of particles by neutron stars: Time evolutions for axial perturbations*, Phys. Rev. D **62**, 107504 (2000).

[167] S. Chandrasekhar, *The Mathematical Theory of Black Holes.* Oxford University Press, New York (1983)

[168] V. Cardoso, A. S. Miranda, E. Berti, H. Witek, and V. T. Zanchin, *Geodesic stability, Lyapunov exponents and quasinormal modes*, Phys. Rev. **D79**, 062016 (2016).

[169] V. Cardoso, P. Pani, *The observational evidence for horizons: from echoes to precision gravitational-wave physics*, arXiv:1707.03021

[170] A. Urbano, H. Veermäe, *On gravitational echoes from ultracompact exotic stars*, J. Cosm and Astrop. Phys. **04** (2019).

[171] The Event Horizon Telescope Collaboration, *First M87 Event Horizon Telescope Results. VI.The Shadow and Mass of the Central Black Hole.* Astrophys. J. Lett. **875**, 1 (2019).

[172] V. Ferrari and B. Mashhoon, *New approach to the quasinormal modes of a black hole*, Phys. Rev. **D30**, 295-304 (1984).

[173] E. Berti, V. Cardoso, and A. O. Starinets, *Quasinormal modes of black holes and black branes*, Class. Quantum Grav. **26** 163001 (2009).

[174] K. D. Kokkotas, *Pulsating Relativistic Stars*, in Relativistic Gravitation and Gravitational Radiation, Eds J-A. Marck and J-P Lasota, Cambridge Cantemporary Astrophysics page 89 (1997).

[175] K. D. Kokkotas, B. F. Schutz, *Normal Modes of a Model Radiating System*, Gen.Rel.Grav. **18**, 913 (1986).

[176] K. D. Kokkotas, B. F. Schutz, *W-modes: A New family of normal modes of pulsating relativistic stars*, Mon.Not.Roy.Astron.Soc. **255**, 119 (1992).

[177] Y. Kojima, N. Andersson, K. D. Kokkotas, *On the oscillation spectra of ultra compact stars*, Proc. R. Soc. Lond. **A471**, 341 (1995).

[178] N. Andersson, Y. Kojima, K. D. Kokkotas, *On the oscillation spectra of ultracompact stars: An Extensive survey of gravitational wave modes*, Astrophys.J. **462**, 855 (1996).

[179] N. Andersson, K. D. Kokkotas, B. F. Schutz, *Space-time modes of relativistic stars*, Mon.Not.Roy.Astron.Soc. **280**, 1230 (1996).

[180] H. A. Buchdahl, *General Relativistic Fluid Spheres*, Phys. Rev. **116**, 1027 (1959).

[181] P. O. Mazur and E. Mottola, *Gravitational vacuum condensate stars*, Proc. Nat. Acad. Sci **101**, 9545-9550 (2004).

[182] P. O. Mazur and E. Mottola, *Gravitational condensate stars: An alternative to black holes*, arXiv:gr-qc/0109035

[183] M. S. Morris, K. S. Thorne, and U. Yurtsever, *Wormholes, Time Machines, and the Weak Energy Condition*, Phys. Rev. Lett. **61**, 1446-1449 (1988).

[184] V. Cardoso, S. Hopper, C. F. B. Macedo, C. Palenzuela, and P. Pani, *Gravitational-wave signatures of exotic compact objects and of quantum corrections at the horizon scale*, Phys. Rev. D **94**, 084031 (2016).

[185] E. Barausse, V. Cardoso, and P. Pani, *Can environmental effects spoil precision gravitational-wave astrophysics?*, Phys. Rev. D **89**, 104059 (2014).

[186] P. Bueno, P. A. Cano, F. Goelen, T. Hertog, and B. Vercnocke, *Echoes of Kerr-like wormholes*, Phys. Rev. D **97**, 024040 (2018).

[187] S. D. Mathur, *The Fuzzball proposal for black holes: An Elementary review*, Fortsch. Phys. **53**, 793-827 (2005).

[188] J. Abedi, H. Dykaar, and N. Afshordi, *Echoes from the abyss: Tentative evidence for Planck-scale structure at black hole horizons* Phys. Rev. **D96**, 082004 (2017).

[189] R. S. Conklin, B. Holdom, and J. Ren, *Gravitational wave echoes through new windows*, Phys.Rev. D **98** no.4, 044021 (2018).

[190] J. Westerweck, *et al.*, *Low significance of evidence for black hole echoes in gravitational wave data*, Phys. Rev. D **97**, 124037 (2018).

[191] G. Ashton, *et al.*, *Comments on: "Echoes from the abyss: Evidence for Planck-scale structure at black hole horizons"*, arXiv:1612.05625

[192] B. Abbott *et al* (Virgo, LIGO Scientific),*Search for post-merger gravitational waves from the remnant of the binary neutron star merger GW170817*, Ap. J. L., **851** :L16 (2017).

[193] F. Zappa, S. Bernuzzi, D. Radice, A. Perego, and T. Dietrich, *Gravitational-Wave Luminosity of Binary Neutron Stars Mergers*, Phys. Rev. Lett. **120**, 111101 (2018).

[194] J. Abedi, H. Dykaar, and N. Afshordi, *Echoes from the Abyss: The Holiday Edition!*, arXiv:1701.03485 (2017)

[195] J. Abedi, N. Afshordi, *Echoes from the Abyss: A higly spinning black hole remnant for the binary neutron star merger GW170817*, JCAP 1911, **11**, 010 (2019).

[196] Binary black hole signals in LIGO open data, https://www.gw-openscience.org/s/events/GW150914/LOSC_Event_tutorial_GW150914.html

[197] M. Mannarelli and F. Tonelli, *Gravitational wave echoes from strange stars*, Phys. Rev. D **97**, 123010 (2018).

[198] E. Annala, T. Gorda, A. Kurkela, and A. Vuorinen, *Gravitational-Wave Constraints on the Neutron-Star-Matter Equation of State*, Phys. Rev. Lett. **120**, 172703 (2018).

[199] E. R. Most, L. R. Weih, L. Rezzolla, and J. Schaffner-Bielich, *New constraints on radii and tidal deformabilities of neutron stars from GW170817*, Phys. Rev. Lett. **120**, 261103 (2018).

[200] Y. Lim and J. W. Holt, *Neutron star tidal deformabilities constrained by nuclear theory and experiment*, Phys. Rev. Lett. **121**, 062701 (2018).

[201] D. Radice, A. Perego, F. Zappa, and S. Bernuzzi, *GW170817: Joint Constraint on the Neutron Star Equation of State from Multimessenger Observations*, Astrophys. J. **852**, L29 (2018).

[202] R. Nandi and P. Char, *Hybrid Stars in the Light of GW170817*, Astrophys. J. **857**, 12 (2018).

[203] G. F. Burgio, A. Drago, G. Pagliara, H.-J. Schulze, and J.-B. Wei, *Are small radii of compact stars ruled out by GW170817/AT2017gfo?*, Astrophys.J. **860** (2018).

[204] O. G. Benvenuto and J. E. Horvath, *Evidence for strange matter in supernovae?*, Phys. Rev. Lett. **63** (1989).

[205] G. Pagliara, M. Herzog, and F. K. Röpke, *Combustion of a neutron star into a strange quark star: The neutrino signal*, Phys. Rev. D **87**, 103007 (2013).

[206] A. Ouyed, R. Ouyed, and P. Jaikumar, *Numerical simulation of the hydrodynamical combustion to strange quark matter in the trapped neutrino regime*, Phys. Lett. B **777**, 184 (2018).

[207] C. V. Flores, Z. B. Hall II, and P. Jaikumar, *Nonradial oscillation modes of compact stars with a crust*, Phys. Rev. C **96**, 065803 (2017).

[208] P. Demorest, T. Pennucci, S. Ransom, M. Roberts, and J. Hessels, *A two-solar-mass neutron star measured using Shapiro delay*, Nature (London) **467**, 1081 (2010).

[209] P. Pani, V. Ferrari *On gravitational-wave echoes from neutron-star binary coalescences*, Class. Quantum Grav. **35** 15LT01 (2018).

[210] E. Gourgoulhon, *Simple equations for general relativistic hydrodynamics in spherical symmetry applied to neutron star collapse* , Astron. Astrophys. **252**, 651 (1991).

[211] M. Shibata, *Collapse of Rotating Supramassive Neutron Stars to Black Holes: Fully General Relativistic Simulations*, Astrophys. J. **595**, 992 (2003).

[212] L. Baiotti, I. Hawke, P. J. Montero, F. Loffler, L. Rezzolla, N. Stergioulas, J. A. Font, and E. Seidel, *Three-dimensional relativistic simulations of rotating neutron-star collapse to a Kerr black hole*, Phys. Rev. D **71**, 024035 (2005).

[213] N. Andersson, Y. Kojima, and K. D. Kokkotas, *On the Oscillation Spectra of Ultracompact Stars: an Extensive Survey of Gravitational-Wave Modes*, Astrophys. J. **462**, 855 (1996).

[214] S. L. Shapiro *Differential Rotation in Neutron Stars: Magnetic Braking and Viscous Damping*, ApJ **544**, 1 (2000).

[215] K. Hotokezaka, K. Kiuchi, K. Kyutoku, T. Muranushi, Y.-i. Sekiguchi, M. Shibata, and K. Taniguchi, *Remnant massive neutron stars of binary neutron star mergers: Evolution process and gravitational waveform*, Phys. Rev. D **88**, 044026 (2013).

[216] T. D. Lee and C. N. Yang, *Question of Parity Conservation in Weak Interactions*, Phys. Rev. **104**, 254 (1956).

[217] S. Weinberg, *The quantum Theory of Fields*, Cambridge University Press. (1996).

[218] A. Zee, *Quantum field theory in a Nutschell*, Princeton University Press. (2010).

[219] B. Holdom, *Two $U(1)$'s and epsilon charge shifts*, Phys. Lett. B **166**, 196 (1986).

[220] S. L. Glashow, *Positronium versus the mirror Universe*, Phys. Lett. B **167**, 35 (1986).

[221] E. D. Carlson and S. L. Glashow, *Nucleosynthesis versus the mirror universe*, Phys. Lett. B 193, 168 (1987).

[222] L. B. Okun, *Mirror particles and mirror matter: 50 years of speculations and search*, Phys. Usp. **50**, 380 (2007).

[223] P. Panci, *Dark Matter Phenomenology*, Phd Thesis, L'Aquila University, http://inspirehep.net/record/1653612

[224] Z. Berezhiani, *Unified picture of the particle and sparticle masses in SUSY GUT*, Physics Letters B **417**, 287 (1998).

[225] Z. Berezhiani, L. Gianfagna, M. Giannotti, *Strong CP problem and mirror world: the Weinberg Wilczek axion revisited*, Phys.Lett. B **500**, 286-296 (2001).

[226] Z. Berezhiani, A. Drago, *Gamma Ray Bursts via emission of axion-like particles*, Phys.Lett. B **473**, 281-290 (2000).

[227] E. Akhmedov, Z. Berezhiani and G. Senjanovic, *Planck scale physics and neutrino masses*, Phys. Rev. Lett. **69**, 3013 (1992).

[228] R. Foot, H. Lew and R. Volkas, *Possible consequences of parity conservation*, Mod. Phys. Lett. A **7**, 2567 (1992).

[229] R. Foot and R. Volkas, *Neutrino physics and the mirror world: How exact parity symmetry explains the solar neutrino deficit, the atmospheric neutrino anomaly and the LSND experiment*, Phys. Rev. D **52**, 6595 (1995).

[230] Z. Berezhiani and R. N. Mohapatra, *Reconciling present neutrino puzzles: Sterile neutrinos as mirror neutrinos*, Phys. Rev. D **52**, 6607 (1995).

[231] Z. Berezhiani, A. D. Dolgov and R. N. Mohapatra, *Asymmetric inflationary reheating and the nature of mirror universe*, Phys. Lett. B **375**, 26 (1996).

[232] Z. Berezhiani, *Astrophysical implications of the mirror world with broken mirror parity*, Acta Phys. Polon. B **27**, 1503 (1996).

[233] R. N. Mohapatra, S. Nussinov and V. L. Teplitz, *Mirror matter as selfinteracting dark matter*, Phys. Rev. D **66**, 063002 (2002).

[234] V.S. Berezinsky, A. Vilenkin, *Ultrahigh-energy neutrinos from hidden sector topological defects*, Phys. Rev. D **62**, 083512 (1999).

[235] Z. Berezhiani, *Mirror world and its cosmological consequences*, Int. J. Mod. Phys. A **19**, 3775 (2004).

[236] Z. Berezhiani, *Through the looking-glass: Alice's adventures in mirror world*, In *From Fields to Strings, Circumnavigating Theoretical Physics*, Eds. M. Shifman et al., vol. 3, pp. 2147-2195 (2005)

[237] Z. Berezhiani, D. Comelli and F. L. Villante, *The Early mirror universe: Inflation, baryogenesis, nucleosynthesis and dark matter*, Phys. Lett. B **503**, 362 (2001).

[238] A. Y. Ignatiev and R. R. Volkas, *Mirror dark matter and large scale structure*, Phys. Rev. D **68**, 023518 (2003).

[239] Z. Berezhiani, P. Ciarcelluti, D. Comelli and F. L. Villante, *Structure formation with mirror dark matter: CMB and LSS*, Int. J. Mod. Phys. D **14**, 107 (2005).

[240] Z. Berezhiani, S. Cassisi, P. Ciarcelluti and A. Pietrinferni, *Evolutionary and structural properties of mirror star MACHOs*, Astropart. Phys. **24**, 495 (2006).

[241] A. Penzias, R. Wilson, *A Measurement of excess antenna temperature at 4080-Mc/s*, Astrophys. J. **142**, 419 (1965).

[242] L. Bento and Z. Berezhiani, *Leptogenesis via collisions: The Lepton number leaking to the hidden sector*, Phys. Rev. Lett. **87**, 231304 (2001).

[243] L. Bento and Z. Berezhiani, *Baryon asymmetry, dark matter and the hidden sector*, Fortsch. Phys. **50**, 489 (2002).

[244] L. Bento and Z. Berezhiani, *Baryogenesis: The Lepton leaking mechanism*, [hep-ph/0111116]

[245] Z. Berezhiani, *Sterile Neutrinos and Leptogenesis of Matter and Dark Matter*, Nucl. Phys. Proc. Suppl. **237-238**, 263 (2013).

[246] Z. Berezhiani, *Anti-dark matter: a hidden face of mirror world*, arXiv:1602.08599 [astro-ph.CO].

[247] Z. Berezhiani and L.Bento, *Neutron - mirror neutron oscillations: How fast might they be?*, Phys. Rev. Lett. **96**, 081801 (2006).

[248] Z. Berezhiani, *More about neutron - mirror neutron oscillation*, Eur. Phys. J. C **64**, 421 (2009).

[249] V. Kuzmin, *Cp violation and baryon asymmetry of the universe*,JETP Lett. **12**, 335 (1970).

[250] R. N. Mohapatra and R. E. Marshak, *Local B-L Symmetry of Electroweak Interactions, Majorana Neutrinos and Neutron Oscillations*, Phys. Rev. Lett. **44**, 1316 (1980).

[251] D. G. Phillips II *et al.*, *Neutron-Antineutron Oscillations: Theoretical Status and Experimental Prospects*, Phys. Rept. **612**, 1 (2016).

[252] Z. Berezhiani and L. Bento, *Fast neutron: Mirror neutron oscillation and ultra high energy cosmic rays*, Phys. Lett. B **635**, 253 (2006).

[253] Z. Berezhiani and A. Gazizov, *Neutron Oscillations to Parallel World: Earlier End to the Cosmic Ray Spectrum?*, Eur. Phys. J. C **72**, 2111 (2012).

[254] R. N. Mohapatra, S. Nasri and S. Nussinov,*Some implications of neutron mirror neutron oscillation*, Phys. Lett. B **627**, 124 (2005).

[255] A. Coc, J. P. Uzan and E. Vangioni,*Mirror matter can alleviate the cosmological lithium problem*, Phys. Rev. D **87**, no. 12, 123530 (2013).

[256] Y. N. Pokotilovski, *On the experimental search for neutron -> mirror neutron oscillations*, Phys. Lett. B **639**, 214 (2006).

[257] G. Ban *et al.*, *A Direct experimental limit on neutron – mirror neutron oscillations*, Phys. Rev. Lett. **99**, 161603 (2007).

[258] A. Serebrov *et al.*, *Experimental search for neutron – mirror neutron oscillations using storage of ultracold neutrons*, Phys. Lett. B **663**, 181 (2008).

[259] I. Altarev *et al.*, *Neutron to Mirror Neutron Oscillations in the Presence of Mirror Magnetic Fields*, Phys. Rev. D **80**, 032003 (2009).

[260] A.Serebrov *et al.*, *Search for neutron mirror neutron oscillations in a laboratory experiment with ultracold neutrons*, Nucl. Instrum. Meth. A **611**, 137 (2009).

[261] Z. Berezhiani *et al.*, *New experimental limits on neutron - mirror neutron oscillations in the presence of mirror magnetic field*, Eur. Phys. J. C **78**, 717 (2018).

[262] Z. Berezhiani, *Neutron lifetime puzzle and neutron-mirror neutron oscillation* , Eur. Phys. J. C **79**: 484 (2019).

[263] Z. Berezhiani and F. Nesti, *Magnetic anomaly in UCN trapping: signal for neutron oscillations to parallel world?*, Eur. Phys. J. C **72**, 1974 (2012).

[264] Z. Berezhiani, M. Frost, Y. Kamyshkov, B. Rybolt and L. Varriano, *Neutron Disappearance and Regeneration from Mirror State*, Phys. Rev. D **96**, 035039 (2017).

[265] L. J. Broussard *et al.*, *New Search for Mirror Neutrons at HFIR*, arXiv:1710.00767 [hep-ex].

[266] W. Q. Zhang, S. E. Woosley and A. Heger, *Fallback and Black Hole Production in Massive Stars*, Astrophys. J. **679**, 639 (2008).

[267] J. Schwab, Ph. Podsiadlowski, and S. Rappaport, *Further evidence for the bimodal distribution of neutron-star masses*, Astrophys. J. **719**, 1 (2010).

[268] C. E. Rhoades, Jr. and R. Ruffini, *Maximum mass of a neutron star*, Phys. Rev. Lett. **32**, 324 (1974).

[269] *ATNF Pulsar Catalogue*, https://www.atnf.csiro.au/people/pulsar/psrcat/

[270] J.G. Martinez, K. Stovall, P.C.C. Freire, J.S. Deneva, F.A. Jenet, M.A. McLaughlin, M. Bagchi, S.D. Bates and A. Ridolfi, *Pulsar J0453+1559: A Double Neutron Star System with a Large Mass Asymmetry*, ApJ **812**, 2 (2015).

[271] S. Chandrasekhar, *Dynamical instability of gaseous masses approaching the Schwarzschild limit in general relativity* Phys. Rev. Lett. **12**, 114 (1964).

[272] S. Chandrasekhar, J. L. Friedman, *On the stability of axisymmetric systems to axisymmetric perturbations in general relativity, I. The equations governing nonstationary, and perturbed systems* Astrophys. J. **140**, 417 (1964), [Erratum: Astrophys. J.140,1342(1964)].-

[273] J. M. Bardeen, K. S. Thorne, D. W. Meltzer, *A catalogue of methods for studying the normal modes of radial pulsation of general-relativistic stellar models*, Astrophysical Journal **145**, p.505 (1966).

[274] W. A. Fowler, *Massive stars, relativistic polytropes, and gravitational radiation*, Rev. Mod. Phys. **36**, 549 and 1104 (1964).

[275] K. D. Kokkotas, J. Ruoff, *Radial oscillations of relativistic stars*, A&A **366**, 565-572 (2001).

[276] E. N. Glass and Amos Harpaz, *The stability of relativistic gas spheres*, Mon. Not. R. astr. Soc. **202**, 159-171 (1983).

[277] E. N. Glass and L. Lindblom, *The radial oscillations of neutron stars*, Astrophysical Journal Supplement v.71, p.173 (1983).

[278] J. H. Wilkinson, *The Algebraic Eigenvalue Problem*, Oxford University Press, London (1965).

[279] H. M. Vaeth and G. Chanmugam, *Radial oscillations of neutron stars and strange stars*, Astronomy and Astrophysics **260**, no. 1-2, p. 250-254 (1992).

[280] G. Chanmugam, *Radial oscillations of zero-temperature white dwarfs and neutron stars below nuclear densities* ApJ **217** ,799 (1977).

[281] O.G.Benvenuto and J.E. Horvath, *Radial pulsations of strange stars and the internal composition of pulsars* MNRAS **250**, 679 (1991).

[282] D. Gondek, P. Haensel and J.L. Zdunik , *Radial pulsations and stability of protoneutron stars*, A& A **325**, 217 (1997).

[283] D. Gondek and J.L. Zdunik , *Avoided crossings in radial pulsations of neutron and strange stars*, A & A **344**, 117 (1999).

Appendix A

Numerical results

Table A.1: Data for a MIT bag model EoS $p = c_s^2(\rho - 4B)$ with $c_s^2 = 1/3$, $B_{eff} = (145MeV)^4$

ρ_c	R	M	ω_0
$(10^{15}\ g/cm^3)$	(km)	$(M_\odot)$	(kHz)
2.000	10.90	2.001	0.20*
1.980	10.91	2.001	0.178
1.950	10.93	2.001	0.349
1.900	10.96	2.001	0.535
1.700	11.08	1.994	1.012
1.500	11.20	1.975	1.395
1.000	11.37	1.792	2.525

Table A.2: Data for parametrized EoS for quark matter $p = 3a_4/(4\pi^2)\mu^4 - 3a_2/(4\pi^2)\mu^2 - B_{eff}$ with $a_4 = 0.7$, $a_2 = 200MeV$ and $B_{eff} = (165MeV)^4$

ρ_c	M	R	ω_0
$(10^{15}\ g/cm^3)$	$(M_\odot)$	(km)	(kHz)
4.800	1.268	7.101	0.65*
4.650	1.268	7.126	0.157
4.500	1.268	7.151	0.694
4.300	1.267	7.186	1.063
4.000	1.263	7.239	2.862
3.000	1.223	7.405	2.695
2.000	1.053	7.404	4.400

Table A.3: Data for a polytropic EoS with $\Gamma = 2$ and $K = 10^{12}G$

ρ_c	M	R	ω_0
$(10^{15}\ g/cm^3)$	$(M_\odot)$	(km)	(kHz)
1.000	0.802	10.812	2.147
1.200	0.891	10.548	2.229
1.400	0.965	10.305	2.281
1.500	0.998	10.189	2.299
1.700	1.056	9.971	2.319
2.000	1.126	9.672	2.32
2.200	1.164	9.488	2.303
2.400	1.196	9.316	2.276
2.500	1.211	9.235	2.258
2.700	1.236	9.078	2.216
3.000	1.267	8.861	2.138
3.200	1.283	8.726	2.075
3.500	1.303	8.537	1.968
3.700	1.314	8.42	1.887
4.000	1.327	8.255	1.751
4.400	1.339	8.054	1.539
4.500	1.341	8.006	1.479
4.700	1.345	7.915	1.35
5.000	1.349	7.786	1.125
5.100	1.349	7.745	1.038
5.200	1.35	7.704	0.942
5.300	1.351	7.665	0.836
5.400	1.351	7.627	0.712
5.500	1.351	7.589	0.562
5.600	1.352	7.552	0.353
5.650	1.352	7.534	0.169
5.700	1.352	7.516	$0.26i$
5.800	1.352	7.481	$0.51i$
5.900	1.351	7.446	$0.673i$

Table A.4: Data for the EoS BBB2 [99]

ρ_c	M	R	ω_0
$(10^{15}\ g/cm^3)$	$(M_\odot)$	(km)	(kHz)
1.000	1.241	10.677	2.971
1.100	1.338	10.68	2.899
1.200	1.437	10.652	2.83
1.300	1.514	10.609	2.748
1.400	1.587	10.546	2.674
1.500	1.646	10.478	2.601
1.600	1.697	10.403	2.513
1.700	1.742	10.321	2.436
1.800	1.777	10.245	2.346
1.900	1.808	10.162	2.246
2.000	1.834	10.084	2.139
2.100	1.854	10.008	2.034
2.200	1.871	9.933	1.912
2.300	1.885	9.862	1.81
2.400	1.896	9.793	1.681
2.500	1.904	9.726	1.559
2.600	1.911	9.664	1.412
2.700	1.916	9.604	1.266
2.800	1.92	9.545	1.121
2.900	1.923	9.49	0.926
3.000	1.924	9.437	0.724
3.100	1.925	9.385	0.435
3.150	1.925	9.360	0.180
3.165	1.925	9.352	0.052
3.200	1.925	9.337	$0.34i$
3.300	1.925	9.289	$0.68i$

Table A.5: Data for the EoS SLy [98]

ρ_c	M	R	ω_0
$(10^{15}\ g/cm^3)$	$(M_\odot)$	(km)	(kHz)
0.800	1.124	10.997	3.094
1.000	1.423	11.115	2.974
1.100	1.54	11.102	2.873
1.200	1.638	11.062	2.77
1.300	1.719	11.002	2.66
1.400	1.786	10.929	2.545
1.500	1.841	10.85	2.418
1.600	1.886	10.766	2.298
1.700	1.923	10.679	2.182
1.800	1.953	10.591	2.051
1.900	1.977	10.506	1.923
2.000	1.996	10.422	1.807
2.100	2.011	10.339	1.68
2.200	2.023	10.259	1.528
2.300	2.033	10.183	1.404
2.400	2.039	10.107	1.251
2.500	2.044	10.036	1.083
2.600	2.048	9.967	0.901
2.700	2.05	9.901	0.681
2.750	2.051	9.868	0.570
2.800	2.051	9.837	0.386
2.840	2.051	9.360	0.078
2.900	2.051	9.777	$0.417i$
3.000	2.051	9.718	$0.69i$

Table A.6: Data for the EoS MS1 [100]

ρ_c	M	R	ω_0
$(10^{15}\ g/cm^3)$	$(M_\odot)$	(km)	(kHz)
0.6	1.95	14.263	2.421
0.650	2.111	14.292	2.398
0.700	2.245	14.283	2.312
0.750	2.352	14.248	2.206
0.800	2.442	14.195	2.109
0.850	2.512	14.131	2.004
0.900	2.57	14.059	1.906
0.950	2.616	13.985	1.778
1.000	2.653	13.907	1.673
1.050	2.682	13.829	1.561
1.100	2.706	13.752	1.448
1.150	2.724	13.675	1.334
1.200	2.739	13.6	1.252
1.250	2.75	13.526	1.115
1.300	2.759	13.455	0.98
1.350	2.765	13.386	0.866
1.400	2.769	13.319	0.741
1.450	2.772	13.254	0.558
1.500	2.774	13.191	0.362
1.550	2.774	13.13	$0.18i$
1.600	2.773	13.071	$0.43i$
1.650	2.772	13.014	$0.57i$

Notations, conventions and units

Acronyms

CS - Compact Star
EoS - Equation of State
GW - Gravitational Wave
M - Mirror
MS - Mixed Star
NS - Neutron Star
O - Ordinary
QCD - Quantum Chromodynamics
SS - Strange Star
TOV - Toleman Oppenheimer Volkoff
TS - Twin Star

Units and Conventions

In this thesis we use geometrical units in which $G = c = 1$, and we often use some fundamental astrophysical quantities:

$$M_\odot = 1.989 \times 10^{33}\text{g},$$
$$\rho_s = 2.66 \times 10^{14}\text{g/cm}^3$$